GEOCOMPOSITE MOISTURE BARRIERS IN ROADWAY APPLICATIONS

Publication No. FHWA-CFL/TD-12-003 **January 2012**

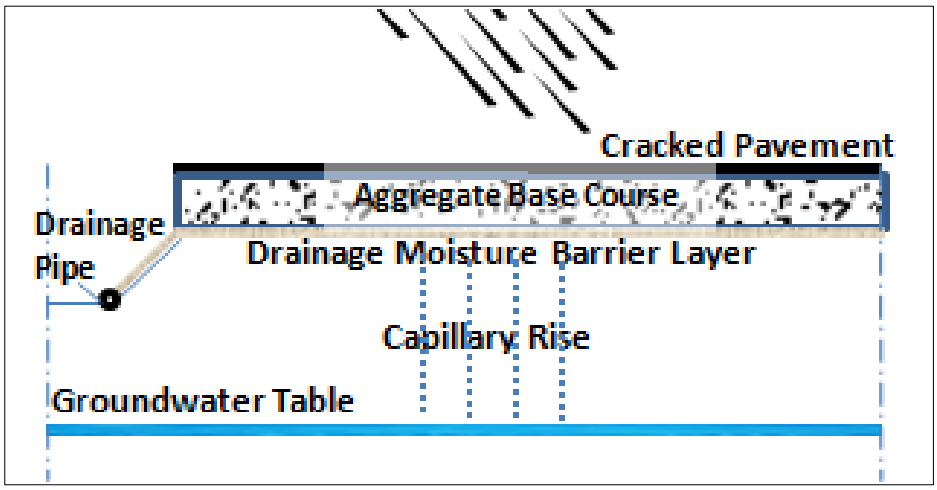

U.S. Department of Transportation
Federal Highway Administration

CTIP

Federal Lands Highway
Commitment to Excellence

Central Federal Lands Highway Division
12300 West Dakota Avenue
Lakewood, CO 80228

FOREWORD

The Federal Lands Highway (FLH) of the Federal Highway Administration (FHWA) promotes development and deployment of applied research and technology applicable to solving transportation related issues on Federal Lands. The FLH provides technology delivery, innovative solutions, recommended best practices, and related information and knowledge sharing to Federal agencies, Tribal governments, and other offices within the FHWA.

This report, *Geocomposite Moisture Barriers in Roadway Applications,* offers reasonable and effective solutions for roadway engineers faced with addressing localized issues of moisture intrusion.

F. David Zanetell, P.E., Director of Project Delivery
Federal Highway Administration
Central Federal Lands Highway Division

Notice

Quality Assurance Statement

The FHWA provides high-quality information to serve the Government, industry, and the public in a manner that promotes public understanding. Standards and policies are used to ensure and maximize the quality, objectivity, utility, and integrity of its information. FHWA periodically reviews quality issues and adjusts its program and processes to ensure continual quality improvement.

Technical Report Documentation Page

1. Report No.	2. Government Accession No.	3. Recipient's Catalog No.
FHWA-CFL/TD-12-003		

4. Title and Subtitle	5. Report Date
Geocomposite Moisture Barriers in Roadway Applications	January 2012
	6. Performing Organization Code

7. Author(s)	8. Performing Organization Report No.
Mohammed A. Gabr, Ph.D., P.E., T. Matthew Evans, Ph.D., Mahdi Bahador, Matthew Ranando	

9. Performing Organization Name and Address	10. Work Unit No. (TRAIS)
North Carolina State University Department of Civil, Construction and Environmental Engineering Raleigh, North Carolina 27695	11. Contract or Grant No. DTFH68-08-E-00058

12. Sponsoring Agency Name and Address	13. Type of Report and Period Covered
Federal Highway Administration Central Federal Lands Highway Division 12300 W. Dakota Avenue, Suite 210B Lakewood, CO 80228	Final Report September 2008 – August 2011
	14. Sponsoring Agency Code HFTS-16.4

15. Supplementary Notes

COTR: Marilyn Dodson, FHWA CFLHD. Advisory Panel: Roger Surdahl, FHWA-CFLHD; Daniel Alzamora, FHWA-RC; Khalid Mohamed and Jason Dietz, FHWA-EFLHD, and Rich Barrows, FHWA-FLH. This project was funded under the FHWA Federal Lands Highway Coordinated Technology Implementation Program (CTIP).

16. Abstract

Geosynthetic capillary barriers are gaining acceptance for use in mitigating the moisture variations and corresponding volume changes found in roadways. The modeling and experimental results from this study indicate that adequate system performance can be achieved with the placement of drainage moisture barrier layers (DMBLs) at the subgrade-aggregate base course (ABC) interface. This location is consistent with that reported in the literature. The recommended configuration for the DMBLs is a two-layered system that contains a geosynthetic layer with a low air entry value (AEV) (on the order of 1 psf) underneath a capillary break layer with a relatively high AEV, and ensures that the AEV of the upper layer remains lower than that of the ABC. The higher AEV of the upper layer over the lower AEV of the capillary break layer minimizes suction reduction in the subgrade while leaving the degree of saturation of the ABC relatively unchanged. Using a geomembrane underneath the DMBL is not recommended as its placement leads to an increase in the degree of saturation of the ABC, which may ultimately lead to a higher degree of rutting.

17. Key Words	18. Distribution Statement
BARRIER, DRAIN, GEOSYNTHETICS, LOADING, MODEL, MOISTURE, PAVEMENT, ROADS, UNPAVED, UNSATURATED	No restriction. This document is available to the public from the sponsoring agency at the website http://www.cflhd.gov.

19. Security Classif. (of this report)	20. Security Classif. (of this page)	21. No. of Pages	22. Price
Unclassified	Unclassified	144	

Form DOT F 1700.7 (8-72) **Reproduction of completed page authorized**

SI* (MODERN METRIC) CONVERSION FACTORS

APPROXIMATE CONVERSIONS TO SI UNITS

Symbol	When You Know	Multiply By	To Find	Symbol
		LENGTH		
in	inches	25.4	millimeters	mm
ft	feet	0.305	Meters	m
yd	yards	0.914	Meters	m
mi	miles	1.61	kilometers	km
		AREA		
in^2	square inches	645.2	square millimeters	mm^2
ft^2	square feet	0.093	square meters	m^2
yd^2	square yard	0.836	square meters	m^2
ac	acres	0.405	hectares	ha
mi^2	square miles	2.59	square kilometers	km^2
		VOLUME		
fl oz	fluid ounces	29.57	milliliters	mL
gal	gallons	3.785	liters	L
ft^3	cubic feet	0.028	cubic meters	m^3
yd^3	cubic yards	0.765	cubic meters	m^3
		NOTE: volumes greater than 1000 L shall be shown in m^3		
		MASS		
oz	ounces	28.35	grams	g
lb	pounds	0.454	kilograms	kg
T	short tons (2000 lb)	0.907	megagrams (or "metric ton")	Mg (or "t")
		TEMPERATURE (exact degrees)		
°F	Fahrenheit	5 (F-32)/9 or (F-32)/1.8	Celsius	°C
		ILLUMINATION		
fc	foot-candles	10.76	lux	lx
fl	foot-Lamberts	3.426	$candela/m^2$	cd/m^2
		FORCE and PRESSURE or STRESS		
lbf	poundforce	4.45	Newtons	N
lbf/in^2	poundforce per square inch	6.89	kilopascals	kPa

APPROXIMATE CONVERSIONS FROM SI UNITS

Symbol	When You Know	Multiply By	To Find	Symbol
		LENGTH		
mm	millimeters	0.039	inches	in
m	meters	3.28	feet	ft
m	meters	1.09	yards	yd
km	kilometers	0.621	miles	mi
		AREA		
mm^2	square millimeters	0.0016	square inches	in^2
m^2	square meters	10.764	square feet	ft^2
m^2	square meters	1.195	square yards	yd^2
ha	hectares	2.47	acres	ac
km^2	square kilometers	0.386	square miles	mi^2
		VOLUME		
mL	milliliters	0.034	fluid ounces	fl oz
L	liters	0.264	gallons	gal
m^3	cubic meters	35.314	cubic feet	ft^3
m^3	cubic meters	1.307	cubic yards	yd^3
		MASS		
g	grams	0.035	ounces	oz
kg	kilograms	2.202	pounds	lb
Mg (or "t")	megagrams (or "metric ton")	1.103	short tons (2000 lb)	T
		TEMPERATURE (exact degrees)		
°C	Celsius	1.8C+32	Fahrenheit	°F
		ILLUMINATION		
lx	lux	0.0929	foot-candles	fc
cd/m^2	$candela/m^2$	0.2919	foot-Lamberts	fl
		FORCE and PRESSURE or STRESS		
N	newtons	0.225	poundforce	lbf
kPa	kilopascals	0.145	poundforce per square inch	lbf/in^2

*SI is the symbol for the International System of Units. Appropriate rounding should be made to comply with Section 4 of ASTM E380. (Revised March 2003)

TABLE OF CONTENTS

LIST OF FIGURES

LIST OF TABLES

ACRONYMS, ABBREVIATIONS AND SYMBOLS

ABC: aggregate base course

α and n: Van Genuchten parameters

AEV: air entry value

AOS apparent opening size

DMBL: drainage moisture barrier layer

EPC: earth pressure cell

FDR: frequency domain reflectometry

FWD falling weight deflectometer

GCBD: geosynthetic composite barrier drain

GSD grain size distribution

LVDT: linear variable differential transformer

MCC: moisture characteristics curves

N.T.S. not-to-scale

SWCC: soil water characteristics curve

TDR: time domain reflectometry

θ : volumetric water content

θ_s: saturated water content

UDL: unsaturated drainage layer

USCS unified soil classification system

WEV: water entry value

ACKNOWLEDGEMENTS

The work described in this report is supported by Federal Highway Administration, Central Federal Lands Highway Division. The authors acknowledge Daniel Alzamora, Rich Barrows, Jason Dietz, Marilyn Dodson, Khalid Mohamed, and Roger Surdahl for serving on the project committee. Their input and guidance is greatly appreciated.

(blank page)

EXECUTIVE SUMMARY

The main objective of this study is to develop recommendations to guide and advance the use of geosynthetic materials as moisture barriers and drainage layers in roadways over soils that are susceptible to moisture variation-induced volume changes. The research encompasses experimental work and modeling. The experimental program is designed to provide data for the analytical model and study the performance of drainage moisture barrier layers (DMBLs) under controlled conditions. The modeling work is aimed at providing systematic data to explain the performance of the DMBLs and to propose guidelines for the use of DMBLs in roadway applications.

The experimental work conducted in this research includes laboratory-scale hanging column tests to measure the moisture characteristic properties of fiberglass geosynthetics, a material that is recommended in the literature as appropriate for inclusion in a DMBL. A composite DMBL was tested in a large-scale test pit to determine its ability to prevent water from infiltrating the subgrade of a simulated road section. Cyclic loading of the two large-scale simulated sections, with and without a DMBL, also was carried out. The scope of the large-scale experimental testing was limited to two tests due to budget constraints. The modeling effort undertaken in this research includes one-dimensional analysis using the computer program UNSAT-H to investigate the effects of temperature gradient on moisture distribution within a soil layer that contains a geotextile. Two-dimensional finite element modeling was performed using SIGMA/W to study the pore pressure distribution throughout a simulated roadway section under loading and to study the roadway section response when the DMBL is located within the aggregate base course (ABC) versus when it is located at the interface between the ABC and the subgrade, as recommended in the literature.

The laboratory-scale experimental testing confirms the results of Stormont and Ramos (2004) with regard to the unsaturated properties of TGLASS material. The large-scale test results provide data regarding the performance of the composite DMBL in a simulated road section and show the DMBL's ability to prevent the infiltration of water into the subgrade during rainfall events. The DMBL's performance under loading conditions indicates that the section with the DMBL performs better than a control section with similar soil properties, although it is not clear whether the improvement in performance is due to the effect of the moisture control or the reinforcement effect of the DMBL, or a combination of the two. However, the types of geosynthetics used for the DMBL system are not traditionally used for reinforcement.

The results of the series of simulations using UNSAT-H indicate that, based on assumed hydraulic and thermal parameters, the temperatures investigated in this study affect the hydraulic conductivity of the geotextile, with no significant effect on the hydraulic conductivity of the soils. Although the conductivity of the geotextile is not a direct function of temperature, it is a function of suction. As suction changes with temperature under simulated drainage conditions when the geotextile is placed at the bottom of the profile and water moves downward due to gravitational force, the geotextile exhibits lower conductivity and works better as a moisture barrier at high temperatures. Under simulated capillary conditions wherein water moves upward due to capillary force, a lower temperature decreases the hydraulic conductivity of the geotextile and induces the geotextile to work more efficiently as a moisture barrier. This phenomenon is important, especially in cold regions where it is desirable to prevent capillary rise and minimize frost heave. The two-dimensional finite element modeling results show that when only one layer system (geotextile in this case) is used, suction in the ABC decreases under infiltration and drainage conditions, whereas suction increases in the subgrade layer. The decreased suction in the ABC results in a decrease in shear strength and consequently leads to higher deformation under applied loading. One way to minimize the decrease in suction in the ABC is to increase the unsaturated hydraulic conductivity of the DMBL under suction by increasing its air entry value (AEV). However, when only a geotextile layer is used as the DMBL, a higher AEV of the DMBL leads to a decrease in the subgrade suction due to downward water flow during rainfall infiltration. Thus, the AEV of the DMBL needs to be increased while the downward water flow into the subgrade decreases; hence, a two-layer system is recommended.

Using composite DMBLs can decrease the downward water flow into the subgrade if the AEV of the lower DMBL is very low (on the order of 1 psf). In this case, increasing the AEV of the upper layer leads to the minimization of suction reduction in the subgrade for both rainfall and drainage conditions, while the ABC remains unsaturated. The results also show that increasing the saturated hydraulic conductivity of the upper layer does not have a significant effect on the pore pressure distribution in the profile as long as the upper layer is associated with a suction level above 2 psf. The findings indicate that placing the DMBL at the interface of the ABC and subgrade minimizes the decrease in the suction level of the subgrade and ABC during infiltration as compared to the case where the DMBL is placed in the middle of the ABC.

The following recommendations are based on the experimental results and the modeling that considers the profile, initial and boundary conditions, and infiltration rates (0.07 ft/hr and 0.035 ft/hr) used in this study:

i. The use of composite DMBL, composed of a transmission layer (geotextile) underneath a capillary break layer (geonet), is recommended to protect the subgrade from infiltrating water. During the load testing phase, the composite DMBL section is found to outperform the control section under both static and cyclic loading.

ii. The composite DMBL should be placed at the interface of the ABC and subgrade. This placement is in concert with and confirms results reported in the literature.

iii. To mitigate water flow into the subgrade and to drain the ABC during rainfall infiltration, the lower layer of the DMBL must have an AEV that is lower than that of the upper layer.

iv. A high AEV for the upper layer of the DMBL minimizes the decrease in the subgrade suction level, whereas the degree of saturation of the ABC remains relatively unchanged. However, the AEV of the upper layer of the DMBL should not exceed the AEV of the overlying soil (ABC); otherwise, the DMBL will act as a barrier to drainage under unsaturated conditions.

v. Although using a geomembrane underneath the DMBL helps maintain the suction level of the subgrade layer, it causes an increase in the degree of saturation of the ABC. This increase may cause positive pore pressures in the ABC that can lead to a decrease in shear strength and, therefore, a higher degree of rutting. Thus, the use of a geomembrane is not recommended.

vi. The best configuration for moisture barriers is the use of two layers, as recommended by Stormont et al. (2000): a layer with a low AEV (1 psf) underneath a layer with a relatively high AEV. The upper layer of the composite section should have an AEV lower than that of the ABC. Although it is tempting to suggest ratios of the AEV between layers, the guiding design principle should be that the AEV is as low as possible for the lower layer, and as high as possible for the upper layer, but that the AEV should not exceed the AEV of the ABC.

vii. Although TGLASS is tested in this study, this material is not commonly used in mass geotechnical applications, and, as such, its cost can be five to ten times higher than that of traditional polypropylene geotextiles. The least expensive type of material should be used as long as conditions related to the relative values of the AEVs are satisfied. The challenge in this case is the dearth of information in the literature regarding the unsaturated hydraulic properties of geosynthetics.

(blank page)

CHAPTER 1 – INTRODUCTION

Overview

Soils found in roadway applications are subjected to a wide variation of moisture conditions due to rainfall, storms and seasonal variations of groundwater elevations. In some cases, subgrade soils are expansive and thus susceptible to volume change and heave due to shrinkage and swelling. In other cases, an increase in the degree of saturation leads to a reduction in shear strength that, in turn, leads to excessive rutting of the constructed roadway sections. One possible approach for addressing these issues is the use of geosynthetics for the drainage of moisture under both unsaturated and saturated conditions such that significant increases in moisture content and the degree of saturation in the layers within a constructed roadway section are minimized. The use of geosynthetics as moisture barriers is not specified explicitly in Federal Lands Highway Division (FLHD) Standard Specifications (FP-03) and, therefore, information regarding specifications and selection criteria is needed to advance the use of geosynthetic materials as moisture barriers in pavement sections.

Several moisture barrier configurations have been investigated and used in geotechnical and geo-environmental projects. For example, an unsaturated drainage layer (UDL), such as sand, placed over a coarse-grained soil, such as gravel, is commonly used in landfill applications, whereas a geocomposite section, composed of a geotextile placed over a geonet, is commonly used in roadway applications. Moisture barrier layers that use geosynthetics have been reported in the literature, and among such moisture barrier systems is a patent by Henry and Stormont (2000) for a configuration termed the *geocomposite capillary barrier drain* (GCBD). In general, capillary barriers are composed of layers of highly permeable and transmissive materials and are installed within profiles of fine-grained soils that are susceptible to volume change. These layers function to minimize moisture variations within soils in pavement sections. These moisture variations are due primarily to two factors: i) the infiltration of water due to rainfall, and ii) the upward flow of groundwater due to capillary force. Geocomposite capillary barriers function to prevent the build-up of positive pore water pressure by removing water from the unsaturated soil; that is, they remove the pore water that is held under tension in the soil matrix. In soil and geocomposite moisture barriers, the unsaturated hydraulic conductivity of the coarse material is relatively low, with a narrow range of variation with changes in suction head. It is essential that flow occurs under unsaturated conditions, and the relative hydraulic conductivity values of the various layers are chosen such that capillary break and moisture transmission take place under a wide range of hydraulic head conditions.

In this report, both the configuration and function of drainage moisture barrier layers (DMBLs) are investigated, with the goal of studying the factors that affect their configuration as well as the parameters that are essential for the DMBL specifications and design. A review of previous work on moisture barriers is presented. Specifically, a comprehensive review of experimental and field work on moisture barriers and their various configurations found in previous studies is presented. The results of the experimental characterization of several geotextile materials and analyses are documented with a focus on the various aspects of moisture barrier performance.

The work plan encompasses modeling and limited experimental testing. The experimental program provides data for the analytical model and examines the performance of DMBLs under controlled conditions. The modeling work includes one-dimensional (1-D) and two-dimensional (2-D) analyses of sections that contain a DMBL. Simulations are performed using the computer programs UNSAT-H and SIGMA/W. UNSAT-H is a finite difference program that simulates water and heat flow in porous media and is used here to investigate the effects of heat flow and temperature on moisture distribution within a soil-geotextile column. SIGMA/W is a 2-D finite element program that is used to simulate unsaturated flow and associated deformation under applied stress. SIGMA/W is used here to model performance aspects of moisture barriers and roadway section responses under loading, with and without the inclusion of moisture barriers. The 2-D seepage program SEEP/W also is used in this research to study the effects of key parameters, such as air entry values (AEVs) and the hydraulic conductivity of the DMBL, on unsaturated moisture distribution within the simulated profile. Results from the experimental and modeling work are used to explain the performance of DMBLs and to propose guidelines for their inclusion in roadway applications. In this report, the term *drainage moisture barrier layer* (i.e., DMBL) is used instead of *geocomposite capillary barrier drain* (GCBD) because the GCBD term refers to a specific patent. The term *GCBD* is used in this report only when referring to the patented configuration by Henry and Stormont (2000).

Geocomposite Capillary Barrier Drain (GCBD)

A geocomposite DMBL provides drainage in unsaturated soil profiles to minimize moisture variations and susceptibility to volume change (Henry and Stormont 2000, Henry et al. 2000, Stormont et al. 2001). Such a system was patented by Henry and Stormont (2000) and termed *geosynthetic composite barrier drain*, or GCBD. The system contains a transport layer, a capillary barrier, and a separator, from top to bottom, as shown in Figure 1 (Stormont et al. 2009).

A defining aspect of the GCBD is that it provides drainage in subsurface applications under unsaturated and saturated conditions. The advantage is that it protects the subgrade layer from saturation. Saturated

conditions reduce the strength of the roadway base and subgrade layers, thus leading to an increase in rutting levels. Frost heave also increases under saturated conditions, as both the pore fluid and the soil grains are incompressible (or can be considered as such within the range of near-surface stresses).

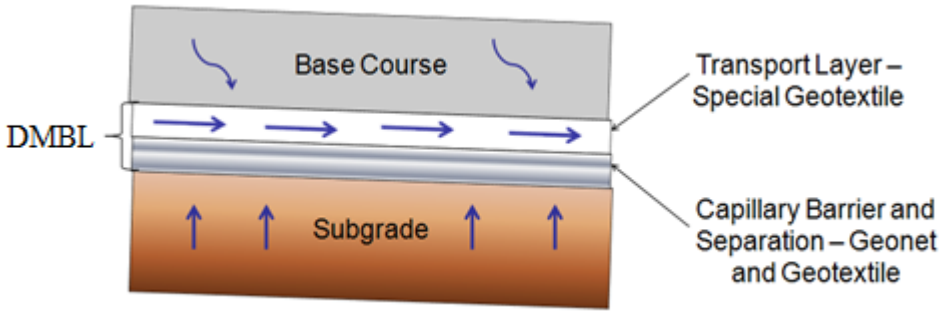

Figure 1. Schematic. DMBL between base and subgrade layers (after Stormont et al. 2009).

Figure 2 shows three possible configurations of a DMBL (Christopher et al. 2000). In scenario A, a GCBD is located at the interface of the roadway base course and the subgrade material. Water is drained laterally to side drainage pipes. The base course material is protected from the upward migration of groundwater and water percolating into the soil through the pavement. A similar configuration is presented in scenario B where Portland cement concrete (PCC) is used. In scenario C, a GCBD is placed at a depth that allows it to protect frost-susceptible soil from the upward migration of groundwater. Rising groundwater is drained laterally by the GCBD into side drainage pipes. In scenario C the frost-susceptible material may be excavated to the required depth for frost protection, the GCBD then placed, and the excavated soil used as back fill.

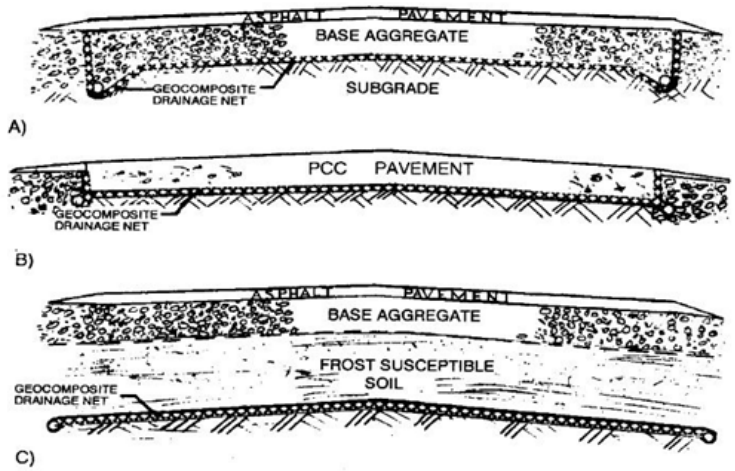

Figure 2. Schematic. Potential use of horizontal geocomposite drainage layers, including: a) drainage of roadway base or sub-base aggregate, b) drainage of surface asphalt or concrete pavement, and c) drainage of subgrade to form a capillary break (Christopher et al. 2000).

Problem Statement

Currently, national guidelines do not exist for the design of moisture capillary barriers to mitigate volume changes due to moisture variation. In the survey of FLHD and U.S. Forest Service (USFS) engineers conducted by Gabr et al. (2006) and reported in "Promoting Geosynthetics Use in Federal Lands Highway Projects," one respondent reported the use of capillary barriers in drainage, and six respondents noted the use of capillary barriers in frost heave projects. Three of the six respondents reported the use of geosynthetics materials in these projects. Based on this small, but targeted, sample, the survey results suggest a need for improved quantitative understanding of the functionality of DMBLs and their use as moisture or capillary barriers for minimizing water infiltration and the associated volume changes within different soil profiles. Although the use of DMBLs is gaining ground as a control technology to mitigate volume change in unstable soils, specific analysis data to aid in understanding the function and performance limitations of DMBLs are lacking in the literature. A thorough investigation of key DMBL engineering parameters and their impact on performance is needed in order to realize a wider application of this technology.

Study Objectives

The main objective of this study is to provide information that will lead to the improved design of geosynthetic capillary barriers to mitigate moisture variations and, therefore, volume changes in roadway sections. Although laboratory and field work has been conducted and reported in the literature, a gap remains with regard to the application of the results to understand the key parameters that ensure the adequate performance of DMBLs. Work herein includes a limited laboratory testing program and numerical parametric analyses to provide information for specifying moisture barrier layers to minimize moisture changes in subgrade soils. The project results are used to propose criteria for specifying DMBLs and for quantifying the effects of key parameters on their performance.

Study Scope

The study scope includes the development of information that can be used to establish guidelines for the use of geosynthetics as moisture barriers in highway applications, with specific emphasis on roadways. In comparison to capillary barrier applications for groundwater remediation or landfill covers, the use of these types of systems in roadways calls for preserving the strength of the roadway section layers, minimizing the variability of suction levels due to moisture infiltration associated with seasonal changes, and conveying water to edge drains under unsaturated conditions.

The study scope includes a literature review of the current state-of-the-art practice for geosynthetic moisture barriers and their use with drainage layers. An experimental program is conducted to characterize the performance parameters of barrier/drain materials using configurations identified in the literature as the most promising for such an application. Large-scale laboratory testing is used to demonstrate the performance of a simulated roadway section subjected to rainfall events, with and without a DMBL, and under cyclic loading. The subgrade layer is instrumented with moisture sensors, and surface rutting is monitored using a displacement gauge under static and cyclic loading. The modeling effort includes 1-D and 2-D numerical analyses to investigate aspects related to unsaturated flow conditions and the effects of geosynthetics barrier transmissivity and permittivity on facilitating drainage and reducing moisture migration. In addition, the effects of the location of the moisture barrier (i.e., where it is placed) on moisture distribution, as well as the effects of key parameters such as AEV and hydraulic conductivity, are investigated. Recommendations are made regarding the placement within a road section and specifications for DMBLs.

(blank page)

CHAPTER 2 – DRAINAGE MOISTURE BARRIER LAYERS (DMBLs)

Overview

A capillary barrier can control water flow within a soil profile because it accounts for the contrast in the hydraulic conductivity of both fine and coarse layers (i.e., the contrast in potential energy between a filled small pore and an empty large pore[1]). Under unsaturated conditions, the fine-grained layer (also referred to as the *transport* or *drainage* layer) can be used to facilitate the lateral (in-plane) drainage of water, and the coarse-grained layer can be used to prevent cross-plane water flow. Two conditions must be satisfied in this case: 1) adequate conductivity of the transport layer under unsaturated conditions to transmit water in the in-plane direction, and 2) inclusion of a filter such that adjacent soil particles do not enter the drainage layer and clog it. The transport layer is typically sand or geotextile placed underneath a material of high saturated hydraulic conductivity (gravel or geonet) to create a capillary break. The hydraulic conductivity of the transport layer under unsaturated conditions and the contact angle (defining the layer's affinity to moisture, and a function of material type) are important factors to consider. The transport layer should be able to drain water under both saturated and unsaturated conditions.

Previous work on infiltration into a soil moisture barrier system is presented next, and factors that affect moisture barrier function and performance are discussed.

The Unsaturated Response of Geotextiles

The hydraulic properties of geotextiles used as DMBLs constitute a key design issue. The properties of concern are the water retention relationship (also referred to as the *moisture characteristics curve*) and the transmissivity of the transport layer. These properties have been the subject of several studies found in the literature. Geotextile materials used in DMBL applications include nonwoven polypropylene and polyester. An additional product by Stormont et al. (2004) is a fiberglass material that is hydrophilic as opposed to a hydrophobic organic, cross-linked, and polymeric material. Each of these geotextile types will drain water under unsaturated conditions; however, the range of suction heads over which they can function is limited. The suction of unsaturated soils and geotextiles is related to water content and pore size. At higher suction values, the water content of the soil is lower. Low water content in soils generally corresponds to high soil strength. Using a drainage layer with a high water entry potential will enable the DMBL to drain at low water contents. In short, then, an effective design of DMBLs for the diversion of water under unsaturated conditions requires knowledge of the water content-to-matric suction potential relationship, i.e., understanding the water retention or moisture characteristics curves (MCCs) of the

[1] This phenomenon is sometimes referred to as the *ink bottle effect*, particularly in soil physics literature (e.g., Hillel 1980).

materials involved in the design. The capillary rise of water in geotextiles has been the focus of several studies. Table 1 provides a summary of several studies reported in the literature on this subject, including the test methods used and parameters measured.

Table 1. Different testing methods and parameters used in previous studies.

Author	Geotextile Material Tested	Test Method	Properties Measured	t (mm)	AEV (mm)	AOS (mm)
Stormont et al. (1997)	Nonwoven Polypropylene	Hanging Column	MCC	NR	100	A1 = 0.15
Ho (2000)	Nonwoven Unspecified	Pressure Plate	MCC	Nonwoven: 3.8 Woven: 1.83	Nonwoven: 5 Woven: 15	Nonwoven: 0.15 woven: 0.3
Lafleuer (2000)	Nonwoven Polyester	Capillary Rise/ Steady State Flux Method	MCC/Conductivity	A1 = 1.9 A2 = 3.49 B1 = 2.31 C1 = 2.23	A1 = 89.7 A2 = 76.5 B1 = 151.9 C1 = 101.9	NR
Morris (2000)*	Nonwoven Unspecified	Hanging Column/ TDR	MCC/ Transmissivity	NR	Mirafi 1160n Drying = 142.9 Wetting = 0.05 SI Geotex 1601 Drying = 103.1 Wetting = 5.1 Amoco 4516 Drying = 166.7 Wetting = 7.9	NR
Stormont and Morris (2000)*	Nonwoven Polypropylene/Polyester	Hanging Column/TDR	MCC/Conductivity	5.9	26.25 – 57.8	0.18
Knight and Kotha (2001)	Nonwoven Unspecified	Pressure Plate/Hanging Column	MCC	10	40	0.15
Stormont and Ramos (2001)	Woven Fiberglass Nonwoven Polypropylene	Capillary Rise Siphon Permeameter	MCC/ Transmissivity	3.2	75.8	O95 = 0.075
Stormont et al.	Nonwoven Polypropylene	Permeameter	Transmissivity	5.9	26.25-57.8	0.18

Author	Geotextile Material Tested	Test Method	Properties Measured	t (mm)	AEV (mm)	AOS (mm)
(2001)*						
Kuhn et al. (2005)*	Nonwoven Unspecified	Pressure Plate/Centrifuge	MCC/ Conductivity	1.97	83.3	NR
Park and Fleming (2005)*	Nonwoven Polypropylene	Pressure Plate	MCC	4.0	151.7	0.05-0.15
Bouazza et al. (2006)	Nonwoven Polyester	Capillary Rise/Hanging Column	MCC/ Transmissivity	A = 2.3 B = 1.8	A = 30.6 B = 91.7	A = 0.2 B = 0.18
Garcia et al. (2007)	Nonwoven Polypropylene	Hanging Column	MCC	4	Drying: 30.60 Wetting: 15.3	0.89
Nahlawi et al. (2007)*	Nonwoven Polyester	Pressure Cell/Hanging Column	MCC	2.3	119.9 – 161.8	0.18
Krisdani et al. (2008)	Nonwoven Polypropylene	Capillary Rise	MCC	NR	42.61	0.11

* AEV is calculated as (1/α), where α is the Van Genucthen parameter.
** NR = Not Reported.

Iryo and Rowe (2003) concluded that water characteristics curves for geotextiles are steeper than those for most types of soils, and are similar to coarse-grained soils such as gravel or uniform coarse sand. They also concluded that water entry values (WEVs) for geotextiles are smaller than for most soils. This phenomenon allows geotextiles to function as a drainage layer under saturated conditions and as a moisture barrier under unsaturated conditions.

(blank page)

CHAPTER 3 – LITERATURE REVIEW

Infiltration into a Soil-Geotextile Column

Zornberg and Mitchell (1994) concluded that nonwoven geotextiles can function as both a drainage and a barrier layer. They postulated that the difference between these two seemingly opposite functions is attributed to the dependency of the hydraulic conductivity of porous media on the suction level. In geotextile-like porous materials, hydraulic conductivity decreases as suction increases. Thus, if suction in the adjacent soil increases, the cross-plane drainage of water in the geotextile decreases; moreover, if the suction value exceeds the WEV of the geotextile, then the geotextile will function as a moisture barrier. However, if the suction value in the soil around the geotextile is less than the WEV of the geotextile, water can enter the geotextile. Further, if the geotextile becomes saturated, it will reach its saturated hydraulic conductivity and then function as a drainage layer. Stated differently, if the soil surrounding the geotextile is unsaturated, and the suction head at the interface is greater than the WEV of the geotextile, the geotextile will act as a barrier. However, if the soil around the geotextile is saturated, a positive pore pressure is generated at the interface, and the geotextile will function as a drainage layer.

Laboratory soil columns often are used to quantify the 1-D unsaturated-saturated hydraulic behavior of one or more layers that is due to drainage or surface infiltration. Ho (2000) performed soil-geotextile column tests using a needle-punched nonwoven geotextile to investigate the hydraulic behavior of the system during infiltration. Ho demonstrated that during infiltration, when the saturated hydraulic conductivity of the geotextile is less than that of the soil above it, positive pore water pressure develops above the geotextile when the wetting front reaches the geotextile. Ho also tested geotextiles that were rubbed with Kaolin paste to evaluate the effects of soil intrusion. Ho's results show that the intrusion of soil into the geotextile decreases its porosity and saturated hydraulic conductivity and consequently increases the positive pore pressure generated above the geotextile. Stormont and Morris (2000) found that the intrusion of soil fines into nonwoven polypropylene geotextile increases the AEV of the geotextile.

Iryo and Rowe (2004) performed sand-geotextile column testing to investigate pore water pressure and water content distribution during infiltration using needle-punched nonwoven geotextiles. They performed numerical simulations using the finite element program SEEP/W version 5. Iryo and Rowe studied four cases: Case 1 was a uniform sand column; Case 2 was a sand column with a horizontal, circular geotextile rubbed with soil fines and located 0.95 m above the bottom of the column; Case 3 was similar to Case 2, but an unimpregnated geotextile was used; Case 4 used loamy sand, and an initial pore

pressure of -18.4 kPa (which corresponds to the degree of saturation of loamy sand, $S_r = 34\%$) was distributed uniformly throughout the profile to study the pore pressure distribution under different types of soil and initial conditions. Cases 1, 2, and 3 showed that the infiltration rate was higher than the hydraulic capacity of the soil, whereas Case 4 demonstrated that the rate was lower than the hydraulic capacity of the soil. Also, in Cases 1, 2, and 3, pore pressure of about -1 kPa was distributed uniformly throughout the profile after 20 minutes of drainage, which represents an initial condition (based on experimental results). The tests were modeled numerically, and the results compared to experimental data obtained by Ho (2000) to verify the numerical model.

Figure 3 shows the pore pressure distribution along the column for Case 2, and Figure 4 shows the data for Case 3. The results of the numerical modeling, along with the experimental data obtained by Ho (2000), are presented in these two figures. The pore pressure profiles shown in these figures correspond to 0 s (the beginning of the infiltration), 140 s (just before the wetting front reaches the geotextile), 180 s (just after the wetting front reaches the geotextile), and 240 s (well after the wetting front passes the geotextile layer but before it reaches the datum) (Iryo and Rowe, 2004). Iryo and Rowe note that positive pore pressure develops above the geotextile after the wetting front reaches the geotextile. However, the value of the positive pressure in Case 2 (geotextile rubbed with fines) is higher than that for Case 3. It is postulated that some air was entrapped in the geotextile during infiltration.

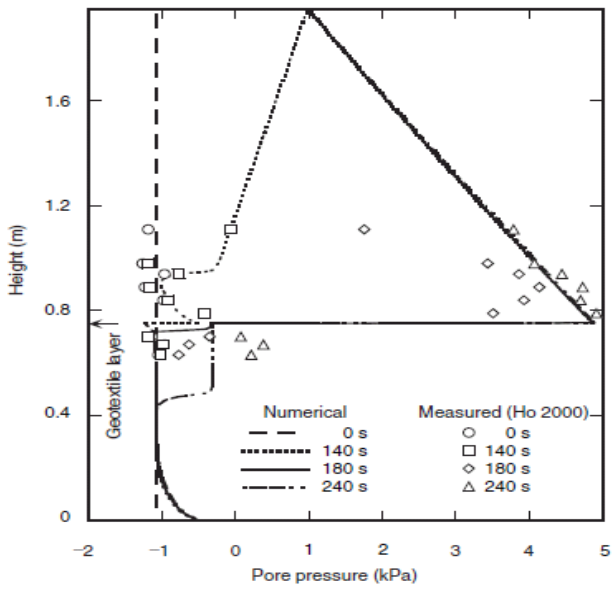

Figure 3. Graph. Pore pressure profile for Case 2 (Iryo and Rowe 2004).

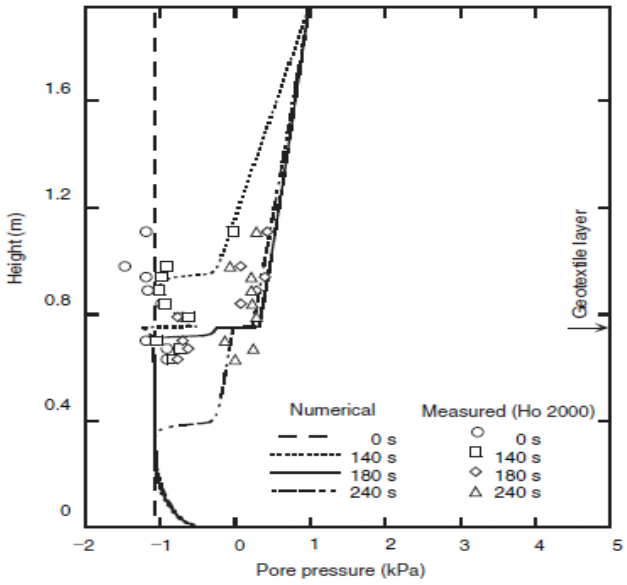

Figure 4. Graph. Pore pressure profile for Case 3 (Iryo and Rowe 2004).

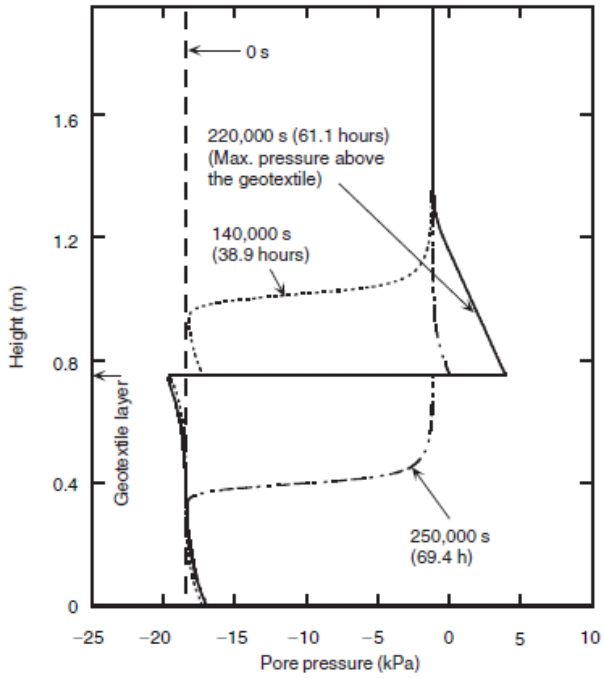

Figure 5. Graph. Pore pressure profile for Case 4 (Iryo and Rowe 2004).

Iryo and Rowe (2004) modeled infiltration by applying a constant positive pore pressure of 0.1 kPa at the top of the column. For Case 4, the infiltration rate was less than the hydraulic conductivity of the loamy sand soil. These results are shown in Figure 5 where it is seen that pore water pressure again develops

above the geotextile due to the difference between the infiltration rate and the hydraulic conductivity of the geotextile.

Based on their study (2004), Iryo and Rowe concluded the following:

- Prior to the arrival of the wetting front, the geotextile is unsaturated and behaves similarly to an impermeable layer.
- After the wetting front reaches the geotextile, the pore pressure increases above the geotextile when the WEV of the geotextile is lower than that of the suction head in the soil. Over time, and when the suction head in the soil above the geotextile reaches the WEV of the geotextile, water passes through the geotextile to the underlying layers, and the developed pore pressure above the geotextile dissipates. However, if the saturated hydraulic conductivity of the geotextile is less than that of the soil, then positive pore pressure may develop above the geotextile.
- After the wetting front passes through the geotextile, the pore pressure profile becomes dependent on the type of boundary conditions and relative hydraulic conductivity of the soil and geotextile. The scenarios are: i) if $K_{sat\_geotextile} < K_{sat\_soil}$ and the infiltration rate is higher than K_{sat_soil}, the positive pore pressure above the geotextile will remain; ii) if $K_{sat\_geotextile} > K_{sat\_soil}$ and the infiltration rate is higher than K_{sat_soil}, the pore pressure above the geotextile will dissipate after the wetting front passes; and iii) if $K_{sat\_geotextile} > K_{sat\_soil}$ and the infiltration rate is lower than K_{sat_soil}, the pore pressure below the geotextile will not become positive because the flux is smaller than K_{sat_soil}. Most of the pore pressure above the geotextile dissipates, but a small pore pressure discontinuity remains at the lower interface of the geotextile.

Krisdani et al. (2008) also performed soil-geosynthetic column testing. The saturated/unsaturated finite element seepage modeling software SVFlux (SoilVision System, Ltd. 2004) was used to model a 1 m fine sand-geosynthetic column with a geocomposite located in the middle of the column. The geocomposite used was Polyfelt Megadrain 2040. This geocomposite is a drainage product composed of a 3-D polypropylene monofilament geonet combined with two layers of polypropylene geotextile. Two types of tests were performed: i) a drawdown test in which the water table is lowered from the top of the column to the bottom, and ii) an infiltration test in which the final condition at the end of the drawdown test is used as an initial condition for a rainfall test (with intensity of 5.8 mm/h for 6 h). Figure 6 shows the results of the numerical and experimental studies for the drawdown tests.

As shown in Figure 6, the geocomposite causes a discontinuity in the pore pressure profile. This discontinuity is due to negative pore pressure induced above the geotextile, which decreases the permeability of the geotextile. Figure 7 shows the results of the rainfall test and drawdown after rainfall,

respectively. Figure 7 also shows that pore pressure above the geotextile does not change and the geotextile functions as a barrier until the suction head reaches the WEV of the geotextile.

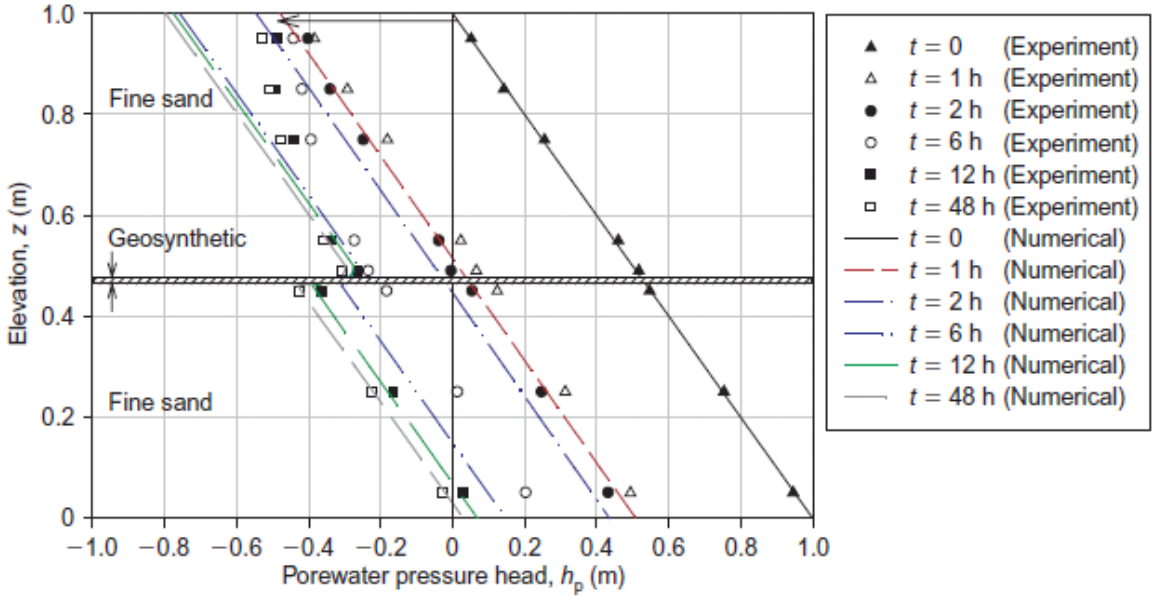

Figure 6. Graph. Pore pressure profile for drawdown test (Krisdani et al. 2008).

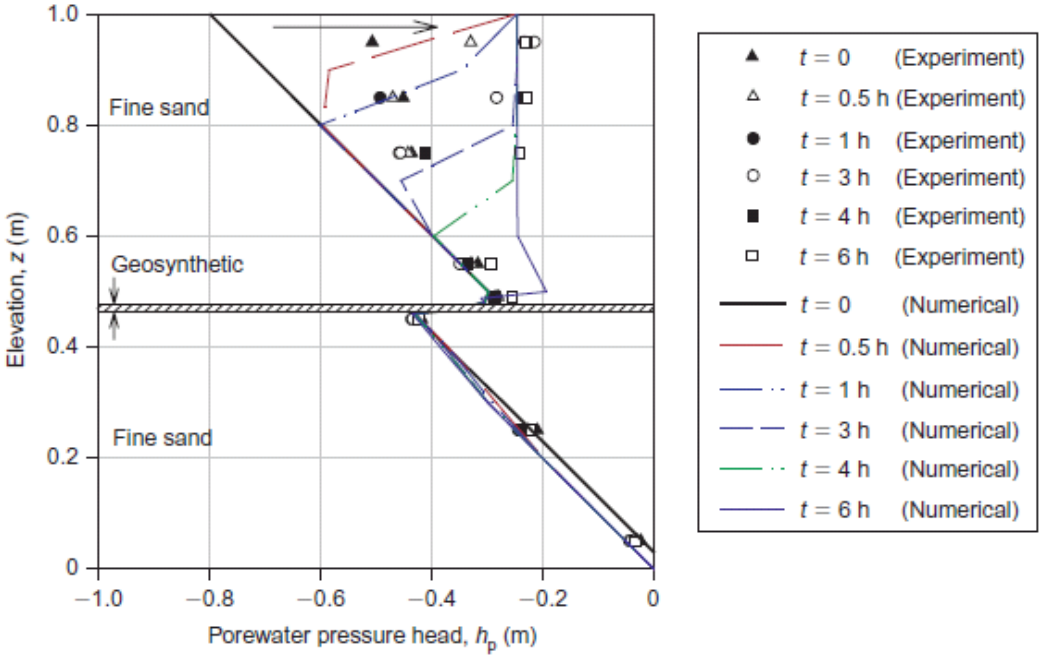

Figure 7. Graph. Pore pressure profile for rainfall test (Krisdani et al. 2008).

Bathurst et al. (2007) performed sand-geotextile column tests to investigate the water content profile within the system. A woven geotextile was used in this study. The column first was saturated, and drainage conditions were observed for 20 min and 24 h. Similar to previous findings, the water content increased at the soil-geotextile interface, but dissipated completely after 24 h, when the suction head at the interface decreased to the WEV of the geotextile.

These previous studies of soil-geotextile columns show that low hydraulic conductivity of initially unsaturated geotextiles may lead to the ponding of infiltrated water at the soil-geotextile interface. This occurrence can cause the lateral spread of water above the geotextile, which may contribute to the deterioration of the road layers. If $K_{sat\_geotextile} > K_{sat\_soil}$, the pore pressure generated above the geotextile will dissipate over time, because the suction at the interface tends to be lower than the WEV of the geotextile. The time it takes for the pore pressure at the interface to dissipate depends on the infiltration rate, water entry suction of the geotextile, hydraulic conductivity of the overlying soil, initial water content of the geotextile, intrusion of soil fines into the geotextile, and the entrapped air in the geotextile. Of all these factors, the WEV of the geotextile and the intrusion of fines are the most readily controlled through proper selection/specification of the geotextile material. Iryo and Rowe (2004) suggest that the intrusion of soil fines into the geotextile does not change the geotextile's WEV; they came to this conclusion by estimating the wetting curve from the drying curve. (However, their idea is not confirmed by experimental data, and the authors themselves recommend further investigation.) In order to mitigate the generation of pore pressure above the geotextile, a layer of geotextile with appropriate WEVs should be used. Decreasing the pore water pressure above the geotextile means that the geotextile can function as a transmission layer. Thus, if the geotextile is installed on a slope (to induce a gradient), it can transmit moisture laterally. Consequently, if a geotextile is located above a high capacity drainage layer, such as gravel or a geonet, the whole system can function as a moisture barrier that drains moisture laterally in unsaturated mode and prevents water from ponding above the geotextile. Previous studies on inclined moisture barriers are presented next.

Geocomposite Layers on Sloping Ground

Ross (1990) performed analytical analyses on inclined capillary barriers. He showed that a fine-grained soil overlying a coarse-grained soil can function as a capillary barrier under rainfall conditions. In order for a capillary barrier to be effective, the fine-grained layer must be drained; otherwise, water will accumulate above the interface and saturate the coarse layer when the water pressure reaches the WEV of the coarse layer. The simplest way to drain the fine layer is to incline the interface (i.e., the contact

surface) between the two layers. Ross (1990) indicates that the inclined capillary barriers are workable over an effective length. Beyond this length, however, the capillary barrier cannot divert any additional water, and the downward flux into the coarse and fine layers is superimposed on the lateral flux above the contact surface between the two layers. Ross shows that the effective length can be defined as:

$$L \ll \frac{K_s \tan\phi}{q\,\alpha} \tag{1}$$

where L is the effective length; K_s is the saturated hydraulic conductivity of the fine layer; ϕ is the angle of the contact between the layers; q is the infiltration rate; and α is a fitting parameter for the approximation of the hydraulic conductivity of the fine soil as a function of suction. Thus, the maximum diversion capacity of the inclined capillary barrier can be calculated as $Q_{max} < L*q$ (Ross 1990).

Morris and Stormont (1999) performed numerical analyses to investigate the effects of slope and material type on the performance of unsaturated drainage layers (UDLs) and on the lateral diversion capacity of fine-over-coarse moisture barriers. Gravity-driven lateral diversion in fine-over-coarse barriers (assuming the interface is sloped) occurs at the interface, where the hydraulic conductivity can be relatively high. In general, water will flow laterally through the coarse layer (as opposed to across the interface), if the suction head in the fine layer is less than the water entry suction head of the coarse layer. When a UDL is used between the fine and coarse layers, with a decreasing suction head in the overlying soil that is less than the WEV of the UDL, water can enter the UDL, and the UDL can then function as a drainage layer. However, if the suction head value in the UDL decreases to less than the WEV of the underlying coarse layer, water will enter that layer, and the moisture barrier will no longer work as a barrier because it will conduct water to the underlying layer. Therefore, for a moisture barrier to function properly, the suction head value in the overlying soil must be less than the WEV of the moisture barrier (coarse layer), and the suction head value in the moisture barrier must be greater than the WEV of the underlying layer.

Morris and Stormont (1999) used three types of sand as UDLs and evaluated the effect of each type on the lateral diversion of moisture. These sand types are: i) uniform sand, ii) concrete sand that has a less uniform grain size than the uniform sand, and iii) plain field sand. Morris and Stormont simulated a moisture barrier with and without a UDL over ten years using daily climate data obtained from three locations in the United States: San Francisco, CA, Chicago, IL, and Columbia, SC. They modeled three slopes of 5%, 10%, and 20% using the computer code TRACR3D described by Travis and Birdsell (1991). This finite difference code is capable of simulating 3-D saturated and unsaturated flow behavior in porous media. The results show that including a UDL at the interface of the moisture barrier and the soil significantly decreases water movement into the underlying soil. The UDL allows for more drainage

from the overlying soil and thus mitigates percolation during periods of high infiltration and low evapotranspiration. In addition, Morris and Stormont showed that the length of the diversion (i.e., the distance the water is diverted laterally with no downward flow through the coarse layer) is related directly to the slope of the fine-coarse interface. If the interface slope is doubled (i.e., the slope is made twice as steep in terms of angle/degree), the diversion length also doubles. Morris and Stormont developed the following relationship between lateral diversion length and the material in which the lateral diversion occurs:

$$L \leq \tan\phi \left[a^{-1}\left(\frac{K_s}{q} - 1\right) + \frac{K_s}{q}(h_a - h_w^*)\right] \quad (2)$$

where q = constant or steady-state infiltration rate; h^*_w = water entry head of the coarse layer; ϕ = inclination of the fine-coarse interface; h_a = air entry head of the UDL; K_s = saturated hydraulic conductivity of the UDL; and a = the constant called the *sorptive number*.

Iryo and Rowe (2005) investigated the behavior of initially unsaturated soil-geocomposite layers on slopes under infiltration and post-infiltration conditions using SEEP/W version 5. They modeled a soil layer 5 m long and 0.3 m deep overlying a 3 mm thick geotextile. The geocomposite consisted of a geonet with a nonwoven geotextile on top of it. The WEV for the geonet was assumed to equal zero, and three slopes of 2.5%, 5%, and 10% were modeled. Details of the modeling cases are shown in Table 2.

Table 2. Test program by Iryo and Rowe (2005).

	δ (%)	Q		
		100 mm/h ($2.78*10^{-5}$ m/s)	10 mm/h ($2.78*10^{-6}$ m/s)	1 mm/h ($2.78*10^{-7}$ m/s)
Sand $K_{sat} = 1.0*10^{-4}$ m/s	2.5 5	Case 1 Case 2	Case 4 Case 5 Case 11[(b)] Case 12[(b)]	Case 7 Case 8
Loam $K_{sat} = 1.0*10^{-6}$ m/s	10 5	Case 3	Case 6 Case 10[(a)] (h_p =0.01m)	Case 9

[(a)] Transient analysis was conducted for infiltration and post-infiltration periods.
[(b)] Entrapped air was assumed to occupy 20% of the void within the geotextile at suction = 0 kPa for Case 11, and 60% for Case 12.

Iryo and Rowe first performed a series of transient analysis on sand-geocomposite systems with various slopes and infiltration rates. In this series of analysis, the infiltration rate was lower than K_{sat_soil}. Second, they evaluated the effects of entrapped air in the geotextile during infiltration. Third, they performed transient analysis on a loam-geocomposite slope to investigate the conditions under which the infiltration

rate is higher than K_{sat_soil}. Lastly, they investigated the drainage behavior of the loam-geocomposite after Infiltration.

Results of the Iryo and Rowe (2005) study indicate that pore pressure and water content increase with the advance of the wetting front, but the soil remains unsaturated because $q < K_{sat\_soil}$. Flow in the geotextile occurs when the wetting front reaches the geotextile and the suction head at the interface of the geotextile and soil equals the water entry suction of the geotextile (-1 kPa in this case). At this point, the sand immediately above the geotextile is almost saturated. Water flow is halted at the interface of the geotextile and sand and is diverted downward. Once the flow in the geotextile starts, it increases until it reaches the geotextile flow capacity (at the lower end of the slope, where the bottom of the geotextile is open to atmospheric pressure), and then water starts to flow into the geonet. Over time, the saturation zone wherein the water flows into the geonet is shifted toward the upper part of the slope. The flow in the geonet increases until it reaches the steady state. This behavior is similar to that observed numerically by Morris and Stormont (1999) for UDLs constructed of sand. As mentioned earlier, in order for the geotextile to function as a drainage layer and the geocomposite to function as a barrier, the suction head value in the overlying soil must be less than the WEV of the geotextile, and the suction head value in the geotextile must be more than the WEV of the geonet. Iryo and Rowe (2005) showed that the geocomposite is more likely to work as a barrier for low infiltration rates and/or steep slopes. They concluded that when a geotextile is used above a geonet as a drainage layer, its capacity to transmit water must exceed the potential infiltration, as presented in the following relationship (Iryo and Rowe 2005):

$$T_{geotextile} > qL/\delta \tag{3}$$

where $T_{geotextile}$ is the capacity of the in-plane flow for the geotextile; q is the infiltration rate; L is the length of the soil-geocomposite system; and δ is the slope of the soil-geocomposite system.

Moisture Barriers and Upward Water Flow

As mentioned earlier, moisture barriers also serve to prevent or reduce upward moisture flow. This function is important in cold regions where soil water may freeze and cause frost heave. In general, three factors are required to cause frost heave: i) water within the freezing zone, ii) freezing temperatures, and iii) frost-susceptible soil (Henry and Holtz 2001). Thus, in order to prevent frost heave in soil, either the susceptible soil must be removed or the water flow into the susceptible soil must be stopped. Replacing the susceptible soil is costly. Thus, the more viable approach is to prevent the upward water flow. Taber (1929) found that placing a layer of coarse sand above the water level eliminates frost heave in frost-susceptible soil. Casagrande (1938) and Beskow (1946) reported the use of a layer of sand or gravel

above the water table to reduce frost heave in overlying fine-grained soil in road construction. Since then, other researchers have shown that placing a coarse-grained layer above the water table reduces frost heave in overlying fined-grained soil. This section presents factors that affect the function of moisture barriers for controlling upward flow.

The upward flow of water in soils above the groundwater table occurs in the capillary fringe zone due to surface tension forces. Capillary barriers can halt the upward water flow because of the differences in hydraulic conductivity between the underlying soil and the barrier material. Similar to the mechanics involved in downward flow control, if the moisture barrier prevents the upward flow of water, the water will accumulate at the soil-barrier interface. In this case, if a moisture barrier with a drainage layer is used, water can be diverted laterally. Thus, a geocomposite that consists of a geonet between two geotextile layers (e.g., a double-sided geocomposite) can divert upward flow laterally. As is the case for the upper geotextile layer, the drainage geotextile under the geonet can divert and drain water if the suction head value in the underlying soil is less than the WEV of the geotextile layer. However, other parameters can also control upward water flow. These parameters include the location of the water table, the location of the frost line, and the suction head in the overlying layers.

Henry (1988) showed that hydrophobic geotextiles are more effective in reducing frost heave than hydrophilic geotextiles. Henry (2000) also indicates that the intrusion of soil fines into a geotextile causes the geotextile to fail as a moisture barrier, whereas a geocomposite that consists of a geonet between two geotextiles can behave as a moisture barrier when the suction head value in the overlying soil is high (>1800 mm). Henry and Holtz (2001) performed tests on 150-mm tall geocomposite soil columns whereby water was at a constant head of 25 mm above the base of the column, and the geocomposite was located 5 mm above the water table. They concluded that if the moisture barrier is located above the water table, where the suction head in the soil is greater than the water entry suction of the moisture barrier, water will not enter the moisture barrier. Generally, if a geonet is used as part of the moisture barrier, it is likely to be effective at any distance above the water table due to its high transmissivity. However, this type of moisture barrier cannot reduce frost heave when the suction head value in the soil overlying the geonet is relatively low and the moisture barrier is initially moist. This condition can exist during precipitation, when downward flow can decrease the suction head in the overlying soil.

Hanging Column Testing: DMBLs

ASTM D 6836, *Standard Test Methods for Determination of the Soil Water Characteristic Curve for Desorption Using Hanging Column, Pressure Extractor, Chilled Mirror Hygrometer, or Centrifuge* (ASTM 2008), outlines an approach for measuring the moisture characteristics curves (MCCs) of porous

materials. Hanging column tests are used to characterize the sorption and desorption curves of materials at low values of suction (typically, up to about 150 cm of water). A hanging column test apparatus is presented in Figure 8 and its function is described in the experimental testing portion of this report.

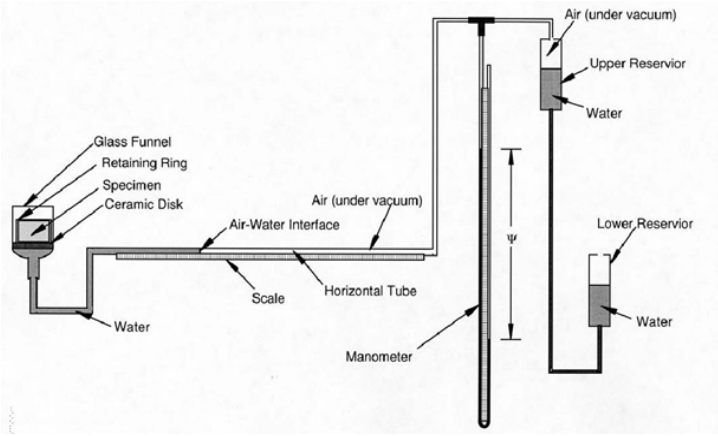

Figure 8. Schematic. Hanging column test apparatus (ASTM D 6836).

Ramos (2001) tested a range of materials for DMBL application. These tests were used to determine the MCCs of the materials. The testing program included capillary rise tests and hanging column tests. Sixteen geotextile materials were considered, including nonwoven polypropylene, nonwoven polyester, nonwoven nylon, and fiberglass products. The fiberglass products currently are used as industrial insulation in composite plastic reinforcement and in wick drains. Based on the results of the capillary rise tests, a smaller group of textiles was selected for further testing using the hanging column apparatus. The capillary rise tests were performed by hanging strips of geotextiles vertically and placing the lower end of the strips in a reservoir of water. The geotextile strips were covered in plastic wrap to prevent evaporation. The capillary rise was measured as the height of the wetting front on the strips. From the results of the capillary rise tests four materials were selected for further testing. These material designations are *Silica* and *TGLASS* (used as industrial insulation), *CSFM* (used for composite plastic reinforcement), and *Nylon* (a nonwoven nylon used for scouring pads). The silica product performed the best in the capillary rise tests, followed by CSFM, TGLASS, and nylon. However, the nylon product performed substantially better than the other nonwoven polypropylene geotextiles and, therefore, was selected for hanging column testing. The fiberglass products were selected based primarily on their high capillary rise when compared with that of the nonwoven polypropylene geotextiles.

The hanging column tests were used to measure the MCCs of the geotextiles. After analyzing the TGLASS product, it was determined that the unsaturated transmissivity of the material should be

evaluated. The TGLASS material has a mass per unit area of 2,370 g/m^2 with a thickness of 3.2 mm (Henry et al. 2002).

Stormont and Ramos (2004) and Stormont et al. (2001) described the test methods and apparatus used to determine the transmissivity, or unsaturated in-plane flow characteristics. Their results indicate that a TGLASS layer becomes transmissive at a suction head of 100 mm. Using a siphon test, TGLASS first becomes transmissive at a suction of 340 mm. Ramos attributes the difference in these values to the type of test apparatus and the time length of the test. When compared to the transmissivity of a geotextile, the TGLASS material becomes transmissive at higher suction head values and lower water contents.

NCHRP-IDEA Project 68

The laboratory proof-of-concept project for DMBLs was funded by an Innovations Deserving Exploratory Analysis (IDEA) grant and undertaken by Henry and Stormont (2002). Figure 9 shows the device used to measure the outflow from a laboratory-scale DMBL system (Stormont et al. 2001).

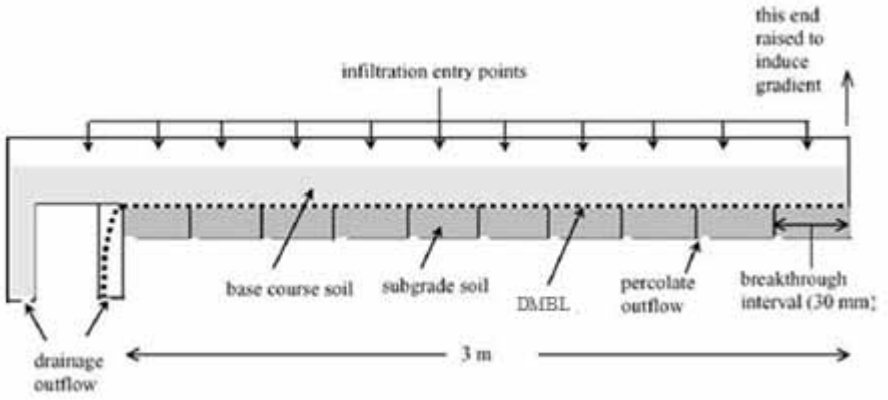

Figure 9. Schematic. DMBL lab configuration 1 (after Stormont et al. 2001).

The system simulates a base course material over a DMBL. Separate outflow volumes are recorded for the two layers. To create a gradient, one end of the box is elevated relative to the other. The DMBL used in this test consists of a TGLASS layer over a high-density polyethylene geonet (to serve as the capillary break). A layer of TGLASS is placed on top of the subgrade, and the geonet/TGLASS composite layer is then placed on top of the first layer of TGLASS. Figure 10 presents a graph taken from test results that are based on the configuration presented in Figure 9. As can be seen in Figure 10, a significant amount of water is drained by the transmission layer. The water collected from the soil is from the soil layer overlaying the transport layer (not the subgrade soil). The transport layer drained approximately 4,000 cc of water, whereas 500 cc of water was drained from the soil layer above it. This amount of drainage demonstrates the ability of the DMBL to drain water from unsaturated soils subject to infiltration.

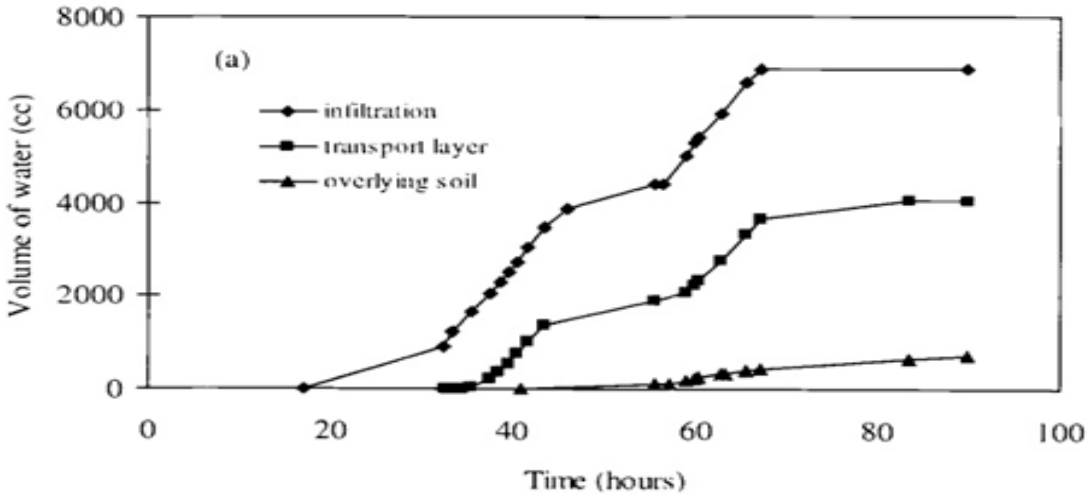

Figure 10. Graph. DMBL drainage data (Stormont and Stockton (2000)).

Figure 11 presents a laboratory set-up with a simulated road section that is 1.3 m (into the page) in length. A crack in the pavement surface is included to simulate the potential infiltration of surface runoff. Each of the laboratory set-ups employs tensiometers to measure the suction in the soil at various depths.

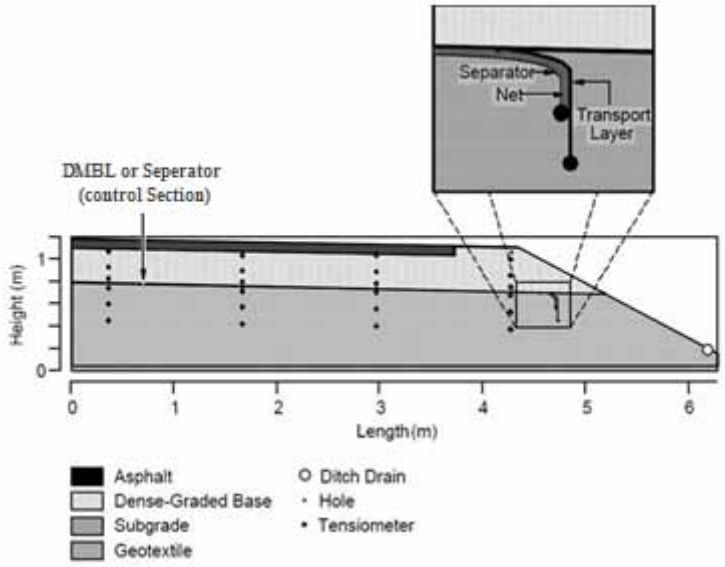

Figure 11. Schematic. DMBL lab testing configuration 2 (after Henry et al. 2002).

Stormont and Ramos (2004) performed tests using the test set-up shown in Figure 11. They did not observe any breakthrough of water through the DMBL into the subgrade material. However, a separate testing program that used an earlier device (Stormont and Stockton 2001) did show breakthrough into the subgrade material at an infiltration rate of 4.7×10^{-7} m/s with a slope of 2.5 percent. Water was added at a

flux rate of 10^{-7} m/s for a period of 88 hours. During constant rate infiltration, the suction in the soil above the DMBL dropped rapidly. As infiltration continued, the TGLASS layer drained at an average suction of 70 mm. A peak suction of 260 mm was observed. Saturation of the base course material did not occur during this test. The second portion of the test involved terminating the constant rate infiltration and measuring the outflow and water content. A flow volume equivalent to 12.6 mm of simulated rainfall, of which 11.3 mm was from the TGLASS layer, was drained during this period. The test was run for 14 hours at which point the TGLASS layer was still draining at suctions of 600 mm.

Henry et al. (2002) demonstrated the use of DMBLs at laboratory scale also using the test set-up displayed in Figure 11. A drainage pipe was connected to the DMBL by wrapping the TGLASS transport layer around a perforated high-density polyethylene pipe. Nine tests were performed using control sections and DMBL sections and assuming infiltration from ten-year and one-hour design storms. The results indicate that the DMBL drains when a suction of 100 mm or higher is applied. During testing a breakthrough to the subgrade material was observed. However, in subsequent tests the DMBL was observed to recover from the breakthrough and protect the subgrade. Figure 12 presents test data from the DMBL lab configuration shown in Figure 11 from Henry et al. (2002). The graph represents the soil suctions as measured by tensiometers. A zero value on the vertical axis indicates saturated conditions in the soil, positive values indicate partially saturated soils, and negative values indicate positive pore water pressures. The tensiometer data presented in Figure 12 were obtained from tensiometers located 25 mm below the DMBL shown in Figure 11.

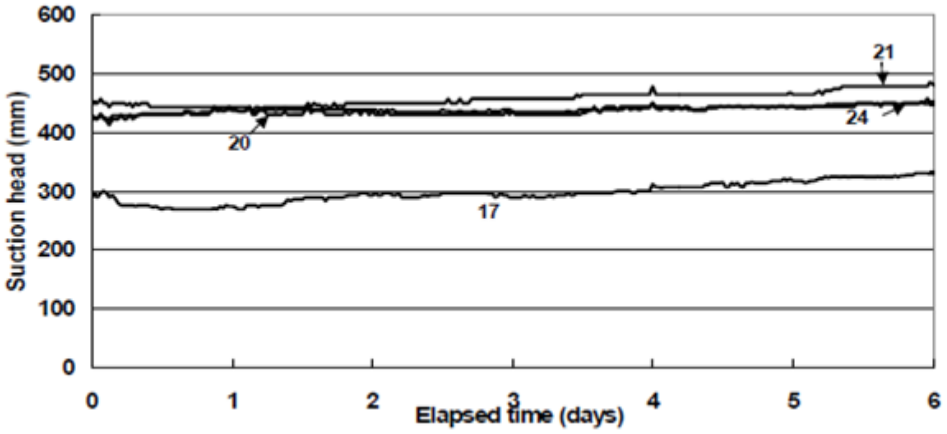

Figure 12. Graph. Measured suction head in subgrade layer (Henry et al. 2002).

The tensiometer measurements indicate that the water content of the soil in the subgrade remains constant during an infiltration event. Several similar tests were run, and the same performance was observed. An increase in the water content of the subgrade soil is represented by a rapid decrease in the suction head

values. Therefore, here the constant values of soil suction indicate that the DMBL protects the subgrade from infiltrating water.

Field Testing: Vermont Muddy Roads/Cold Regions Research and Engineering Laboratory (CRREL)

The purpose of the Vermont Muddy Roads/CRREL field project was to investigate potential road improvement methods for unsurfaced rural roads. Both gravel and plain subgrade roads were considered, and six testing scenarios were implemented. However, the specific test set-up of interest to the current work is the one that employs a DMBL, as shown in Figure 13.

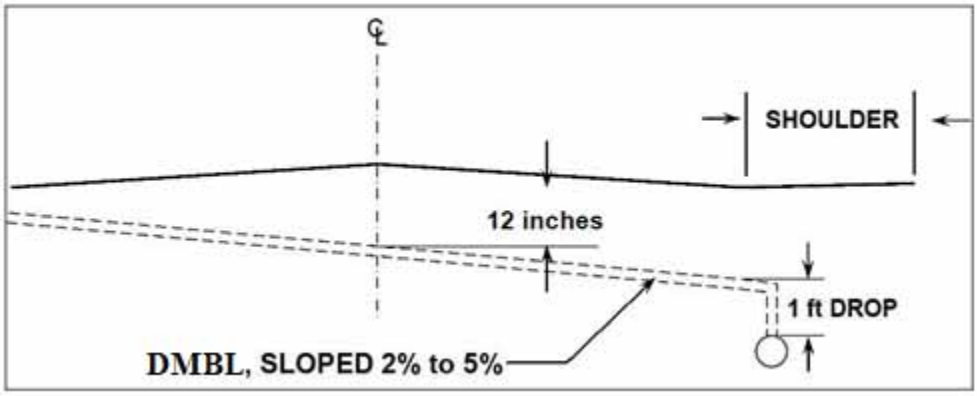

Figure 13. Schematic. Vermont Muddy Roads/CRREL Project: DMBL configuration (after Henry et al. 2005).

The transport layer used in this DMBL configuration is the TGLASS material discussed previously. The edge connection to the drain pipe does not wrap around the pipe but instead is placed into a slot on the pipe. The roadway sections were instrumented with thermocouples for temperature measurement in order to determine the performance of the road under freeze-thaw conditions. Difficulties in data acquisition made accurate measurements impossible. However, in terms of rut formation, the DMBL roadway sections performed better than the other test sections.

Field Testing: CRREL/Maine DOT

A full-scale road test was implemented in the CRREL/Maine DOT project using a DMBL product termed Tendrain 102™. The Tendrain 102™ consists of a geonet core sandwiched between two geotextile drainage layers. Figure 14 presents a schematic of the test set-up. The structure of the Tendrain 102™ DMBL and the connection to a drainage pipe are also shown. The DMBL shown is wrapped around a perforated drainage pipe.

A tipping bucket device (a bucket with a calibrated volume) was used to measure outflow. The bucket has a divider to allow two equal volumes of water and is on a hinge. Water flows into one side of the bucket. Once the appropriate volume of water is collected, the bucket tips, spilling out the water. The number of tips is recorded to determine the outflow. Tensiometers were installed to measure the soil suction. Time domain reflectometry (TDR) probes were used to measure the water content of the roadway sections. Frost heave surveys also were conducted to measure the amount of heave that the roadway test sections experienced. Falling weight deflectometers (FWDs) were used also to measure the roadway stiffness.

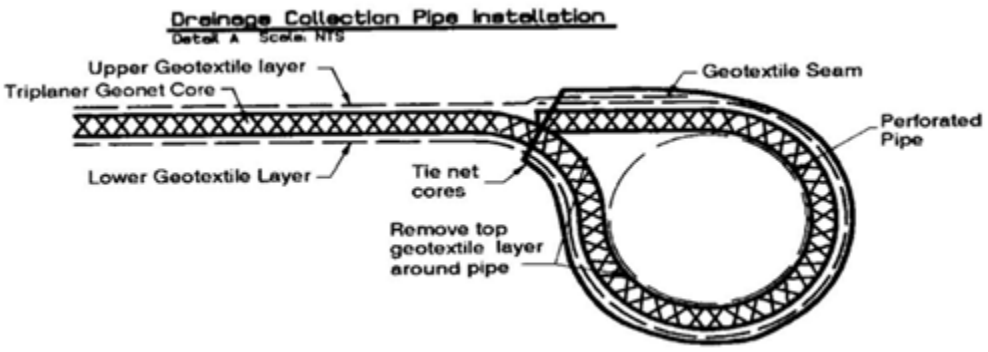

Figure 14. Schematic. Maine DOT DMBL test layout (Christopher et al. 2000).

Figure 15 displays the different test sections used in the testing program. A control section and three configurations were used. Section D-1 presents a configuration in which the DMBL (referred to as *drainage geocomposite* in the figure) is placed a certain depth into the subgrade. Such a configuration may be used to protect a frost-susceptible subgrade from a rising water table.

Section D-2 places the DMBL at the interface between the subgrade and the base course material. Section D-3 shows a section in which a DMBL is placed at the subgrade-base course interface and the asphalt base course interface.

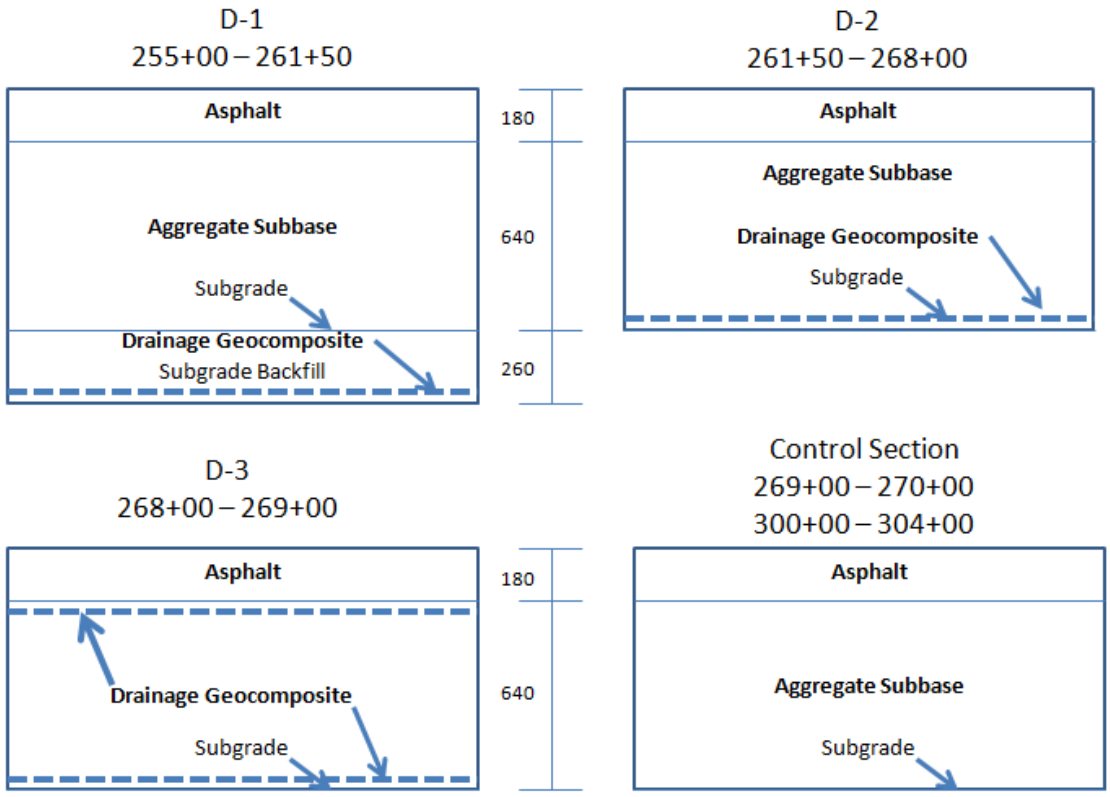

Figure 15. Schematic. Maine DOT DMBL test configurations (Christopher et al. 2000).

After the two-year testing period, the 3.0 km roadway displayed very little evidence of frost heave damage or rutting (Christopher et al. 2000). Averaged tensiometer readings were reported for the fall of 1997 and summer of 1998. Measurements during the spring thaw period were unavailable due to technical problems with the tensiometers. The reported heads for all three sections containing DMBL systems were negative. The control section reported positive piezometric heads averaged over the same period.

The tipping bucket data were considered to be very conservative. The maximum flow capacity was reached in the roadway sections. The tipping bucket devices were capable of measuring flows of only 7 l/min. Also, the tipping bucket devices were not adequate for measuring flow rates less than 0.25 l/min. FWD data indicated an increase in stiffness in all of the roadway sections at the end of the testing period.

Field Testing: MnROAD/MnDOT (NCHRP No. 113)

At the Minnesota Department of Transportation's (MnDOT's) testing facility, a full-scale test of a DMBL was demonstrated under NCHRP Contract No. 113. Laboratory testing of the materials and the development of an edge drain collection system were completed in addition to full-scale field testing. Details concerning the roadway construction and laboratory testing are documented in Stormont et al.

(2008). The DMBL tested at the MnROAD site used a fiberglass transport layer characterized by Stormont and Ramos (2004). Full-scale test sections were constructed during the summer of 2006. Testing was conducted for a section containing a DMBL system and one control section (without a DMBL). Figure 16 shows a cross-section of the full-scale profile (Stormont et al. 2009).

Figure 16. Schematic. MnROAD test section (Stormont et al. 2009).

Sensors were placed at depths of 6, 10, 13, and 24 inches, as indicated in Figure 16. The roadway test sections were instrumented to measure temperature, water content, suction, and drainage volume. Tipping bucket mechanisms were implemented to measure outflow. TDR probes were used to measure the water content of the base course and subgrade material. Other methods of measuring the water content were not considered due to complications with the data acquisition system. Volume outflow measurements from the tipping buckets were not considered in the analysis because of calibration issues. The measurements of the outflow from the DMBL were further complicated by evaporation during the summer months. The nominal amount of water collected during the summer months is evidence of this problem. As noted by Stormont et al. (2009) , the tipping bucket data do not necessarily reflect the drainage from the DMBL because roadway runoff may have infiltrated the collection system. FWD measurements also were taken to determine any effects the DMBL may have had on the subgrade.

The data collected demonstrate that a DMBL system is able to reduce the steady-state water content in the sub-base layer and consequently improve the modulus of the roadway section. The development of positive pore water pressures was minimized in the sub-base material, and wetting of the subgrade due to infiltration was prevented. The prevention of the capillary rise of the groundwater also was observed. Little effect on the water content of the subgrade material was observed in the roadway test sections. A method for connecting a DMBL to a conventional edge drain system also was demonstrated. For future

development of DMBL technology, Stormont et al. (2009) recommend the development of a less expensive geotextile transport layer.

Summary

In summary, a geocomposite moisture barrier can function as a barrier if the drainage geotextile layers above and below the geonet can laterally transmit moisture under unsaturated conditions and prevent water from percolating into the geonet. In order for the geotextile layer to drain water, it should be installed as inclined (on a slope), and the suction head value in the overlying and underlying soil must be lower than the WEV of the geotextile. The suction head value in the geotextile must be higher than the WEV of the geonet. To achieve this goal, the slope angle of the geocomposite may be increased. Alternatively, or along with a sloped installation, a geotextile with saturated hydraulic conductivity that is greater than the saturated hydraulic conductivity of the soil can be used. In this case, there will be a suction head in the geotextile that has a higher value than that of the WEV of the geonet, thereby preventing water from infiltrating the geonet.

Other important factors to consider are the effects of heat flux and temperature gradient on moisture movement and moisture barrier functionality. Henry (2001) notes that net heat flux and temperature gradients in freezing soils are important variables for controlling frost heave and determining the effectiveness of a moisture barrier. For example, if the heat loss in soil occurs at a high rate, causing rapid frost penetration, a capillary moisture barrier will not be helpful (Henry and Holtz 2001).

(blank page)

CHAPTER 4 – NUMERICAL MODELING: SOFTWARE CONSIDERATIONS

Overview

A number of software packages are available for the simulation of moisture movement, heat flow, and/or stress and deformation in partially saturated porous media. However, combining these phenomena for simulation and analysis is particularly burdensome and generally can be accomplished by only the most advanced software packages. Thus, simulations of this nature are expensive, not only from the standpoint of the number of processor cycles to be conducted, but from a software sophistication standpoint as well. Prior to beginning a comprehensive modeling program, it is necessary to evaluate the software currently available for these types of simulations. In this section, some of the computer programs used in previous work on moisture barriers are presented.

UNSAT-H

UNSAT-H is a finite difference program for simulating air/water/heat flow in one dimension. This program can address soil water infiltration, redistribution, evaporation, plant transpiration, deep drainage, and soil heat flow as 1-D processes. The UNSAT-H program simulates water flow using Richard's equation, water vapor diffusion using Fick's law, and heat flow using the Fourier equation. UNSAT-H has been shown (e.g., by Khire et al. 1997, Khire et al. 1999, and Khire et al. 2000) to simulate conditions measured in the field reasonably well. However, it cannot model the freeze/thaw process.

SHAW Model

SHAW is an implicit finite difference, vertical, 1-D model developed by Flerchinger and Saxton (1989). This program can simultaneously model heat, water, and water vapor. Furthermore, it can be used to model freeze/thaw and transpiration processes. This program also can be used to model climate conditions, such as rainfall, snow, runoff, transpiration, etc., although it was developed primarily to simulate snowmelt. The drawback of this program is that it is a 1-D model. Thus, it cannot be used to simulate and investigate lateral diversion caused by moisture barriers.

TOUGH2

TOUGH2 is a finite difference program that can model heat and multicomponent fluid in 2-D or 3-D. This program is used mainly for geotechnical reservoir engineering, nuclear waste isolation studies, environmental applications, and flow in saturated media and aquifers. In general, TOUGH2 can simulate coupled water, vapor and heat flow in soil. The drawbacks of the program are that it cannot simulate freezing and thawing in soil and it does not have provisions to input climate conditions of the soil surface.

HYDRUS 1-D, 2-D, and 3-D

HYDRUS is a finite element model that can simulate water, vapor, and heat flow in saturated and unsaturated soil in 1-D, 2-D, and 3-D. In addition, this program can simulate evaporation and evapotranspiration and hysteresis in MCCs.

SoilVision SVOffice 2009

SVOffice 2009 is a commercially available finite element 2-D and 3-D numerical model that offers the following features:

i. coupling of air/water/thermal flow,
ii. freeze and thaw modeling in soil,
iii. boundary conditions that can be a function of time, space, or any other model variable, and
iv. simulation of precipitation, evapotranspiration, and transpiration processes. The input data can be a constant, expression, or data sheet.

This program also has the features of HYDRUS 2-D. In addition, SVOffice allows for coupled seepage and stress analyses and consolidation due to drainage of the soil.

SIGMA/W and SEEP/W 2007

Both SIGMA/W and SEEP/W 2007 are two of the modules of the GEOSLOPE package. SIGMA/W is a finite element model that is capable of stress deformation and seepage analyses. It is also capable of performing seepage-stress coupled analyses, but with the limitation that the soil strength parameters are not a function of matric suction. However, a user-defined constitutive model can be developed to consider this effect. This software allows the study of unsaturated water flow and soil deformation due to seepage forces and applied stress. SEEP/W is only focused on the saturated/unsaturated seepage attributes of the domain and is therefore simpler to use when the deformation aspects are not evaluated.

Summary

The computer program UNSAT-H is selected for this research effort to study the effects of heat flow on matric suction and moisture distribution throughout a soil-geotextile column. The computer programs SIGMA/W and SEEP/W are used herein to investigate the effects of unsaturated water flow with and without DMBLs and the significance of changes in moisture distribution on rutting under loading. These software packages are verified in the literature and are commercially available. They are selected for this project because they provide the means of addressing the study scope and are readily available without additional costs incurred by the study institution.

CHAPTER 5 – EXPERIMENTAL PROGRAM

The experimental program of this research project focuses on defining the water characteristics relationship (also known as the water retention relationship) of the soil and geosynthetic materials and focuses also on the large-scale performance of a drainage moisture barrier in a simulated road section. A fiberglass geosynthetic material was selected as the transmission layer of the barrier, as recommended by Stormont et al. (2009). The suction-moisture relationships of the geotextile were measured and compared to the data reported in the literature. These data also were needed for modeling the transient water flow through the DMBL under unsaturated conditions. Large-scale testing was conducted to investigate the behavior of a simulated roadway section with a moisture barrier under the conditions of rainfall events and loading (an aspect of research that the authors were not able to find reported in the literature). The DMBL system was tested for its ability to control infiltrating water and prevent it from entering the subgrade and to prevent the corresponding section from rutting under static and cyclic loading. Due to budget constraints, the large-scale experimental program was limited to two tests.

Testing Materials

The experimental program used subgrade soil provided by the North Carolina Department of Transportation (NCDOT) and retrieved from an area located north of Greenville, NC. The ABC materials used in testing were obtained from a quarry in Raleigh, NC. The geosynthetic materials that comprised the DMBL system were as specified by Stormont et al. (2009) and were selected based on extensive testing of various products in the market.

Coastal Plain Subgrade

The subgrade used in the test pit is referred to as the *coastal plain* subgrade. Geologically, the site is located within the so-called *coastal plain physiographic province*. The topography of the area is nearly flat to gently sloping and generally exhibits poor surface drainage. Surficial soils in this area generally are derived from alluvial deposition and the weathering of existing formational material. These surface units are above the Pliocene marine deposits of the Yorktown Formation.

Table 3 - Index properties of coastal plain subgrade (Borden 2010).

Soil sample	LL	PL	PI	G_s	Maximum dry unit weight, γ_{dmax} (pcf)	Optimal moisture content (%)	Classification	
							USCS	AASHTO
Coastal plain soil	29	18	11	2.66	120.2	13	CL	A-6(3)

The coastal plain subgrade was used in prior testing at North Carolina State University (NCSU) by Borden et al. (2010). Table 3 shows the physical properties of the test soil. Standard Proctor compaction testing was performed to determine the properties of the coastal plain subgrade. As shown in Figure 17, the maximum dry unit weight of the test soil is approximately 120 pcf at an optimal moisture content of approximately 13 percent. The grain size distribution of the material is shown in Figure 18 and shows approximately 28% fines, the majority of which are clay-size particles (less than 2 micron). The soil is classified as CL according to the unified soil classification system (USCS) and A-6 according to the American Association of State Highway and Transportation Officials ***(***AASHTO***)***.

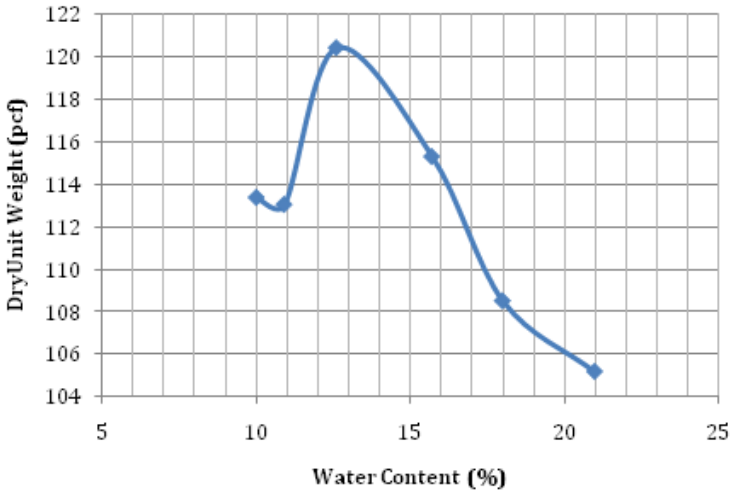

Figure 17. Graph. Compaction curve: coastal plain subgrade.

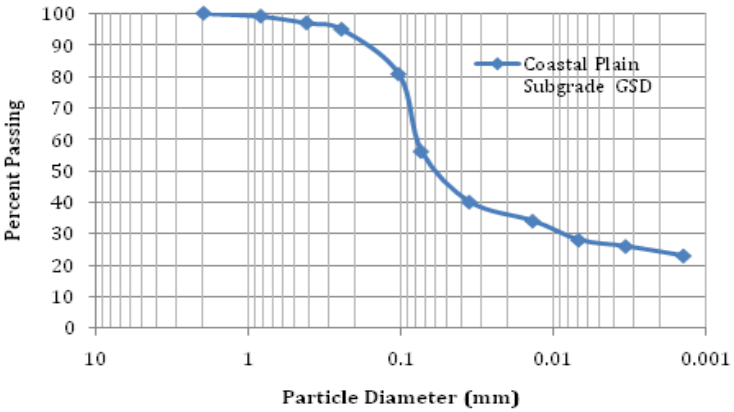

Figure 18. Graph. Grain size distribution: coastal plain subgrade.

Aggregate Base Course (ABC)

Figure 19 shows the grain size distribution of the ABC. The ABC material has a maximum dry unit weight of 138.5 pcf at the optimal moisture content of 5.8 percent. A washed sieve, in accordance with ASTM D6913 *Standard Test Methods for Particle-Size Distribution (Gradation) of Soils Using Sieve Analysis*, was used to obtain the grain size distribution of the ABC. Also plotted in Figure 19 are the upper and lower bound gradations recommended by the NCDOT. The ABC is classified as GW-GM, according to USCS and A-1 according to AASHTO.

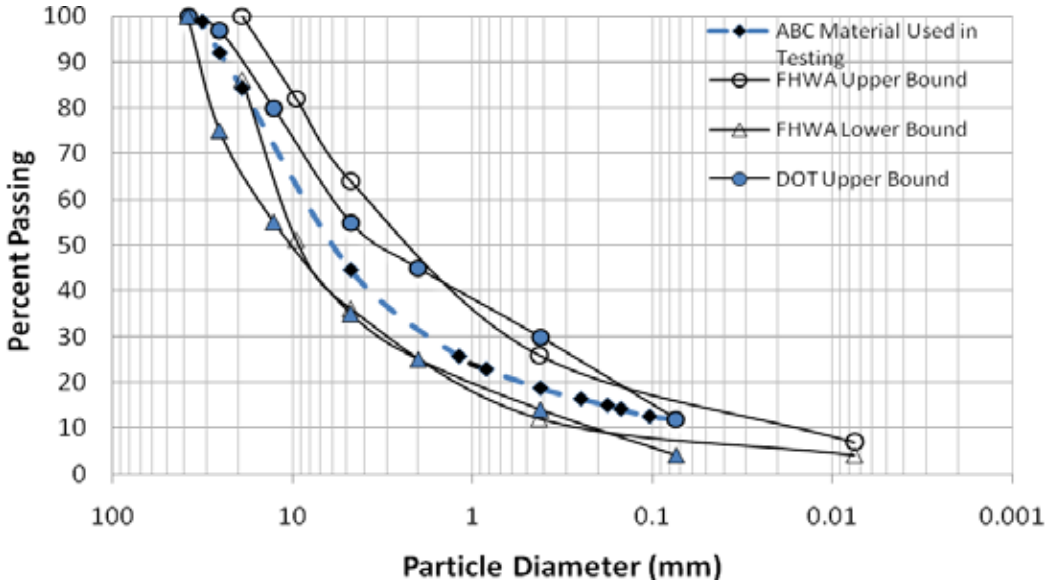

Figure 19. Graph. Grain size distribution: ABC with gradation bounds established by the North Carolina Department of Transportation.

Geosynthetic Materials

Two geosynthetic products were used in the construction of the DMBL section. The geocomposite material consisted of a geonet with nonwoven polypropylene textiles bonded with adhesive to either side of the geocomposite. A photograph of the geocomposite drain is presented in Figure 20.

Figure 20. Photograph. Geocomposite sheet drain.

A fiberglass textile was used as the transmission layer above the sheet drain. The fiberglass material is pictured in Figure 21. In comparison to traditional polypropylene and polyester types of fiberglass that are hydrophobic (i.e., have a high contact angle), the fiberglass material used here is hydrophilic (i.e., has a low contact angle), which aids in spreading and transmitting water. The fiberglass textile has a woven structure with a thickness of 0.126 in. (3.2 mm). Its mass per unit area is 0.471 psf (2.3 kg/m^2), according to manufacturer specifications.

Figure 21. Photograph. Fiberglass textile.

Hanging Column Tests

The hanging column test set-ups were built according to Stormont et al. (1997). The maximum pore size of the ceramic disc, according to manufacturer specifications, is 4 to 5.5 micrometers, with an approximate AEV of 561 psf (27 kPa). Without the ceramic disc, water would simply flow freely from the upper reservoir to the lower reservoir. A hanging column set-up is pictured in Figure 22.

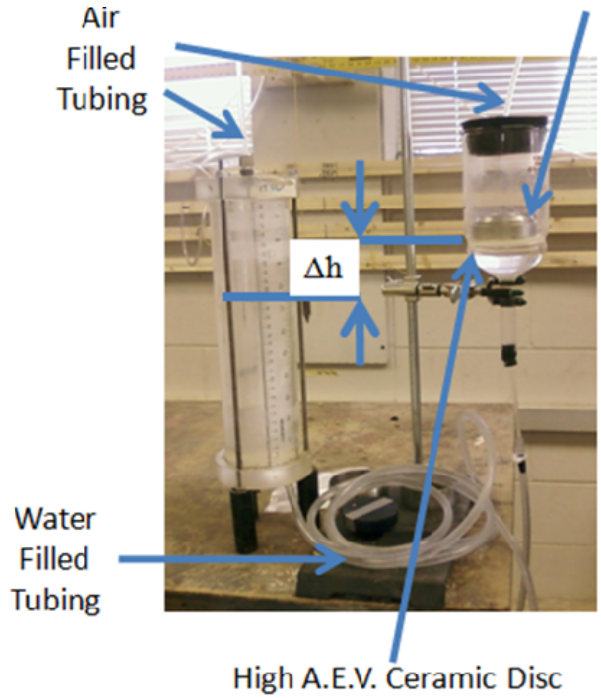

Figure 22. Photograph. Hanging column test set-up.

In this set-up, suction is applied by gravity. A contiguous line of water is established between the water reservoir and the bottom of the ceramic disc. Suction is applied by raising the elevation of the Büchner funnel. As the elevation of the Büchner funnel is decreased or increased, water is allowed to flow out of or into the specimen, respectively. The suction (Δh) is measured as the difference in elevation between the water level in the reservoir and the specimen on top of the ceramic disc in the Büchner funnel.

A digital manometer was used to measure the suction levels. The manometer is capable of measuring levels up to 5 psi at an accuracy of plus or minus 0.3 percent. The manometer was attached as an inline device. The manometer connection was made on the reservoir side of the outflow tubes using a 'T' connector with barbed ends. Hose clamps were placed on the 'T' connections. All connections were covered with a small amount of vacuum grease to maintain a vacuum in the system. A drawback of this system, however, is the need to remove and weigh the specimens in order to determine the water content. All reasonable efforts were made to prevent moisture loss from the specimen and system during geotextile extraction and weighing.

Suction Measurements Using a Dewpoint PotentiaMeter

Measurements taken for the hanging column set-up were supplemented using a WP4-T Dewpoint PotentiaMeter, manufactured by Decagon Devices, Inc. The hanging column test set-up was used to measure the water content at low suctions up to 6.56 ft (2 m) of water, whereas the WP4-T was used to measure high suction values on the order of ksf (MPa) that correspond to low water contents. A photograph of the WP4-T Dewpoint Potentiameter is presented in Figure 23.

Figure 23. Photograph. WP4-T Dewpoint Potentiameter.

The sample preparation for testing in the WP4-T Dewpoint Potentiameter began with an initially dry batch of soil, and water was added gradually. Each time water was added to the batch, a sample was taken. These samples were then placed in the potentiameter and readings of suction were recorded. To determine the water content, the entire sample was oven-dried for 24 hours, and the gravimetric water content was determined.

Hanging Column Sample Preparation

Both geotextile and soil samples were tested in the hanging column apparatus. Figure 24 pictures the type of ring used to confine the samples during testing. To prepare a geotextile sample, a confinement ring with a cloth screen was placed on the textile surface. An outline of the ring was marked on the textile. The circular sample was then cut using a razorblade. Care was taken to create a uniform textile sample that completely filled the ring for testing.

Figure 24. Photograph. Hanging column testing sample containment ring.

To prepare soil samples for the hanging column test, the confinement ring was compacted in a Proctor mold, without the cheesecloth that is visible in Figure 24. One lift of soil was placed in the mold and compacted. The beveled edge of the ring was then pressed lightly into the compacted lift. Next, another lift was compacted on top of the ring, and then a third lift was compacted. Each of the lifts was compacted with 25 blows from a standard Proctor hammer. After compaction was complete, the sample was extruded from the mold and trimmed with a wire saw. Once the sample was completely trimmed and the top and bottom surfaces smoothed, cheesecloth was placed around the bottom of the sample to prevent the migration of fines out of the sample during testing.

Geotextile Suction-Moisture Relationship

The TGLASS wetting and drying MCCs are presented in Figure 25 using gravimetric water content data. Table 4 and Table 5 present best fit parameters for the Van Genuchten-Mualem constitutive relationship (Van Genuchten 1980). The α value of the wetting curve for Test 1 is significantly different from the values measured in Tests 2 through 5. The same sample was used for Tests 1 and 3, but the overburden stress applied was not the same. Test 1 had an overburden stress of 0.16 psi, and Test 2 had an overburden stress of 0.49 psi.

Table 4. Van Genuchten wetting TGLASS fitting parameters: gravimetric water content.

Test	α (1/psi)	n
1	226.21	1.338
2	29.57	1.495
3	20.74	1.576
4	17.53	1.625
5	39.06	1.467

Table 5. Van Genuchten drying TGLASS fitting parameters: gravimetric water content.

Test	α (1/psi)	n
1	19.28	1.508
2	8.72	1.494
3	6.97	1.573
4	9.24	1.497
5	10.49	1.504

With an increase in overburden stress, the pore structure was altered, and better hydraulic contact was imposed between the sample and the ceramic disc. In this case, the high overburden stress led to small pore sizes and high AEVs that correspond to the decrease in the α value.

Different samples were used for Tests 2, 4, and 5. During these tests, overburden stresses of 0.49, 0.67, and 0.49 psi, respectively, were applied. Figure 25 and Figure 26 present plots that combine all five of the wetting curves (Figure 25) and drying curves (Figure 26). The data show the variations in gravimetric water content at saturation. The data obtained for Test 1 are not in concert with the results for the other four tests, most likely due to the relatively applied confining stress and imperfect contact with the ceramic disc. The AEV of the TGLASS is on the order of 0.01 psi with the water entry head being approximately half that value. The variation in the gravimetric water content occurs over a relatively narrow range of suction, similar to that of coarse-grained material. The differences in the shape of the wetting and drying curves can be attributed to hysteresis, as presented by Kool and Parker (1987), as the wetting and drying processes occur differently in relation to pore size and air entrapment.

For the purpose of comparison with previous test results by Stormont and Ramos (2004), the gravimetric water content plots are converted into saturation plots. The saturation of the sample is defined as the ratio of the volume of water in the sample at a given value of suction to the volume of water in the sample at saturation or zero suction.

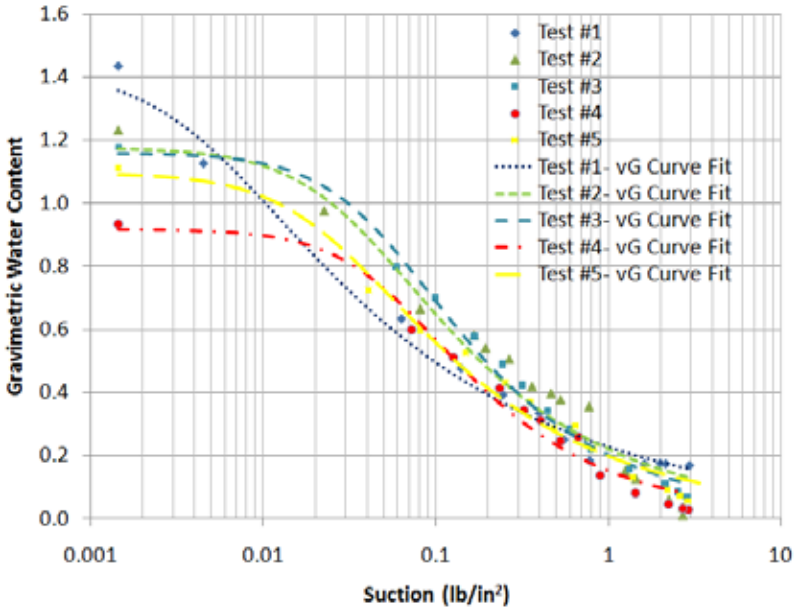

Figure 25. Graph. TGLASS wetting curves.

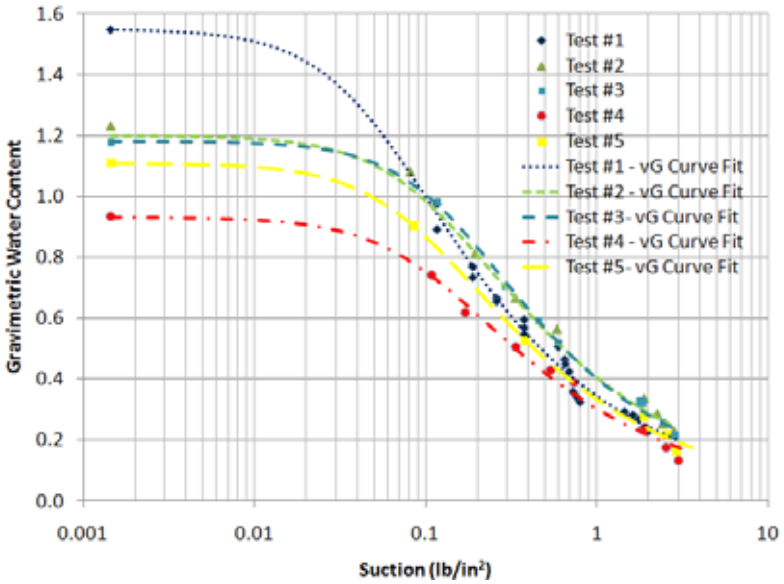

Figure 26. Graph. TGLASS drying curves.

Table 7 and Table 7 show the fitting parameters in relationship to the measured data according to the Van Genuchten (1980) approach. In addition, data obtained by Stormont and Ramos (2004) are included for comparison. The wetting curve parameters for TGLASS Tests 3 and 4, conducted under applied vertical stress values of 0.49 and 0.67 psi, respectively, display the closest agreement to the data presented by Stormont and Ramos (2004). The same agreement is not seen in the drying curve parameters.

Table 6. Van Genuchten wetting TGLASS fitting parameters obtained from saturation data.

Test	α (1/psi)	N
Stormont and Ramos 2004	17.79	1.68
1	305.86	1.333
2	24.90	1.538
3	20.21	1.589
4	17.52	1.625
5	39.17	1.466

Table 7. Van Genuchten drying TGLASS fitting parameters obtained from saturation data.

Test	α (1/psi)	N
Stormont and Ramos 2004	14.83	1.39
1	19.10	1.511
2	8.69	1.495
3	7.10	1.553
4	9.24	1.497
5	10.55	1.504

Figure 27 shows the wetting curves compared to those measured by Stormont et al. (2001). Good agreement is seen between the data measured in this study and the results reported by Stormont et al. (2001). Test 1 is an outlier in the dataset of wetting curves; a possible reason for the slight variation is the application of varying overburden stresses. Stormont and Ramos (2004) report that an overburden of 0.13 psi was applied when measuring the points on the characteristic curves of the TGLASS material in their study.

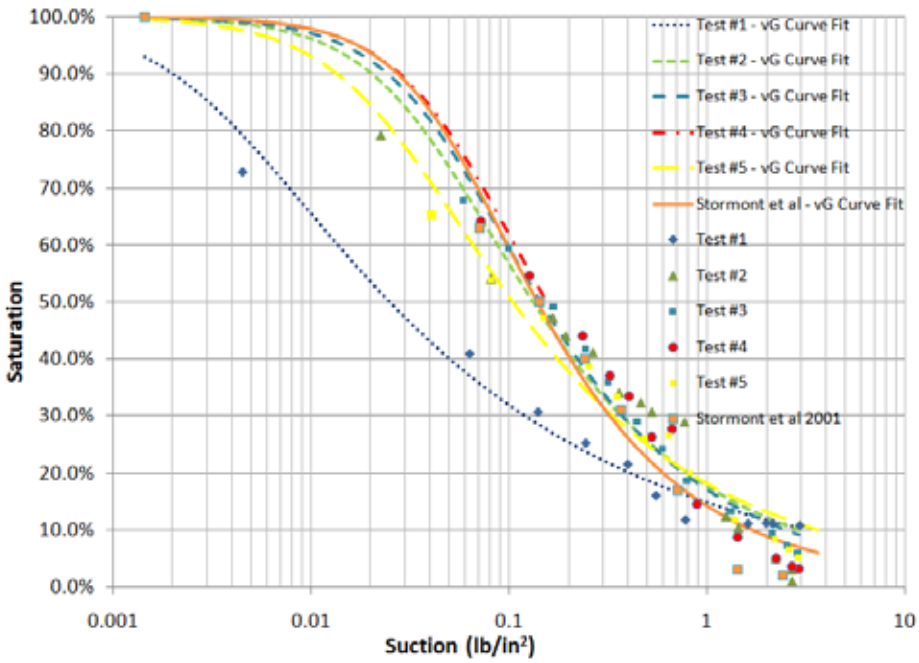

Figure 27. Graph. TGLASS wetting curves compared to Stormont and Ramos (2004) data.

Figure 28 shows the wetting curves plotted against the wetting curves from the Stormont and Ramos study (2004). The wetting curve data obtained from Tests 2, 3, 4, and 5 indicate slightly higher AEVs than the curve data obtained by Stormont and Ramos (2004).

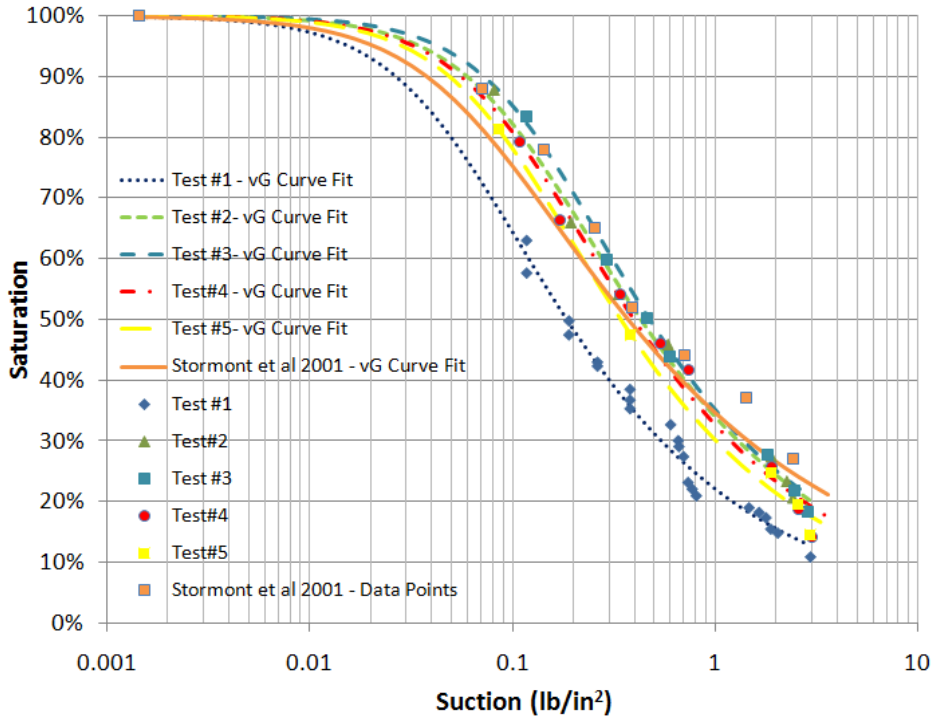

Figure 28. Graph. TGLASS drying curves compared to Stormont and Ramos (2004) data.

Soil-Water Characteristic Relationship: Coastal Plain Subgrade

Samples for testing the coastal plain subgrade were prepared as previously described, and the drying water retention curves of several specimens were determined. The first sample prepared was tested three times on its drying curve were collected. A second sample was also prepared, and data points on its drying curve were measured. Table 8 shows the Van Genuchten (1980) curve fitting parameters for the measured data.

Table 8. Van Genuchten curve fitting parameters for measured coastal plain subgrade data.

Test	Sample	Wetting/Drying	α (1/psi)	n	e
1	1	D	0.23	1.285	0.58
2	1	D	6.32	1.362	0.55
3	1	D	4.23	1.375	0.50
4	2	D	1.61	1.219	0.64
5	1	D	5.91	1.357	0.50

Figure 29 shows the measured drying data and curve fitting for the coastal plain subgrade material. In this case, the variation in gravimetric moisture content occurs over a wide range of suction values, which is typical of fine-grained soils. The AEV is on the order of 1 psi, which is two orders of magnitude higher than the value estimated for the TGLASS material.

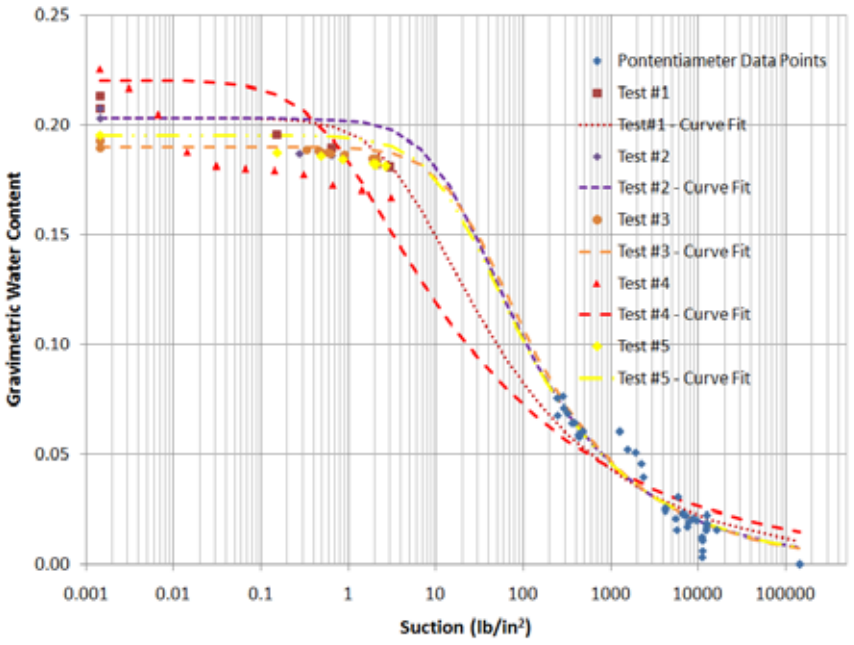

Figure 29. Graph. Drying curves for coastal plain subgrade.

The data obtained from Sample 2 (Test 4) departs from the data measured for Sample 1 due to the difference in void ratios of the samples. The data presented in Figure 30 show such a variation, with data for Sample 4 showing the highest void ratio of 0.64.

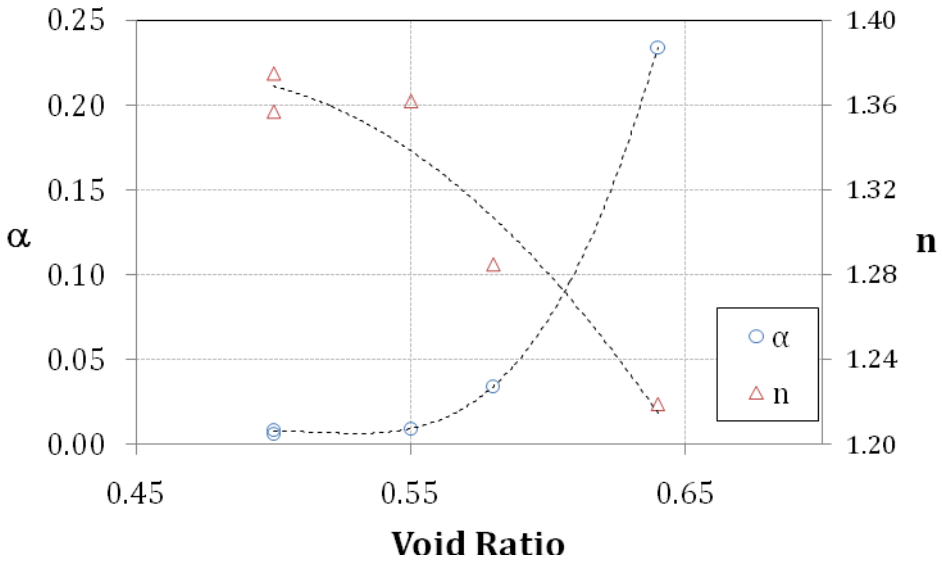

Figure 30. Graph. Variation of α and n as a function of void ratio.

Soil-Water Characteristic Relationship: ABC

To determine the characteristics curves of the ABC material, five tests were conducted. Figure 31 shows the drying curves of the ABC material. The first three tests measured the points for the drying curve. The sample was allowed to saturate for 24 hours after each test at zero suction. The fourth test was conducted on a second sample, and it measured the points for both the wetting and drying curves of the sample. The drying curve data were measured first, followed by the wetting curve data. Test 5 measured the points for the drying curve of Sample 1. Data in Table 9 summarize the estimated Van Genuchten parameters based on the measured behavior of the ABC material.

Table 9. Van Genuchten curve fitting parameters for measured ABC data.

Test	Sample	Wetting/Drying	α (1/psi)	n	e
1	1	D	3.32	1.316	0.57
2	1	D	1.97	1.344	0.53
3	1	D	5.99	1.265	0.48
4-A	2	D	1.44	1.361	0.52
4-B	2	W	1.38	1.327	0.52
5	1	D	3.68	1.260	0.35

the gravimetric water content for the ABC material is approximately 0.15 versus 0.2 for the subgrade material. This difference should be noted because the relative unsaturated permeability of the various materials in the profile plays a major role in the formation of the capillary break and the ability of the layers to drain under unsaturated conditions.

Figure 31 shows the drying curves for the ABC material, with an AEV on the order of 0.01 psi (a few kpa), which is similar to the value observed for the TGLASS material. Results for Test 5 show a notably lower saturated gravimetric water content (0.15) than that (0.2) for the other four tests. The void ratio of the sample changed during testing, which is thought to be due to the migration of the fines from the sample after being retested on its drying path several times. It is also noted that the saturated gravimetric water content of Sample 1 decreased as it was retested.

Figure 32 shows the wetting and drying curves determined from Test 4 and highlights the hysteretic hydraulic response of the material. It should be noted that due to the change in gravimetric water content over the range of suction, the corresponding hydraulic conductivity of the ABC can be lower than that for the subgrade material at some value of suction. For example, at 1 psi (7 kPa), the gravimetric water content for the ABC material is approximately 0.15 versus 0.2 for the subgrade material. This difference should be noted because the relative unsaturated permeability of the various materials in the profile plays a major role in the formation of the capillary break and the ability of the layers to drain under unsaturated conditions.

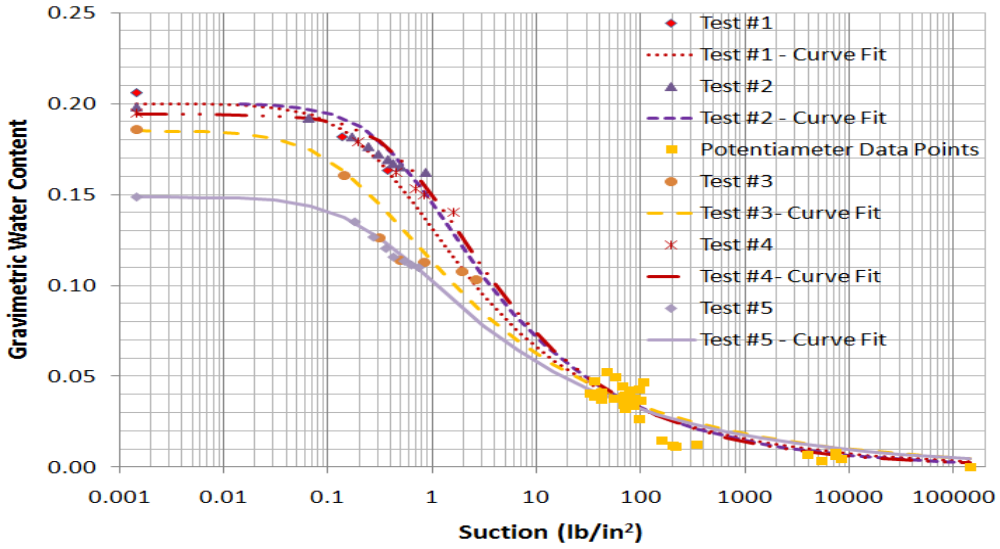

Figure 31. Graph. Drying curves for ABC material.

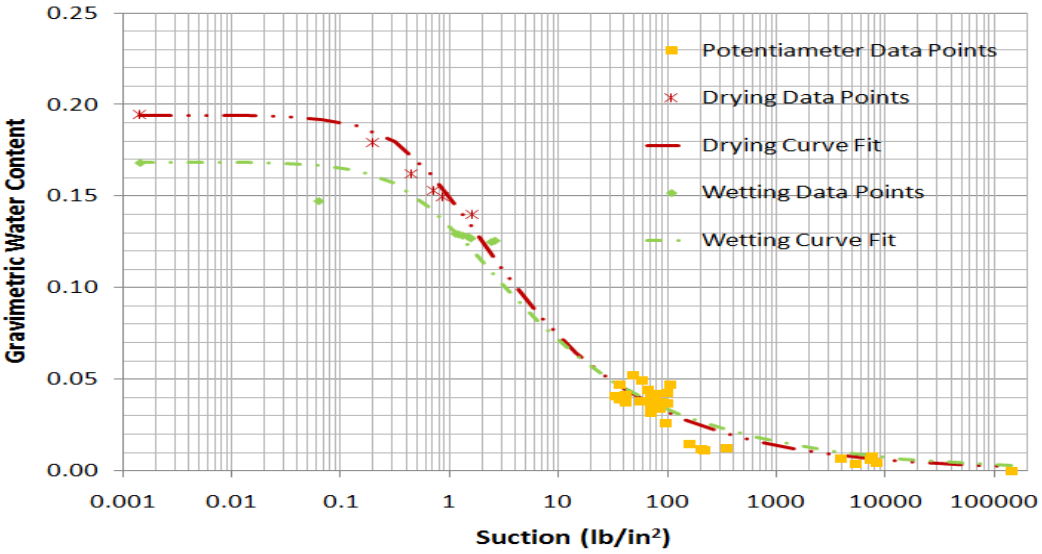

Figure 32. Graph. Moisture characteristic curves for ABC material: Sample 2.

CHAPTER 6 – EXPERIMENTAL PROGRAM: LARGE SCALE TESTING

The large-scale testing for this project was performed at NCSU's Constructed Facilities Laboratory. The testing involved the construction of samples that simulate roadway sections, and encompassed two phases. The first phase included an installed moisture barrier, and the second phase was conducted without a moisture barrier. The large-scale testing program began by simulating rainstorms of various magnitudes, followed by loading the test section with static and cyclic loads in an attempt to discern the effectiveness of the DMBL system. The testing program also involved applying rainfall during static loading to observe changes in deformation over time with the ingress of moisture into the test section.

The tests were conducted in a concrete test pit. A photo of the test pit is provided in Figure 33. The overall dimensions of the test pit are 9 ft wide, 12 ft long, and 7 ft deep. The test pit is at an elevation 3 ft below the floor elevation of the lab. An approximately 6-ft wide ramp provided access to the test pit for sample preparation and compaction.

Figure 33. Photograph. NCSU Constructed Facilities Laboratory test pit.

The test pit was reduced in size to lessen the amount of soil needed to fill the pit during testing. Three concrete panels, each 7 ft tall, 3 ft wide, and 8 in. thick, were placed along one side of the test pit and shored with wooden braces. A prefabricated wall consisting of bolted wooden beams was braced against the back wall to decrease the length of the pit. The dimensions of the reduced test pit are 6 ft wide, 9 ft long, and 7 ft deep. The soil was retained along the ramp side of the test pit by a timber wall composed of beams with a nominal 4-in. square cross-section. The wooden beams comprising the front wall are not shown in Figure 33. The final preparation of the test pit involved the installation of a 1.18-in. (30 mil)

thick vinyl polyester liner. The liner is manufactured by Flexi-Liner™ Corporation. The manufacturer's designation of the vinyl polyester material is J-22. Two test sections were prepared, as shown in Figure 34.

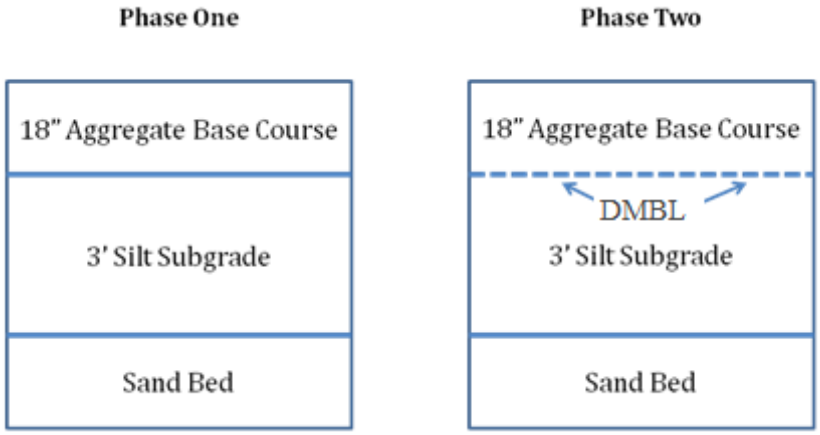

Figure 34. Schematic. Planned test profiles.

Section Construction

Before its placement in the test pit, the coastal plain subgrade was tilled to remove soil clods to ensure a more uniform distribution of moisture and soil properties throughout the test pit. A Poulan-Pro® Model HDF800 front-tine tiller was used to break up the clods. The soil was placed in the pit using a Bobcat® Model 773 skid-steer loader.

A plate compactor and jackhammer were used for the construction of the soil sections. The plate compactor is Northern Industrial Equipment® Model JPC-60 and weighs 152.1 lb (69 kg) with a plate area of 20.08 in. by 12.2 in. (510 mm by 310 mm) and a centrifugal force of 2,270 lb-f (1,030 kg-f). The jackhammer is a Bosch® Model 110304 electric jackhammer with an 8-in. square tamping plate. The jackhammer can impact 1,400 beats per minute at 43 foot-pounds of force.

The soil was broken down section by section using the jackhammer and a pick axe. Water was added to loosen the soil clods. After each work day, the soil pile was covered with a tarp to minimize evaporation of the water from the soil. The Poulan-Pro® tiller was used to till the soil pile until it could no longer reduce the clods into smaller sizes.

During construction of the subgrade layer, the coastal plain soil was placed in lifts with a target thickness of 6 in. After placement with the Bobcat® Model 773 skid-steer loader, the soil was raked to obtain the

desired slope required to simulate a DMBL system in a road section. The plate compactor was then used to smooth the soil surface in preparation for compaction with the jackhammer. After preparation of the subgrade, the ABC was placed in lifts with a target thickness of 3 in. The ABC lifts were compacted using the plate compactor until no loose particles were observed at the surface. The jackhammer was not used in the compaction of the ABC in order to prevent potential crushing of the aggregate particles.

During construction of the test sections, a Troxler nuclear density gauge was used to measure the water content and density of the subgrade. The pit was divided into six quadrants within a three by two grid with square elements. The in-place water content and density were measured periodically during section construction and deconstruction. Readings were taken in both back-scatter and direct transmission modes. Gravimetric samples were taken as well for comparison to those measured by the nuclear density gauge and frequency domain reflectometer (FDR) sensors (to be described later).The DMBL was connected to a drainage pipe used to collect lateral flow from the DMBL. The connection is pictured in Figure 35.

Figure 35. Photograph. Drainage pipe connection.

The pipe used is 4 in. in diameter. A longitudinal slot was cut into the pipe to connect the DMBL. The drainage pipe was sloped at 5% in its flow direction. The PVC pipe connected to the DMBL, as shown in Figure 35, is one of several possible configurations. Although the connection detail shown in this figure is that used in the laboratory study, it should be noted that other equivalent connection configurations are also acceptable.

The thicknesses of the section layers in their as-built condition were measured at several points using a surveying grid with a reference frame placed above the test pit. A flexible tape with a weight on the

underside was lowered in each of the grid locations by one person, while a second person stood eye-level with the grid and took measurements. The average thickness of each layer is presented in Table 10.

Table 10. As-built section thicknesses and moisture-unit weight values.

Section/Layer Thickness	ABC (in.)	Subgrade (ft)
Control	11.4	2.62
DMBL	11.9	2.67

After the DMBL section was loaded, the ABC and top foot of the subgrade were removed in order to prepare the test sample for the control section (without a moisture barrier). The depth of the removed portion was determined to be the zone of stress increase using twice the diameter of the load plate. The removed subgrade material was tilled again and placed using the same procedure as discussed above.

Test Pit Instrumentation

The test sections were instrumented with sensors to measure the moisture content of the soil and the surface displacement during the application of the load. Moisture sensors were calibrated for the specific soil used for testing. All displacement sensors were calibrated using a Mituyo height gauge.

Moisture Sensors

The sensors used to estimate the moisture content of the soil are FDRs. These sensors are manufactured by Decagon Devices, Inc. The manufacturer's sensor designation is 10HS. The FDR 10HS sensors measure the dielectric constant of the soil in a 1-L zone of influence in the area surrounding the sensor and correlate it to the moisture value during calibration. Standard calibration curves are available in the literature for using the FDR sensors to determine the water content of soils. However, the individual response of an FDR sensor can vary significantly amongst soil types. To obtain the best possible accuracy in this research, the FDR sensors were calibrated experimentally to the specific soil used in testing.

To calibrate the FDR 10HS sensors, the soil was compacted in a mold with a nominal diameter of 6 in. and height of 7 in., with a total volume of approximately 3 L. The size of the compaction mold was chosen to minimize interference within the zone of influence of the FDR 10HS sensors.

For the calibration process, the coastal plain subgrade was prepared in batches, each batch having a mass of 17.6 lb. The soil batches were oven-dried for 24 hours. The soil was then pulverized in a grinder to remove any clods and to create uniform samples. After the soil had been pulverized, at least three gravimetric water content samples were taken, and a prescribed amount of water was mixed into the

samples. After the soil was mixed to the desired water content, it was allowed to sit for 24 hours. Each of the three lifts in the mold was compacted with 85 blows from a standard Proctor hammer. This number is scaled up from 25 blows commonly employed in the standard Proctor test by the ratio of the mold volumes used in each test. Accordingly, the same compaction effort was used, and the Proctor curves developed from the FDR calibration can be compared to previously measured compaction curves for the coastal plain subgrade soil.

After the first layer was compacted in the mold, a sensor was inserted a few centimeters into the first lift. The second and third lifts then were compacted. Care was taken not to damage the FDR sensors during compaction. A reading was then taken from each FDR sensor. Pictured in Figure 36 is a sensor being extracted from the compaction mold. Once the soil and sensor were removed from the compaction mold, three gravimetric water content samples were taken. Samples were taken as close as possible to the top, middle, and bottom of the sensor location within the mold.

Figure 36. Photograph. FDR sensor in calibration mold.

Next, the soil was broken down by hand, and more water was added to attain a second water content. This process was repeated with increasing water contents. The soil was allowed to condition for 24 hours between each addition of water. Three gravimetric water content samples were taken from each mold.

Figure 37 shows the calibration curves experimentally developed for the coastal plain subgrade soil using a second order polynomial function. Curves representing errors of plus or minus 3% volumetric water content also are plotted.

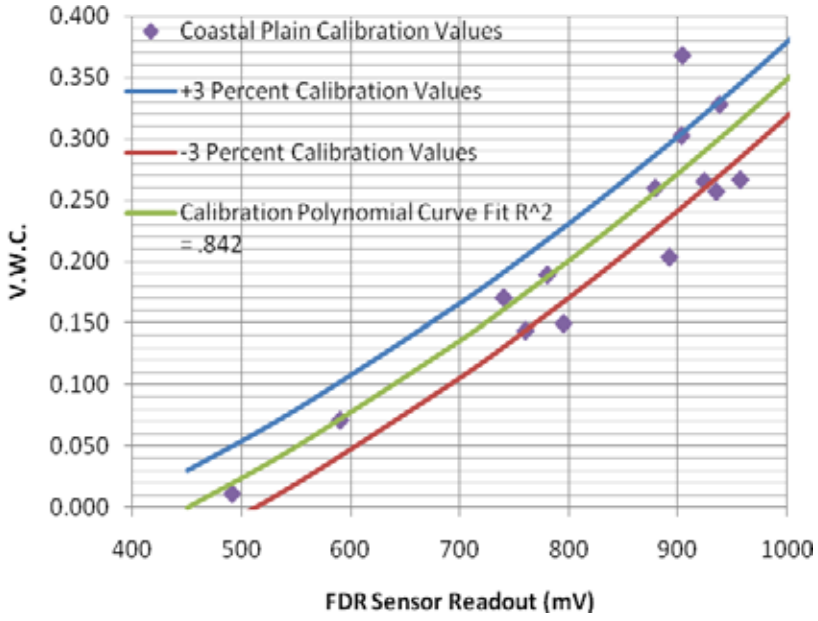

Figure 37. Graph. FDR calibration curves for coastal plain subgrade.

Earth Pressure Cells

The DMBL section was instrumented using dynamic earth pressure cells (EPCs) manufactured by GeoKon. Two 4-in. diameter sensors with a capacity of 60 psi were used. The control section (with no moisture barrier) was instrumented using vibrating wire EPCs manufactured by GeoKon, as shown in Figure 38.

Figure 38. Photograph. GeoKon vibrating wire earth pressure cell with thermistor (18-inch ruler shown).

String Pots and Short Longfellows

Figure 39 shows the string pot sensors used to monitor the displacement of the load plate. The sensors are manufactured by Celesco. The actuator load cell used to measure the applied load and the load plate used in testing are also shown in Figure 39.

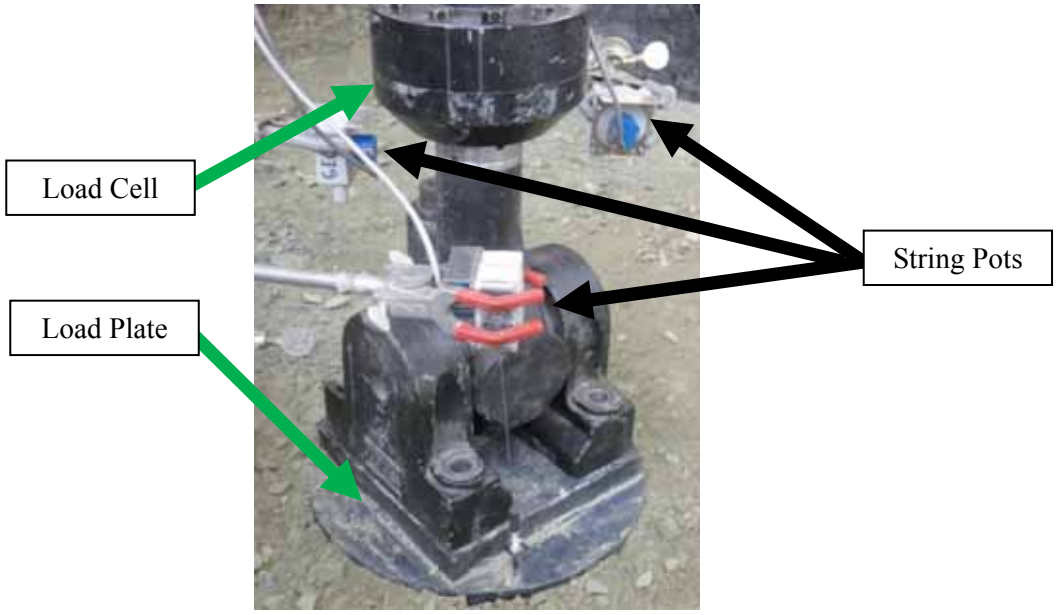

Figure 39. Photograph. String pot sensors.

The actuator loaded the test sections through a steel plate. The plate is 12 in. in diameter by 1 in. thick. An 8-in. square, 1-in. thick steel plate was welded to the top of the circular plate. Figure 40 shows the short Longfellow displacement sensors used to monitor displacements outside the plate in the test section. These sensors were placed at 5 in., 10 in. and 15 in. away from the load plate.

Figure 40. Photograph. Short Longfellow sensors.

A view of all the sensors, string pots, short Longfellows, and the actuator load cell used to monitor displacement is presented in Figure 41.

Figure 41. Photograph. Instrumentation in test pit.

Pictured in Figure 42 is the MTS actuator used to load the test sections. This picture is of the control DMBL section. The actuator is capable of applying a load of 19 kips.

Figure 42. Photograph. MTS actuator used to load test sections.

Sensor Placement

Figure 43 shows the placement of an FDR sensor in the subgrade soil. Care was taken not to damage the prongs of the sensor when placing it in the subgrade. Before pushing the sensor into the soil, two small pilot holes were made using a thin spatula. Approximately one-half inch of the sensor was left above the

lift of the soil in which it was being placed. A PVC elbow was placed over the top of the sensor to prevent damage from the compaction of the next soil lift above the sensor.

Figure 43. Photograph. FDR sensor placement.

The sensor protection for the entire first lift is shown In Figure 44. The PVC pipe used to protect the wires is 1/2 in. in diameter.

Figure 44. Photograph. Sensor wire protection.

Figure 45 shows a plan view of the locations of the FDR and EPC sensors as they were placed in an as-built condition. Eight FDR sensors were used per test sample. Figure 46 and Figure 47 display the depths at which the FDR sensors and EPCs were placed in as-built conditions.

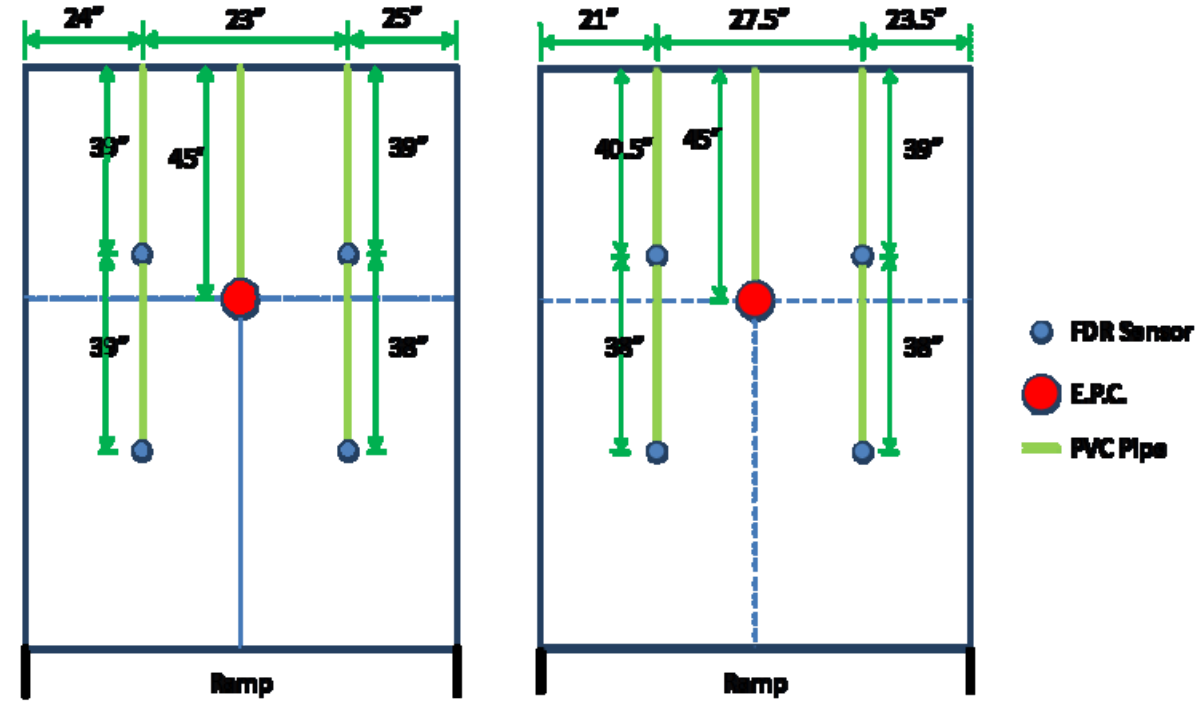

Shallow Moisture Sensors Plan View Deep Moisture Sensors Plan View

Figure 45. Schematic. Plan views of sensor locations (N.T.S.).

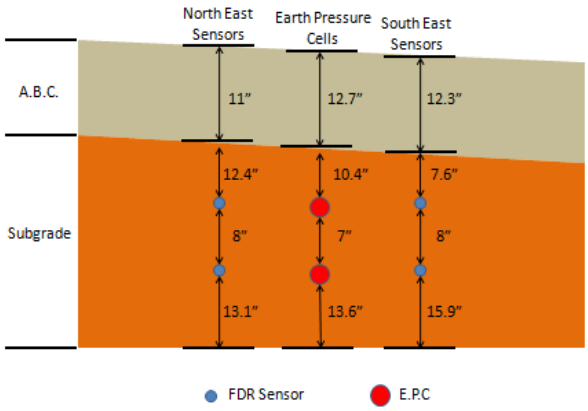

Figure 46. Schematic. Elevation looking east: control section, western sensor depths (N.T.S.).

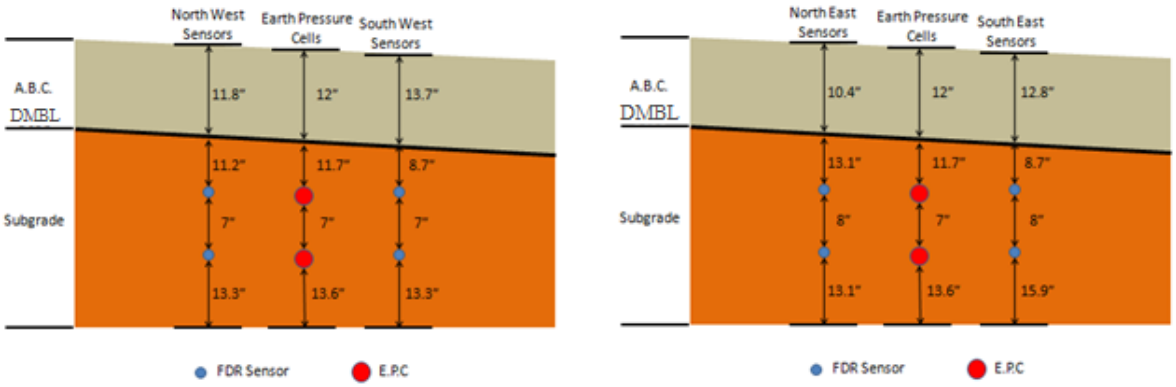

(a) (b)

Figure 47. Schematic. Elevation looking east: DMBL section, (a) western sensor depths (N.T.S.) (b) eastern sensor depths (N.T.S.).

Data acquisition systems

Two data acquisition systems were used in the testing program. The first system, pictured in Figure 48, is manufactured by the Vishay Micro Measurement Division. The Vishay 7000 was used to collect data from readings taken at the rate of every five minutes during static loading and 200 readings per second during cyclic loading.

Figure 48. Photograph. Vishay 7000 data acquisition system.

The Vishay 7000 was used to monitor data from the actuator load cell, actuator linear variable differential transformer (LVDT), string pots, short Longfellows and the dynamic EPCs. A separate data acquisition system was used to monitor data from the FDR sensors, as shown in Figure 49. This second system is an Agilent 34972A and was used to record readings from the FDR sensors every 15 minutes.

Figure 49. Photograph. Agilent 34972A data acquisition system.

Rainfall System

Figure 50 is a schematic representation of the first rainfall application system constructed for the project. This system uses 7 sprinkler heads inserted into a ¼-in. water line, pictured in red with a barbed connection. The sprinklers and hoses are commercially available products. These sprinkler heads allow multiple application directions of 90º, 180º, or 360º and were placed strategically to achieve the best

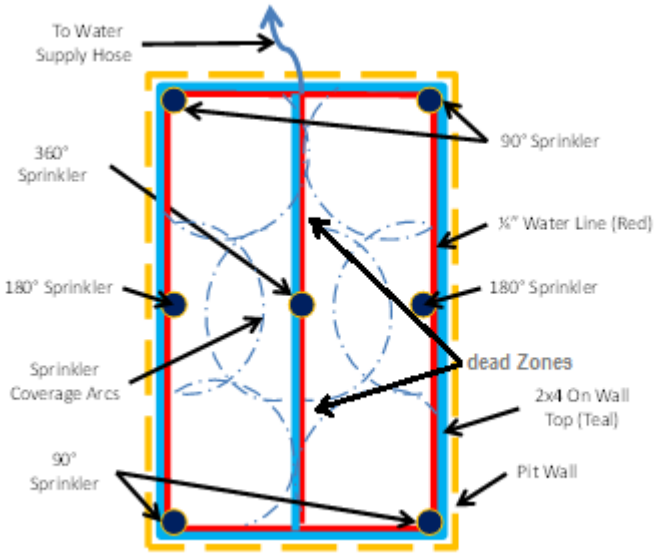

coverage of the test pit.

Figure 50. Schematic. Rainfall application system -1.

Using this system, the flow rates can be as low as 0.5 gal/hr or as high as 2 gal/hr. The distance range of the water from the sprinkler heads can vary from 1 ft to 5 ft. The placement of the system over the sample is shown in Figure 50. Although this system worked, the pattern of spray resulted in some "dead" zones, as shown in Figure 50. Therefore, a second system was developed.

Figure 51. Photograph. Rainfall application system 1 in test pit.

Figure 52 is a schematic representation of the second rainfall application system. This second system employs two sprinkler heads of the same type used in the first system. The system consists of 5-ft long PVC pipes with supply hoses connected at one end. The other end of the pipe is capped and sealed. Located in the middle of each pipe in the long direction are 180º sprinkler heads. These sprinklers were found to be sufficient to apply even rainfall over the test pit.

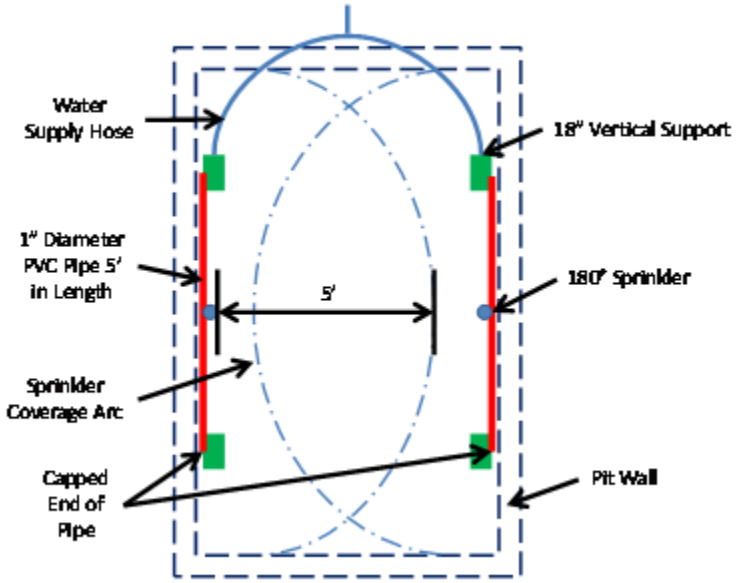

Figure 52. Schematic. Rainfall application system- 2.

Rainfall Test Schedule

The rainfall application schedule includes rainfall with and without loading. Details regarding the duration and intensity of the rainfall events are presented in Table 11.

Table 11. Rainfall event schedule.

Rainfall Event	Date	Duration (hr)	Precipitation Rate (in./hr)	Load Applied (Y/N)	Rainfall System 1 or 2
1	9/23/2010	.5	0.836	N	1
2	9/24/2010	.5	0.836	N	1
3	10/5/2010	.5	0.836	N	1
4	10/7/2010	.5	0.836	N	1
5	10/11/2010	.5	0.836	N	1
6	10/12/2010	.5	0.836	N	1
7	10/19/2010	.5	0.836	N	1
8	10/30/2010	1.25	0.836	N	1
9	2/4/2011	2	0.836	Y	1
10	2/6/2011	.5	0.836	Y	1
11	4/18/2011	4	0.836	N	1
12	4/19/2011	3	0.836	N	1
13	4/23/2001	3	0.607	N	2
14	4/23/2011	2	0.607	N	2
15	5/31/2011	2	0.607	N	2
16	6/1/2011	1.75	0.607	N	2

Before loading, rainfall was applied to both sections to study the distribution of moisture in the sections with and without a DMBL. For the first test (with the moisture barrier), eight rainfall events were simulated prior to the load application on the moisture barrier section. Two rainfall events were applied to this section during loading, and four rainfall events were applied after loading. For the second test, three rainfall events were simulated for the control section (without the moisture barrier). Two of these events were prior to loading and one was during loading. The rainfall events were applied with durations between 0.5 and 4 hours.

Loading Schedule

The apparatus used to load the sections in the test pit was controlled by a Flex Test SE controller manufactured by MTS. Loads were applied in both phases of testing to the control and moisture barrier sections. Each section was subjected to a static load of 72 psi. The static load was maintained until the observed deformation reached a relatively steady state. After this state was reached, a rainfall event was simulated, and the static load was held constant for another 24 hours. At the end of the static loading, a cyclic load was applied. In this case, 72 psi was used as the pulse load to replicate the passing of a truck on a road section. The load was applied in 1-s pulses for 10,000 cycles. Each cycle consisted of 0.1 s of loading and 0.9 s of rest time.

Large-Scale Test Results

The collected data from this testing program include moisture, rainfall event, load, and displacement data. The moisture data are presented in terms of moisture content versus time to show temporal variations. These data are used to observe the performance of the DMBL and control sections. The load displacement data during and after storm applications are presented to investigate the performance of DMBLs under static and dynamic loading conditions.

Moisture Data

Select portions of the data are presented in this section to illustrate the moisture variations in the control section and in the DMBL section. Moisture readings were taken at 15-min intervals from the time of their placement. Water balance calculations were performed to investigate the performance of the moisture barrier section. Figure 53 shows the water balance data for rainfall events 1 to 14. The values are presented in terms of inches of rain per the area of the test samples (54 ft^2). That is, the values for the

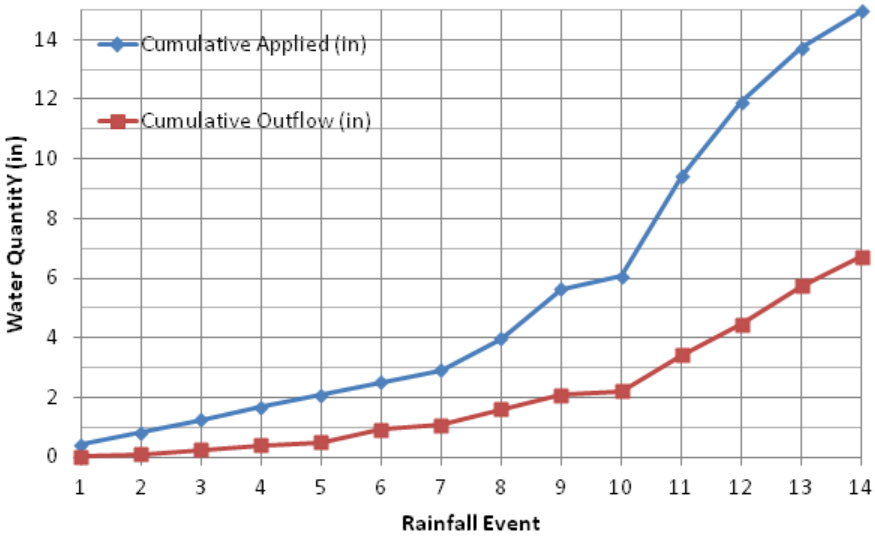

water balance are plotted from rainfall application to rainfall application instead of temporally.

Figure 53. Graph. Water balance data for rainfall events 1 to 14.

To quantify the performance of the moisture barrier section, calculations were made assuming that no unsaturated flow into the subgrade occurs until the ABC is saturated. In addition, after the ABC is saturated, it remains so instead of draining to its field capacity. This assumption was made because no moisture sensors were installed in the ABC to provide information regarding moisture variation as simulated rainfall is induced. Figure 54 shows a balance of water infiltrating the soil system. Infiltrating water is defined as the rainfall applied minus any outflow.

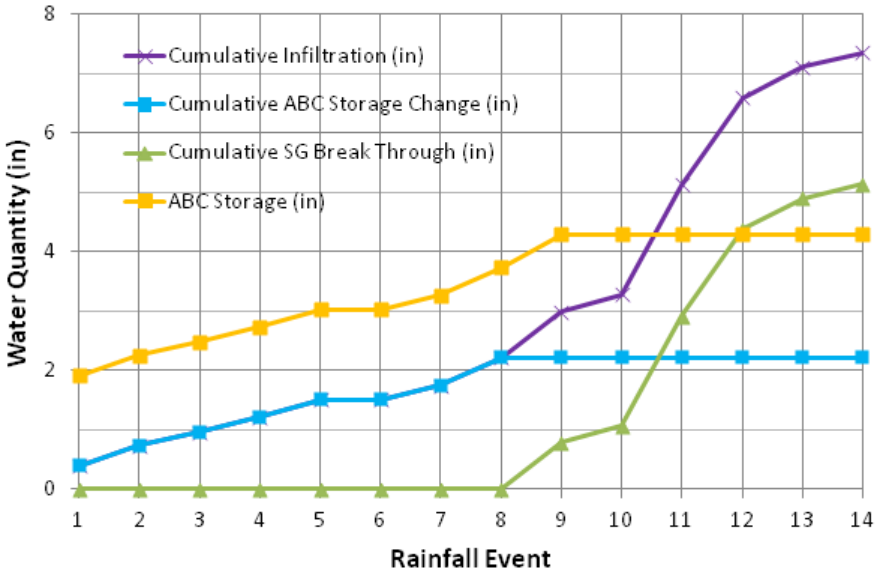

Figure 54. Graph. Computed infiltration: water balance for rainfall events 1 to 14.

The data indicate that the infiltrating water is equal to the change in ABC storage until rainfall event 9. This finding is based on the premise that water cannot flow into the subgrade until the ABC has reached a saturated state. The data presented in Figure 54 indicate that after rainfall event 9, the ABC has reached a saturated state, and approximately 5 in. (168 gal) more infiltrating water can potentially enter the subgrade. The subgrade soil was prepared at a degree of saturation of approximately 87 percent. The estimated amount of water is enough to nearly saturate the subgrade if the water were to break through. As shown in Figure 53, the amount of outflow is approximately 6 in., which seems to indicate that no breakthrough into the subgrade occurred.

The data presented in Figure 55 indicate that after rainfall event 9, the ABC has reached a saturated state, and approximately 5 in. (168 gal) more infiltrating water can potentially enter the subgrade. The subgrade soil was prepared at a degree of saturation of approximately 87 percent. The estimated amount of water is enough to nearly saturate the subgrade if the water were to break through. As shown in Figure 54, the

amount of outflow is approximately 6 in., which seems to indicate that no breakthrough into the subgrade occurred. Figure 55 shows a balance of water infiltrating the soil system. Infiltrating water is defined as the rainfall applied minus any outflow. The data indicate that the infiltrating water is equal to the change in ABC storage until rainfall event 9. This finding is based on the premise that water cannot flow into the subgrade until the ABC has reached a saturated state. The data presented in Figure 55 indicate that after rainfall event 9, the ABC has reached a saturated state, and approximately 5 in. (168 gal) more infiltrating water can potentially enter the subgrade. The subgrade soil was prepared at a degree of saturation of approximately 87 percent. The estimated amount of water is enough to nearly saturate the subgrade if the water were to break through. As shown in Figure 54, the amount of outflow is approximately 6 in., which seems to indicate that no breakthrough into the subgrade occurred.

This observation is confirmed by the data presented in Figure 56, which shows the moisture variation data obtained from the FDR sensors for rainfall events 13 and 14. Note that the FDR sensors are better at providing an indication of the relative change in moisture rather than absolute moisture values. This chart is typical of the moisture data collected during this testing. In Figure 56, a small variation is seen in the moisture readings for the deep and shallow southwest sensors. These small variations observed for several of the sensors are within the error range of the FDR sensors. To verify the performance of the moisture barrier, moisture content measurements taken before the rainfall applications and during section construction are compared to moisture content measurements taken during section deconstruction.

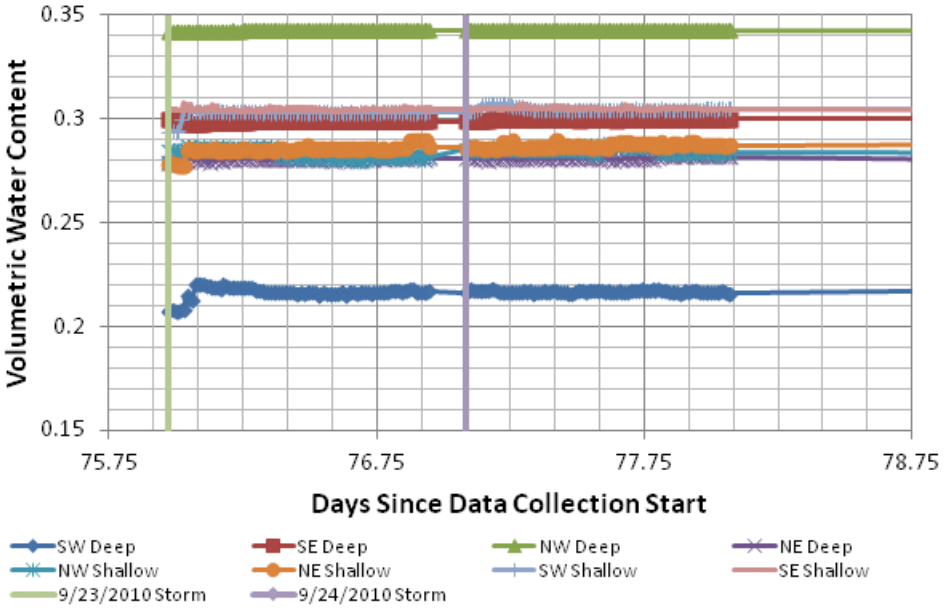

Figure 55. Graph. Moisture data for rainfall events 13 and 14.

Figure 56 presents water content measurements taken from the DMBL section for quality control purposes. Measurements taken after construction of the section and before the application of the rainfall events are marked by the date 8-25-2010.

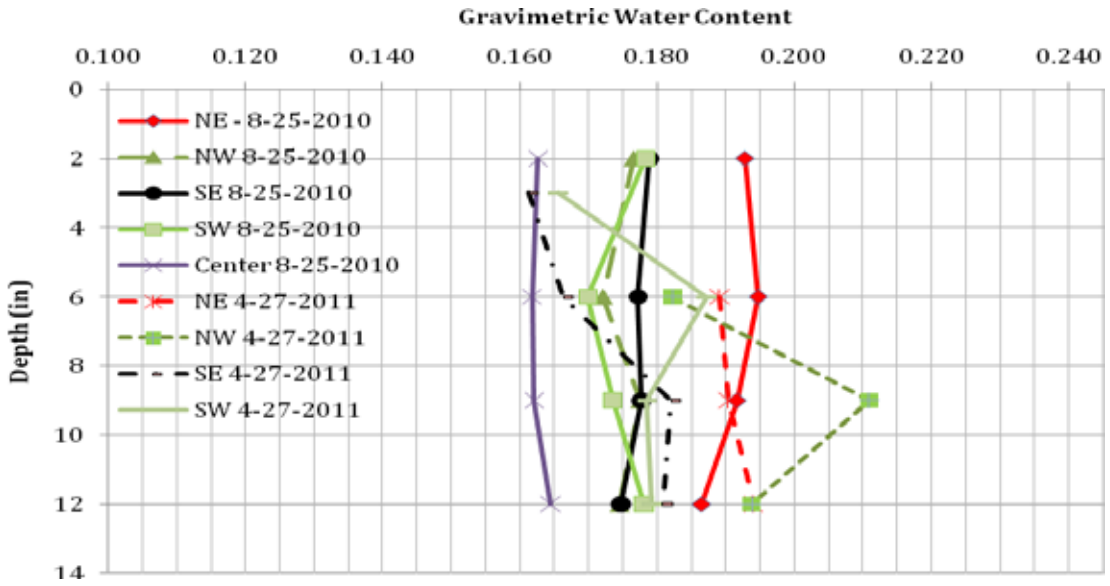

Figure 56. Graph. Water content quality control measurements for coastal plain subgrade.

These water content measurements marked with the date 8-25-2010 were taken using a nuclear density gauge calibrated for the coastal plain subgrade. Water content measurements marked with the date 4-27-2011 were obtained through the use of an oven-drying test process for samples taken directly from the test section, and these measurements conform to the FDR data.

Displacement Data

This section presents the results of static and dynamic loading on the test sections constructed. The static displacements that occurred during constant loading are compared with those that occurred under and after rainfall conditions whereby the static load magnitude was held constant. The displacements under dynamic loading also are discussed. Figure 57 shows the displacements as measured over time by the string pot sensors for the control section. The static load, shown as the red line, was held constant for five days. On the fourth day of loading, a rainfall event was simulated. The rainfall event lasted two hours. An increase in the number of displacements is seen in Figure 57 after the application of the rainfall event.

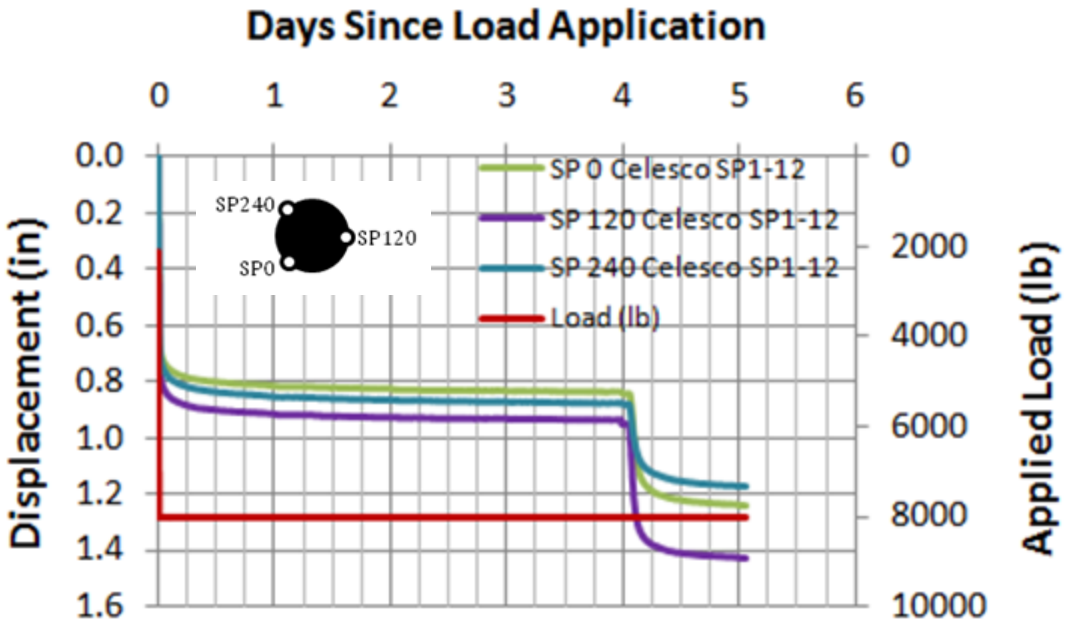

Figure 57. Graph. Static load displacements, as measured by string pot sensors in control section.

Figure 58 plots the displacements as measured by the short Longfellow sensors in the control section during static loading conditions.

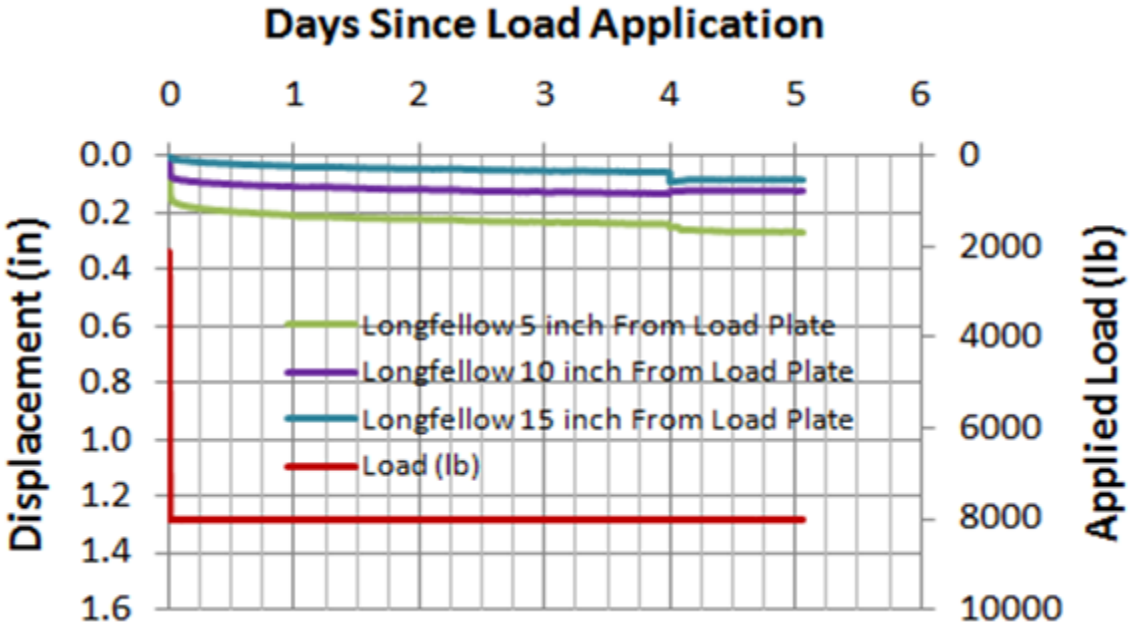

Figure 58. Graph. Static load displacements, as measured by short Longfellow sensors in control section.

The data presented in Figure 58 provide an indication of the shape of the deformation profile, with a slightly discernible increase in deformation outside the load area and show a maximum deformation of 1.4 in., with an increase of 0.4 in. in the deformation level with the introduction of moisture through the rain device. The data also indicate plate rotation with the introduction of rain on the order of 0.75º.

Static loading of the moisture barrier section began on November 15, 2010 as the first test to be performed in the series of the two tests. Several challenges arose, however, with regard to the pumps that drive the actuator loading system, which led to the postponement of the continued static loading until January 31, 2011. In and Figure 60 the displacements, as measured by the string pot sensors and short Longfellow sensors, are presented for the section with the DMBL. Loading was applied incrementally until the displacement was nearly constant for a given load increment. As shown in Figure 60, the load had to be released several times due to equipment problems. Loading was applied incrementally until the displacement was nearly constant for a given load increment. As shown in Figure 59, the load had to be released several times due to equipment problems.

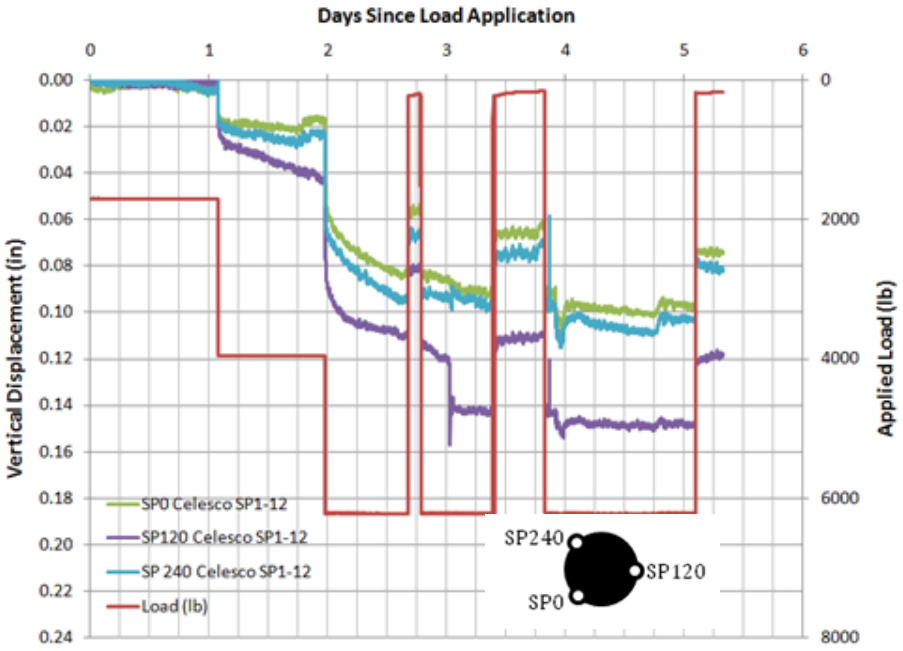

Figure 59. Graph. First static load displacements, as measured by string pots in DMBL section.

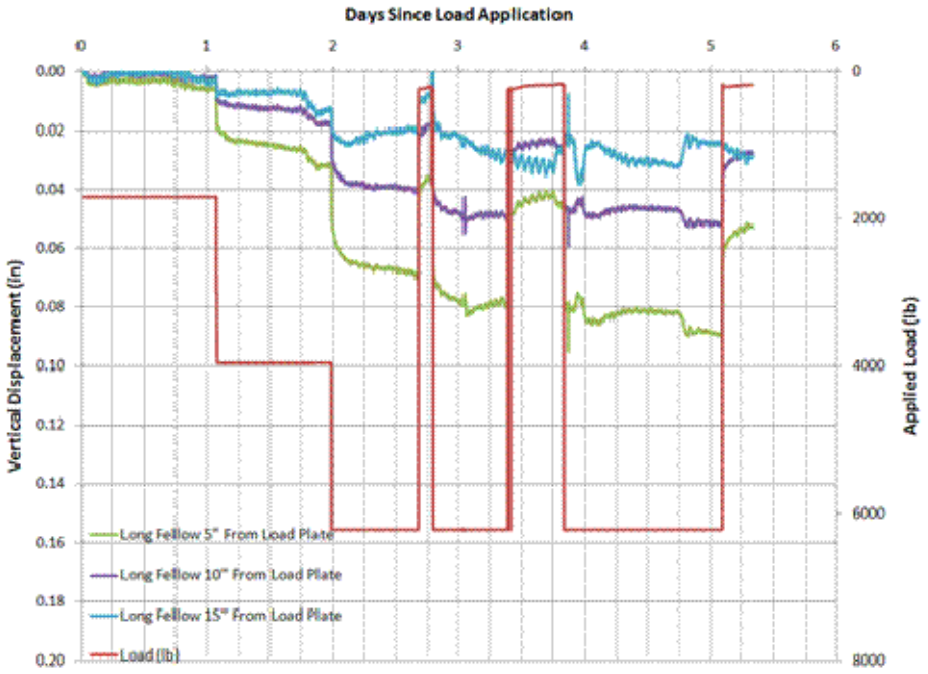

Figure 60. Graph. First static load displacements, as measured by short Longfellow sensors in DMBL section.

During this test, the displacement magnitude with the DMBL was approximately one order of magnitude less than without the DMBL. The total displacement measured during the loading sequence was on the order of 0.15 in. With the introduction of each rainstorm, the increase in displacement was typically less than 0.05 in. The data shown in also indicate a smaller deformation profile in comparison to the case without the moisture barrier.

A second static loading was applied on January 31, 2011 and held for approximately seven days. After four days of static loading a rainfall event was applied. The displacement jump seen at four days corresponds to this application of rainfall. The rainfall event number is 9, and its duration was 2 hours. After the application of rainfall event 9, the static load was held for another two days, and another rainfall event was applied. This rainfall event was number 10, and its duration was one half hour. The static load was released one day after the application of rainfall event 10.

After the application of the first static load on the DMBL section, all of the sensors were left in place for the second static load application. The deformations reported in Figure 62 and Figure 62 include the permanent deformations that resulted from the first static loading. Even with repeated loading and the introduction of moisture into the system, the final total displacement was approximately 0.2 in., with the increase in displacement due to the introduction of the rainfall event being approximately 0.05 in.

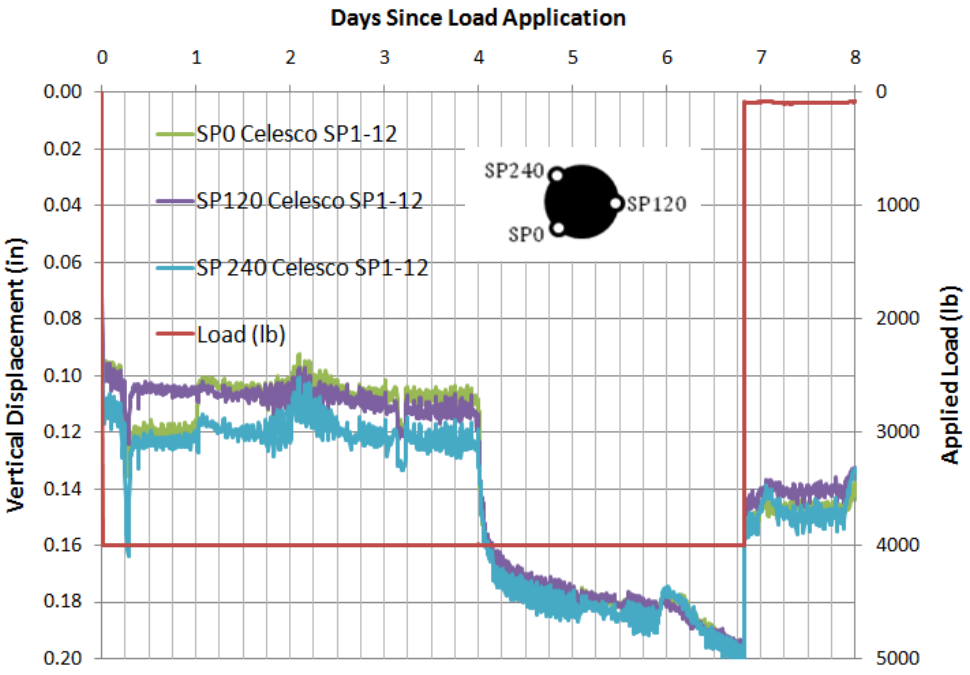

Figure 61. Graph. Second static load displacements, as measured by string pot sensors in DMBL section.

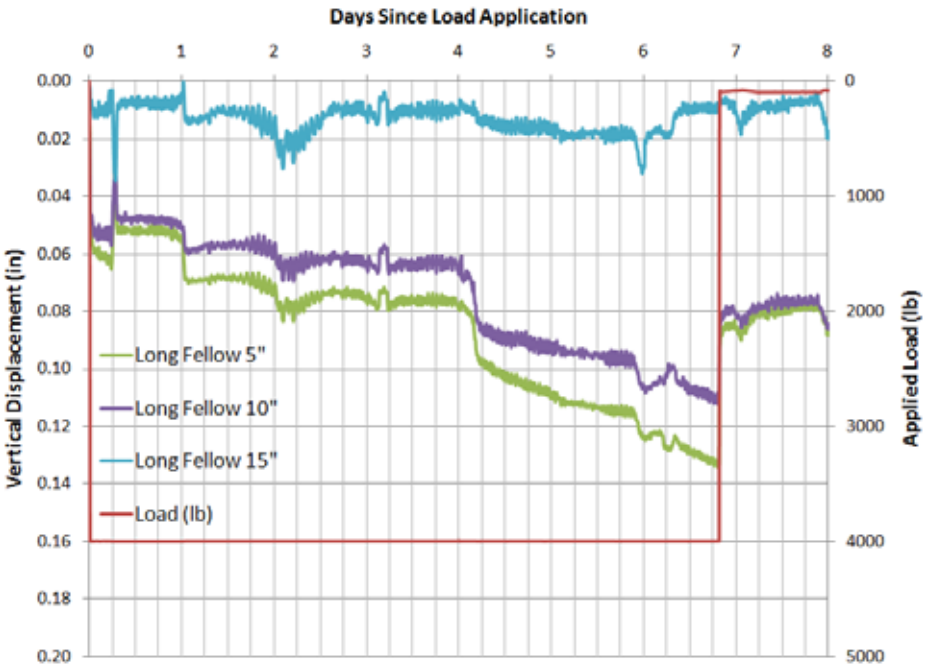

Figure 62. Graph. Second static load displacements, as measured by short Longfellow sensors in DMBL section.

The challenge here, however, is not knowing whether the improved performance was due to the reinforcement effect provided by the inclusion of the DMBL, or to its contribution in maintaining the moisture level with the introduction of the rainstorms and, therefore, minimizing the shear strength of the section soil layers. This question requires further study, especially given that the cost of the TGLASS component of the barrier is typically ten times the cost of traditional polyester and polypropylene products.

Cyclic Loading

Figure 63 displays the cyclic load data as measured by the actuator LVDT for the control and DMBL sections. Forty minutes into the loading of the control section, the actuator slipped off the load plate as excessive plate rotation occurred. A local failure in the section is believed to be the source of this plate rotation. The deflection seen in the control section is greater than 2 in., whereas the deflection seen in the DMBL section is less than .03 in. With two orders of magnitude difference in these displacements under cyclic loading, the better performance of the DMBL section over the control section is apparent.

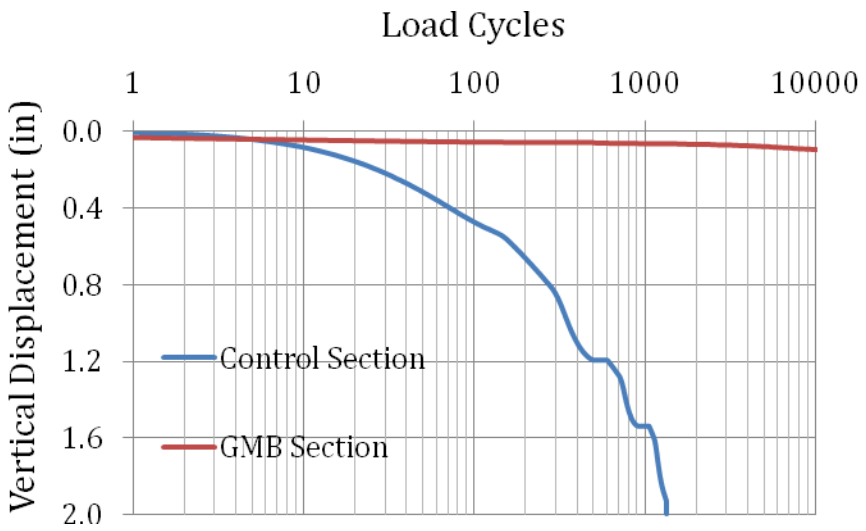

Figure 63. Graph. Cyclic load displacements, as measured by actuator LVDT.

Displacement Comparisons

Table 12 summarizes the displacements measured by the string pot sensors at the end of the seven-day static loading period for both tests. The displacements reported for the DMBL section are total displacements from both of the static loading cycles applied to the section.

Table 12. Static load displacements (in.) (Note DMBL section displacement is from two static load applications).

Section/Sensor	SPO	SP120	SP240
Control	0.835	0.964	0.876
DMBL	0.113	0.123	0.132
DMBL Perm. Deflection	0.071	0.063	0.081

Table 12 also presents the permanent displacements that resulted from the first static loading in the DMBL section. These permanent displacements are presented for comparison and to show the effect of loading the DMBL section twice. Table 13 presents the final displacements after four days of static loading and one rainfall event for the control and DMBL sections. The displacements reported for the DMBL section are one order of magnitude smaller than those observed in the control section.

Table 13. Surface displacements (in.) 24 hours after application of 2-hour rainfall event.

Section/Sensor	SPO	SP120	SP240
Control	1.24	1.43	1.17
DMBL	0.193	0.193	0.193

(blank page)

CHAPTER 7 – ONE-DIMENSIONAL NUMERICAL MODELING

Effect of Temperature on Moisture Barriers

A series of simulations was performed using UNSAT-H to understand the effects of temperature on pore pressure and water content distribution in a soil-geotextile column. Three sets of simulations were performed. For all of the simulations, the height of the soil column was assumed to be 0.98 ft (30 cm), and the thickness of the geotextile layer was modeled as 0.39 in. (1 cm). For comparative purposes, two types of soil were simulated: sand and silty clay. The silty soils are relatively susceptible to frost heave due to capillary retention of water in the soil pores. Sandy soils have higher permeability than silty soils and allow a downward flow of water into the subsurface during precipitation. Three different temperature conditions were considered: 1) a constant temperature of 32°F along the column, 2) a constant temperature of 100°F along the column, and 3) a constant temperature of 32°F at the top and a constant temperature of 66°F at the bottom of the column.

Temperatures of 32°F and 100°F were selected to represent cold and hot regions, respectively. The temperature gradient of 34°F was selected to magnify the effect of temperature gradient on moisture movement and suction head distribution along the soil-geotextile column. However, the typical temperature gradient range for freezing pavements is from 0˚F/m to 54˚F/m (Henry 1988). The thermal conductivity of the soils and geotextile was computed using the following equation (Campbell and Jones 1984):

$$k_h = a + b\left(\frac{\theta}{\theta_s}\right) + (a-d)\exp\left[-c\left(\frac{\theta}{\theta_s}\right)^e\right] \quad (4)$$

where a, b, c, d, and e are constants; θ is the volumetric water content, and θ_s is the saturated water content. The constants for both types of soil and geotextile are the same (a = 0.6, b = 0.7, c = 8.0, d = 0.26, e = 3.0). These values were taken from Cass et al. (1981) for lysimeter sand at 22.5°C.

Figure 64 shows the water characteristic curves for the soils and geotextile considered in the analysis, and Figure 65 shows the hydraulic conductivity variation as a function of suction. The Van Genuchten equation (Van Genuchten 1980) was used to determine the water characteristics curves, and the Van Genuchten-Mualem model (Mualem 1976, Van Genuchten 1980) was used to determine the relative hydraulic conductivity curves. Table 14 shows the parameters for the water characteristics and hydraulic conductivity curves for both the soils and geotextile.

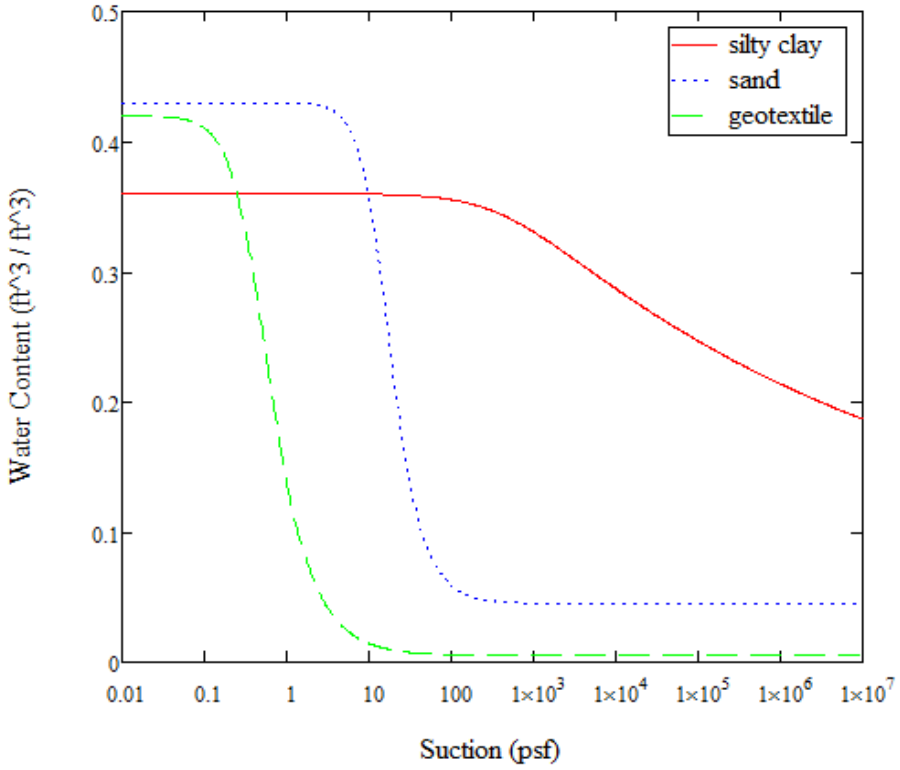

Figure 64. Graph. Water characteristics curves of various materials in the model.

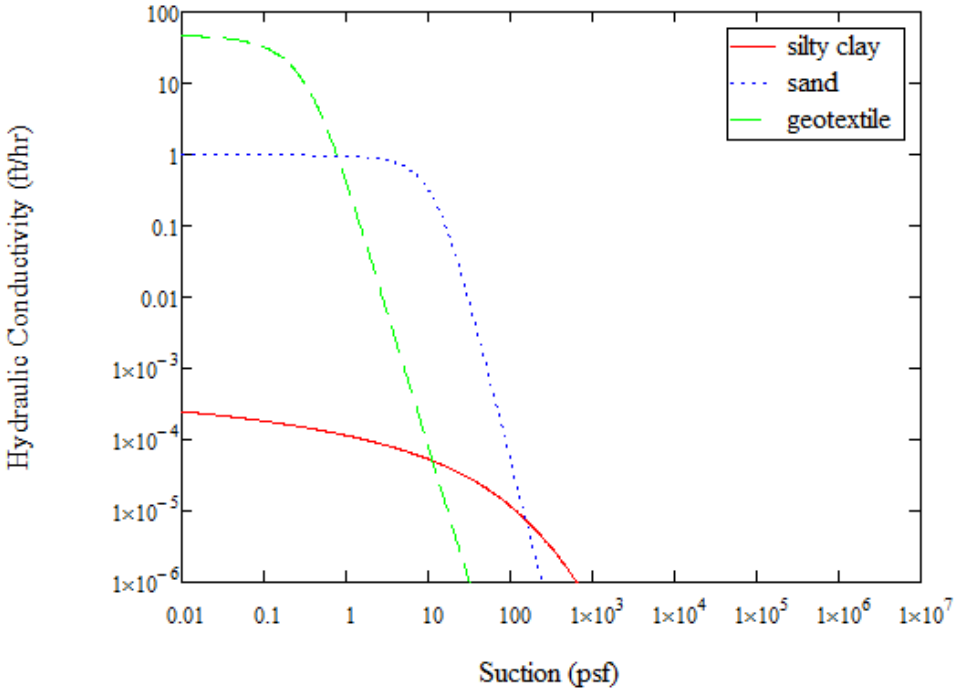

Figure 65. Graph. Hydraulic conductivity curves with suction for modeled materials.

Table 14. Water characteristics and hydraulic conductivity parameters (Carsel and Parrish 1988).

	Saturated Water Content θ_s	Residual Water Content θ_r	α (1/psf)	N	Saturated Hydraulic Conductivity (ft/hr)
Sand	0.43	0.045	$7.10*10^{-2}$	2.68	0.974
Clay	0.36	0.070	$2.442*10^{-3}$	1.09	$6.56*10^{-4}$
Geotextile	0.42	0.005	2.408	2.19	47.23

Modeling Cases

Three cases were simulated in this study: (1) the geotextile placed at the bottom of the column with an initial pressure head of zero along the column (drainage condition); (2) the geotextile placed at the top of the column, and the water table initially placed at the bottom (capillary rise condition); and (3) the geotextile placed in the middle and the water table at the bottom. The conditions for Case 3 describe a scenario in which the geotextile layer may be embedded within the subgrade.

Case 1: Drained Condition;

The initial and boundary conditions for Case 1 are: no flux boundary at the top and along the side walls, unit gradient at the bottom of the column, zero pressure head along the column (as the initial condition), and heat and vapor flow allowed. The geotextile layer was placed at the bottom of the profile. The soil-geotextile column was allowed to drain under gravitational force for three days in the model. Results from the Case 1 analysis indicate the following findings:

i. Increasing the temperature along the column from 32°F to 100°F has no significant effect on suction and water content distribution in the soil;
ii. Applying a temperature gradient (32°F at the top and 66°F at the bottom) causes a decrease in suction and an increase in water content throughout the soil column. However, within the geotextile layer, the water content decreases and the suction increases. In other words, when the heat flow is the opposite direction of the water flow, the water content increases and the suction decreases along the soil profile. The top of the soil shows the most decrease in suction and increase in water content. In the geotextile, keeping the temperature at 66°F, compared to 32°F at the top, leads to some water evaporation and, consequently, the water content decreases and the suction increases. The variation in suction and water content at the top of the soil for both types of soils and after three days of run time is shown in Table 15.

Table 15. Water content and suction differences between the column with a constant temperature of 32°F and the column with a temperature gradient after three days simulation.

	Suction difference at the top of the soil (%)	Water content difference at the top of the soil (%)
Sand	0.7	-0.3
Silty Clay	1.1	0.0

The simulation time was then increased to fifty days. A soil-geotextile column with a constant temperature of 32°F at the bottom and constant temperature of 66°F at the top (the opposite of the previous simulation) was simulated to evaluate the inverse temperature gradient for both types of soil (sand and silty clay.) Results indicate that:

i. Over time, the change in water content and suction in a soil-geotextile column exposed to a constant temperature of 32°F and temperature gradient is 12% for silty clay versus 2.1% for sand. These differences are shown in Table 16.

ii. The temperature gradient has a greater effect on suction than water content, as indicated in Table 16

When the temperature gradient is reversed (66°F at the top and 32°F at the bottom of the column), the water content decreases and the suction increases at the top of the soil. In other words, when the temperature gradient is reversed, the trend for water content and suction distribution is also reversed. Table 17 shows the differences in water content and suction for the simulation with a temperature of 32°F at the top and 66°F at the bottom.

Table 16. Water content and suction differences between the column with a constant temperature of 32°F and the column with a temperature gradient after fifty days simulation.

	Suction difference at the top of the soil (%)	Water content difference at the top of the soil (%)
Sand	2.1	-1.4
Silty Clay	12	-0.1

Table 17. Differences in water content and suction head between the column with a temperature of 32°F at the top and 66°F at the bottom and the column with a reverse temperature gradient.

	Head difference at the top of the soil (%)	Water content difference at the top of the soil (%)
Sand	-3.4	2.1
Silty Clay	-62	0.34

Figure 66 and Figure 67 show the distribution of matric potential at a constant temperature of 32°F in sand and silty clay, respectively. As can be seen from these figures, the suction at the top of the soil after fifty days is approximately 68 psf for the sand and 78 psf for the silty clay. According to the hydraulic conductivity data presented in Figure 65, at suction values between 0.01 psf and 200 psf, the hydraulic conductivity of the silty clay changes less considerably than for the other materials. Thus, the change in suction shown in Table 16 does not have a significant effect on the hydraulic conductivity of the silty clay. As shown in Table 16, the suction difference at the top of the sand is less than that of the silty clay (2.1%), and although the hydraulic conductivity of the sand drops fast as the suction increases, a 2% difference in suction causes only a slight change in the hydraulic conductivity. The same scenario happens with a temperature gradient. Although 62% change occurs in the suction at the top of the silty clay between the temperature gradient simulation with a temperature of 32°F at the top and the simulation with a reverse temperature gradient, the hydraulic conductivity of the silty clay does not change significantly. In all of the simulations, the change in water content is very small (on the order of 10^{-2} to 10^{-4} ft^3/ft^3).

Although temperature does not appear to have a significant effect on the hydraulic conductivity of the soil, it can affect the hydraulic conductivity of the geotextile, because the slope of the hydraulic conductivity curve for the geotextile is relatively steep (Figure 65). As the temperature increases, the suction increases and, consequently, the hydraulic conductivity of the geotextile decrease. Although the suction difference is relatively insignificant, it can have a quantifiable impact on the hydraulic conductivity of the geotextile, especially at low suction. When the temperature is increased from 32°F to 100°F at the geotextile level, the hydraulic conductivity of the geotextile decreases from 6.2×10^{-6} to 3.0×10^{-6} ft/hr and from 8.8×10^{-6} to 1.6×10^{-7} ft/hr for the sand and silty clay simulations, respectively (maximum change in the hydraulic conductivity of the geotextile).

These results show that during desorption, when heat and water flow are in the same direction, the water content decreases and the suction increases throughout the soil-geotextile column. If the heat and water flow are in the opposite direction, the results will be vice versa. These changes have a minor effect on the hydraulic conductivity of the soils whereas they do change the hydraulic conductivity of the geotextile, which can affect the effectiveness of the moisture barrier. Consequently, in hot regions, a geotextile may have a lower water content and higher suction, which leads to low hydraulic conductivity, and therefore, the geotextile functions more efficiently as a moisture barrier.

Case 2: Capillary Rise

Case 2 simulations were performed to investigate the temperature effects on a soil-geotextile column under capillary rise conditions (upward water flow). The boundary and initial conditions are:

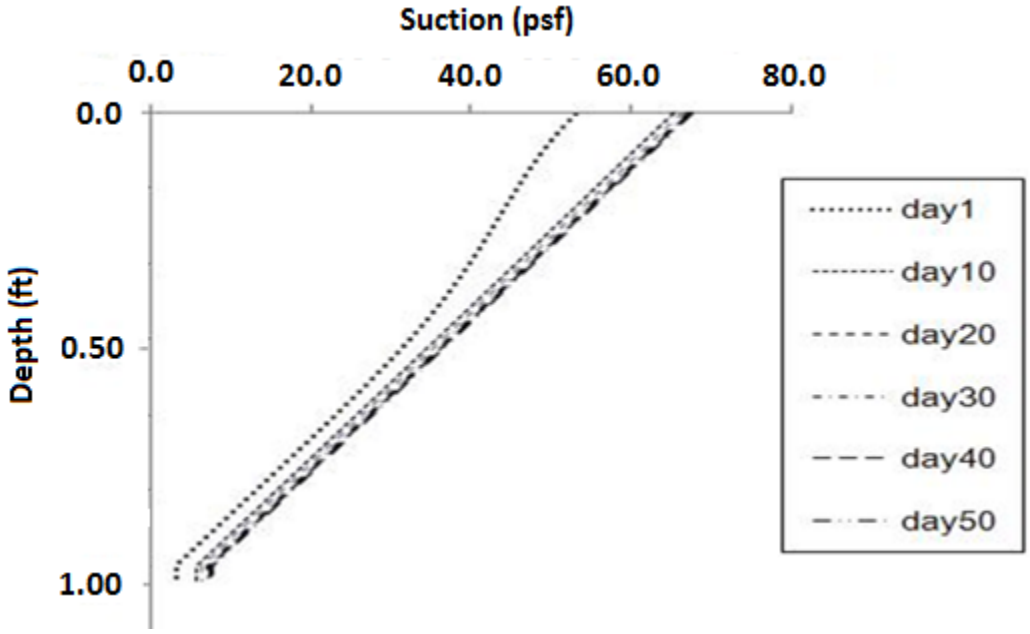

Figure 66. Graph. Suction distribution in sand-geotextile column (constant temperature 32°F).

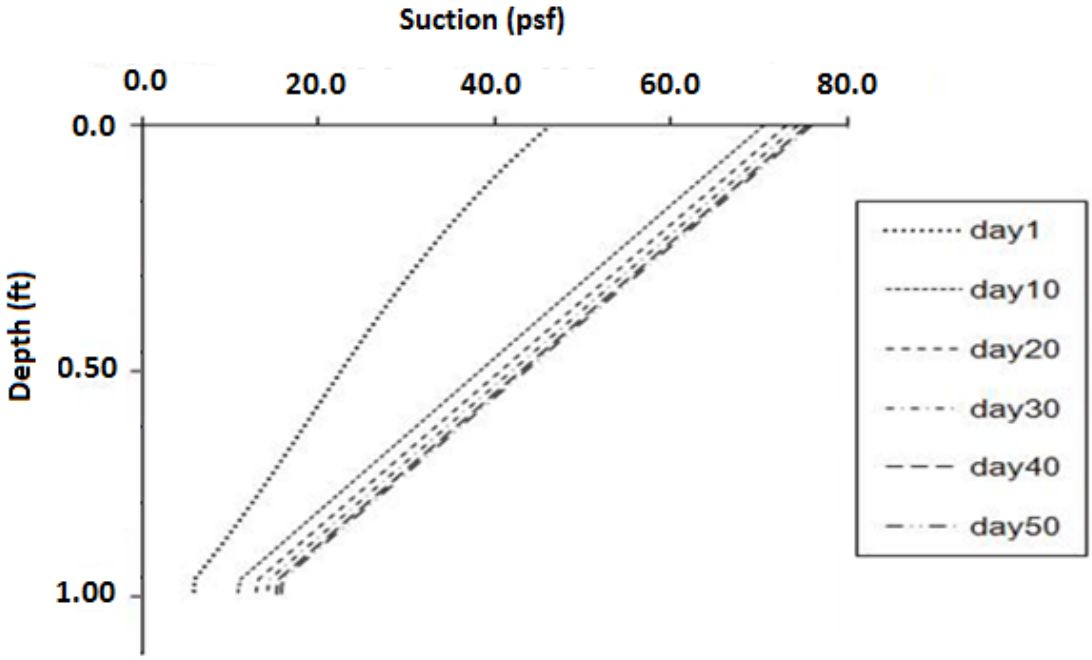

Figure 67. Graph. Suction distribution in silty clay-geotextile column (constant temperature 32°F).

no flux boundary at the top and along the side walls, constant pressure head of zero at the bottom, and heat and vapor flow allowed.

The geotextile was placed at the top of the profile. For the silty clay-geotextile column, an initial suction head of 32.81 ft (1,000 cm) was applied throughout the column, corresponding to a volumetric water content of 32 percent. For the sand-geotextile column, an initial suction head corresponding to a volumetric water content of 32% equals 0.21 ft (6.39 cm). For both soil-geotextile columns, the initial suction head of the geotextile was 32.81 ft.

In this series of simulations, upward water flow occurs due to capillary forces. The results show that changing the temperature from 32°F to 100°F has a slight effect on the water content and suction head profile throughout the soil column. However, the temperature conditions affect the suction head of the geotextile and the soil below it. Figure 68 and Figure 69 show the head differences when the temperature is increased from 32°F to 100°F in the silty clay and sand, respectively.

Unlike the drainage simulation, increasing the temperature decreases the suction head in the geotextile when water flows upward due to capillary rise. This phenomenon can be attributed to the magnitude of the saturation vapor pressure. In fact, saturated vapor pressure increases with increasing temperature, and thus, the moisture capacity of the soil increases, and the soil can absorb more water in the wetting process, which leads to a decrease in the suction head.

As can be observed from Figure 69 and Figure 70, increasing the temperature from 32°F to 100°F causes a 3.54 ft and 1.44 ft decrease in suction in the silty clay and sand, respectively (after 50 days). This decrease in suction leads to an increase in hydraulic conductivity. For the silty clay, the hydraulic conductivity of the geotextile increases from 4.9×10^{-14} to 1.21×10^{-11} ft/hr, and increases for the sand from 1.51×10^{-12} to 6.89×10^{-11} ft/hr with an increase in temperature from 32°F to 100°F. (Note: the values for the hydraulic conductivity are relatively small due to the initial suction of 32.81 ft in the geotextile). Thus, in contrast to the drainage simulation, under capillary conditions the geotextile functions more efficiently as a moisture barrier in cold regions. Because upward water flow is a concern in cold regions, this characteristic of the geotextile can help it to function better as a moisture barrier. Similar to Case 1 (drainage condition), temperature has only a slight effect on the suction head and hydraulic conductivity of the soils.

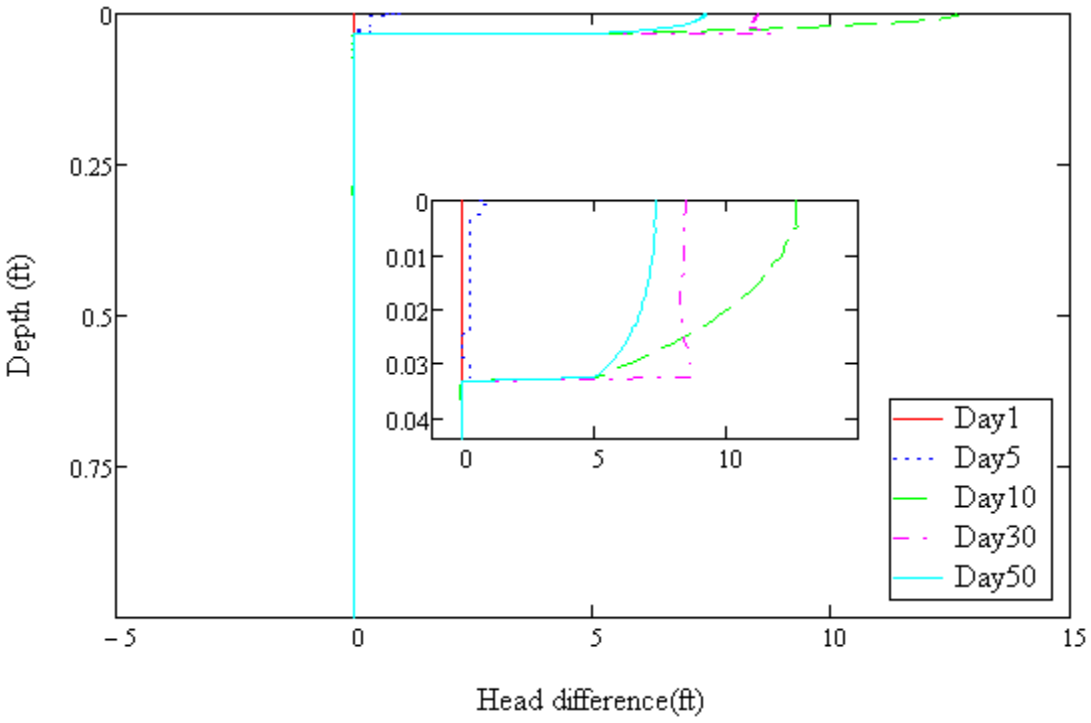

Figure 68. Graph. Head differences between constant temperatures of 32°F and 100°F for silty clay-geotextile column.

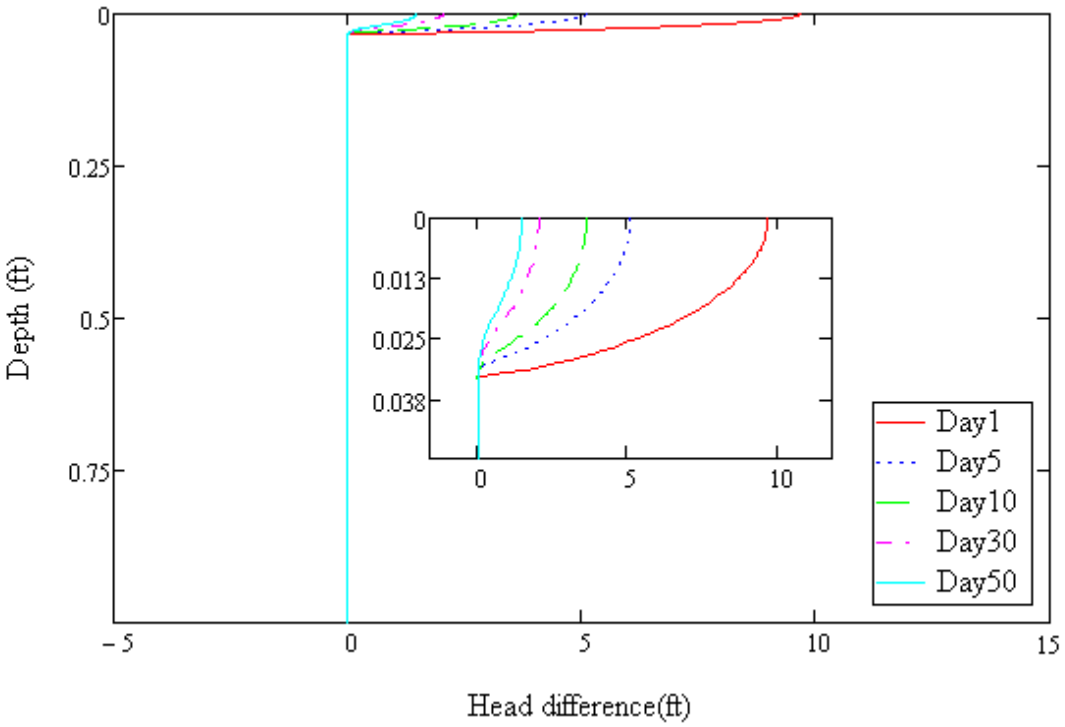

Figure 69. Graph. Head differences between constant temperatures of 32°F and 100°F for sand-geotextile column.

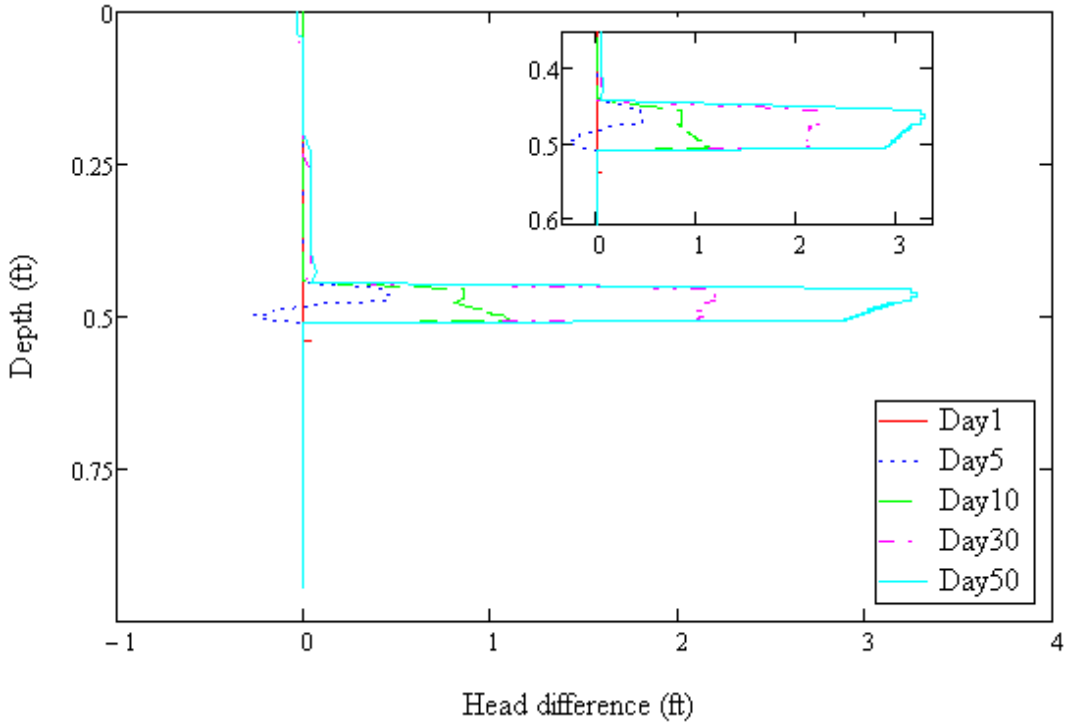

Figure 70. Graph. Head differences between 32°F versus 100°F for silty clay-geotextile column.

Case 3: Geotextile Embedded within Subgrade

For Case 3, the initial and boundary conditions are the same as for Case 2, but the geotextile layer is placed in the middle of the simulated column. The following observations are made based on the results:

i. Similar to the observations made for Cases 1 and 2, temperature does not significantly affect the water content and suction head in the soil column, except in the region immediately below the geotextile.

ii. Similar to Case 2, temperature conditions affect the suction head and hydraulic conductivity of the geotextile. Figure 70 shows the head differences between temperatures of 32°F and 100°F in the silty clay-geotextile column. In this case, increasing the temperature from 32°F to 100°F causes a 3.28 ft decrease in the suction head, which consequently increases the hydraulic conductivity of the geotextile and diminishes its function as a moisture barrier.

Summary

In conclusion, based on the assumed hydraulic and thermal parameters, the temperatures investigated in this study affect the suction head and hydraulic conductivity of the geotextile. Under simulated drainage conditions, where the geotextile is placed at the bottom of the profile and water moves downward due to gravitational force, the geotextile works better as a moisture barrier at high temperatures. Under simulated capillary conditions, where the geotextile is placed at the top of the profile and water moves upward due to capillary force, the geotextile works more efficiently as a moisture barrier at low temperatures.

(blank page)

CHAPTER 8 – TWO-DIMENSIONAL PERFORMANCE MODELING

The finite element computer program SIGMA/W is used in this research to model coupled seepage-stress analysis of a simulated roadway section that includes various moisture barrier configurations. The pore pressure distribution throughout the profile is examined with one and two DMBLs under various configurations that represent rainfall storms and gravity drainage. As noted earlier, a DMBL under unsaturated conditions functions more as a moisture barrier yet nonetheless exhibits some hydraulic conductivity, whereas in the saturated condition, it functions solely as a drainage layer. The analysis is focused on modeling conditions similar to those of the experimental testing in the large-scale test pit. Given the limited scope of the testing program, the modeling is used to understand the impact of key parameters on responses of the sections and to determine the appropriate configuration and properties for the DMBL to be used in actual road applications. The materials, profiles, initial and boundary conditions, and results of the sensitivity analysis on the hydraulic properties of the DMBL are presented.

Materials

Three materials are modeled in the simulations to represent an unpaved road profile: the ABC, the geotextile (the DMBL in this case), and the subgrade. The strength parameters for these three materials are shown in Table 18 (EICM 2006, SIGMA/W 2007). The ABC and subgrade (silty sand) materials are modeled as elastic-perfectly plastic, and the geotextile layer is modeled as a linear elastic material.

Table 18. Material properties assumed in the model for various layers (EICM 2006, SIGMA/W 2007).

Materials	Elastic modulus (psf)	Poisson's ratio	Unit weight (pcf)	Effective cohesion (psf)	Effective friction angle (degree)
Crushed stone	8,640,000	0.40	147	0	35
Geotextile	21,600,000	0.40	96	N/A	N/A
Silty sand	1,440,000	0.35	114	400	30

Figure 71 and Figure 72 show, respectively, the MCCs and hydraulic conductivity curves selected as representative of the three materials (EICM 2006, SIGMA/W 2007). The values for the strength and hydraulic parameters are chosen as typical values from GEOSLOPE and from the Enhanced Integrated Climate Model (EICM) database. Fiberglass hydraulic properties are used for the geotextile, crushed stone is used for the ABC material, and the subgrade layer is modeled as silty sand.

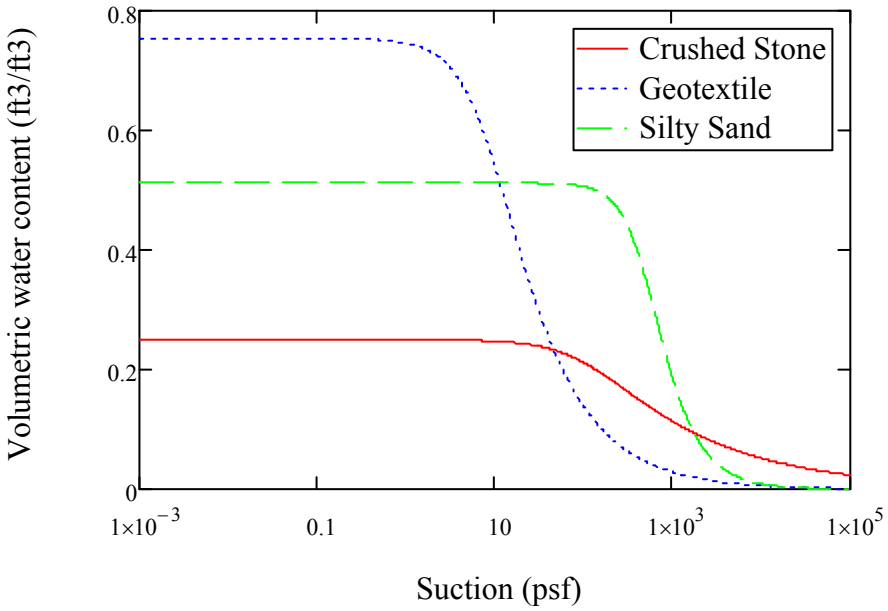

Figure 71. Graph. Moisture characteristics curves (EICM 2006, SIGMA/W 2007).

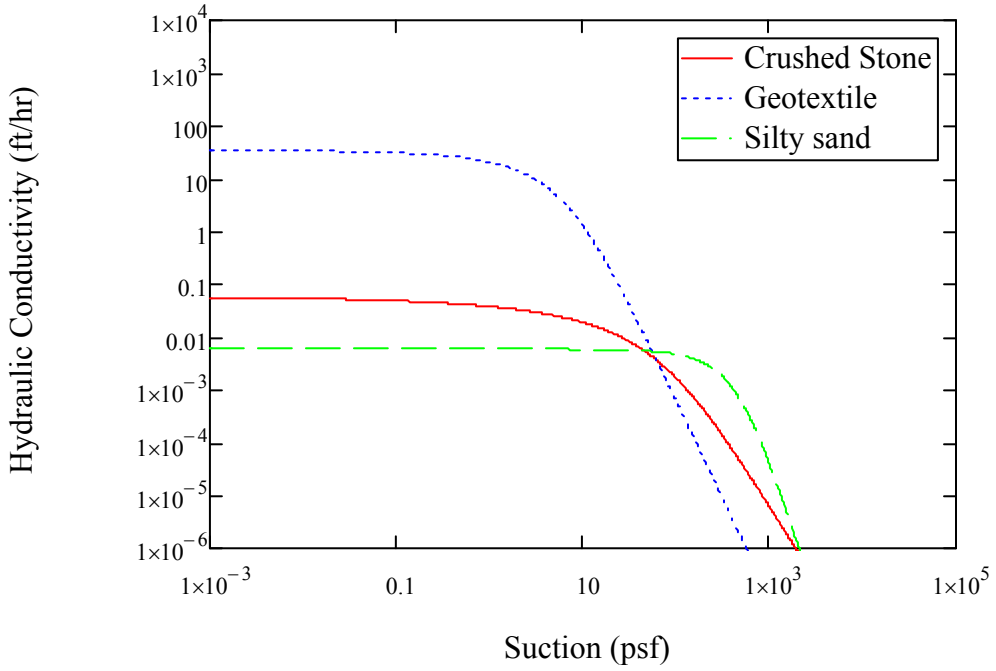

Figure 72. Graph. Hydraulic conductivity curves (EICM 2006, SIGMA/W 2007).

Modeling of Experimental Profile

The modeled experimental profile used to simulate the layers during laboratory testing is shown in Figure 73. The thicknesses of the ABC, geotextile, and silty sand layers are 1.5 ft, 0.01 ft, and 4 ft, respectively. Rectangular and triangular elements were used to discretize the domain. The layer of geotextile was used as the drainage/moisture barrier; i.e., it functions as either a moisture barrier or drainage layer depending on the developed pore pressure in it and in the adjacent soil layer. Very small elements were necessary to represent the geotextile layer due to its relative thinness. Some of these elements were as small as 0.003 ft, such that four nodes were located within the geotextile layer. Transition elements were used to increase the size of these elements for the remaining area of the mesh. Nonetheless, the model size is quite large (nearly 51,000 elements), and the run time took several days.

Other factors that affected the simulation time include the type of constitutive models used for the materials and the unsaturated condition of the layers. Initial simulations were performed to investigate the accuracy of the simulation results.

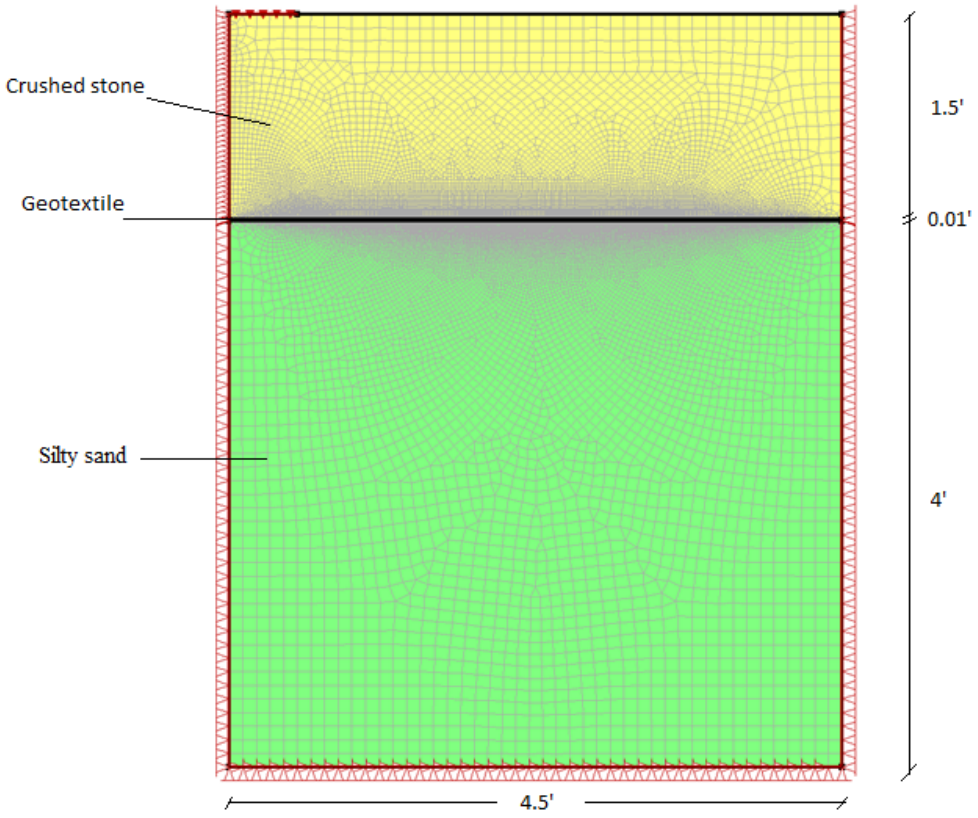

Figure 73. Graph. Discretized experimental profile.

A series of simulations was performed on a smaller profile to investigate the effects of applying more than one DMBL on the pore pressure distribution throughout the profile. Sensitivity analysis was performed on the hydraulic properties of both DMBLs to find the most appropriate configurations and properties to be used in a road section.

First Sets of Experimental Profile Modeling: Boundary Conditions

The first set of experimental simulations was performed in three stages:

1. *In situ* stress analysis due to body forces
2. Seepage-stress analysis under drainage conditions to achieve steady state
3. Seepage-stress analysis under loading conditions

In Stage 1, the soil was loaded under its own weight to model initial *in situ* stress. The water table was placed at the top of the profile to model a saturated profile. In Stage 2, water was drained at the bottom of the profile by gravity. Drainage was continued for 8 days to reach a steady state representing a general condition prior to the stress event (such as a rainstorm and/or rise in the water table.) In Stage 3, a stress equal to 10,080 psf (70 psi) was applied at the top of the profile 0.5 ft from the right-side boundary to represent tire pressure with a contact width and length of 0.4 m and 0.28 m, respectively. The following boundary conditions were applied during these modeling stages:

Stress-deformation boundary conditions:

- Zero displacement in the x direction for the right and left boundaries
- Zero displacement in the x and y directions for the bottom boundary
- Y-stress on 0.5 ft of the top right boundary

Hydraulic boundary conditions for Stages 2 and 3:

- Zero pressure head at the bottom of the profile (representing the groundwater table)
- No flow boundary condition at the left and right boundaries (except at the right side of the ABC and geotextile)

Different boundary conditions were used for the right side of the ABC based on the simulation type. (These boundary conditions are explained later for each set of simulations.) Three series of simulations were performed with two cases modeled for each series. Case 1 is a profile that contains a geotextile as the DMBL, and Case 2 is without a geotextile.

First Sets of Experimental Profile Modeling: Layers Oriented Horizontally for No Flow Boundary Condition for the ABC

In these sets of simulations, both the geotextile and ABC surfaces were oriented horizontally. The results show that during Stage 2 (the drainage stage), the water ponds above the geotextile and cannot drain from the ABC, leading to a high moisture content and low suction in the ABC. This occurrence is due to the no flow boundary at the ABC and the placement of the geotextile between the ABC and subgrade layers with low hydraulic conductivity under suction. As a result, applying the tire stress in Stage 3 led to higher displacement compared to the profile without the geotextile. This occurrence can be attributed to the effective stress (and therefore strength) of the ABC prior to application of the tire load. Negative pore pressure increases the effective stress and consequently the stiffness of the ABC, but quickly dissipates with ponding. This situation shows that the geotextile has a negative effect in terms of displacement and perhaps points out the importance of considering the drainage potential of the three layers as a system within the profile. However, in the field, water can flow laterally out of the ABC. To consider this scenario, a second series of simulations was performed

First Sets of Experimental Profile Modeling: Inclined Geotextile and Flat Surface: Potential Seepage Boundary Condition for the Right Side of the ABC

In this set of simulations, a special boundary condition, termed the *potential seepage boundary*, is used so that the ABC can drain water laterally. The geotextile is placed inclined at a slope of 4.4% to drain water outward due to the gradient. Nodes in the potential seepage boundary were reviewed after each iteration and modified based on the calculated results (SEEP/W v.5 manual). In other words, after each iteration the heads were calculated and the nodes at the boundary were checked to discern whether a seepage face had developed in the potential seepage boundary. In this simulation, ponding did not occur, and negative pore pressure was generated above the geotextile. However, the magnitude of the developed pore pressure above the geotextile was less than that which developed in the profile without the geotextile. Despite the fact that the geotextile was inclined and water could flow from the geotextile and ABC, the geotextile layer prevented water from breaking through, which led to less suction above it. The lower effective stress yielded more displacement. In order to simulate a condition that is closer to field conditions, the surface of the ABC also was inclined to prompt water flow from the ABC.

First Sets of Experimental Profile Modeling: Inclined Geotextile and Ground Surface: Potential Seepage Boundary Condition for the Right Side of the ABC

Previous results show that the inclination of the ABC surface has a slight effect on the suction generated above the geotextile layer. Figure 74 shows the pore water pressure contours at the end of drainage, with and without the geotextile.

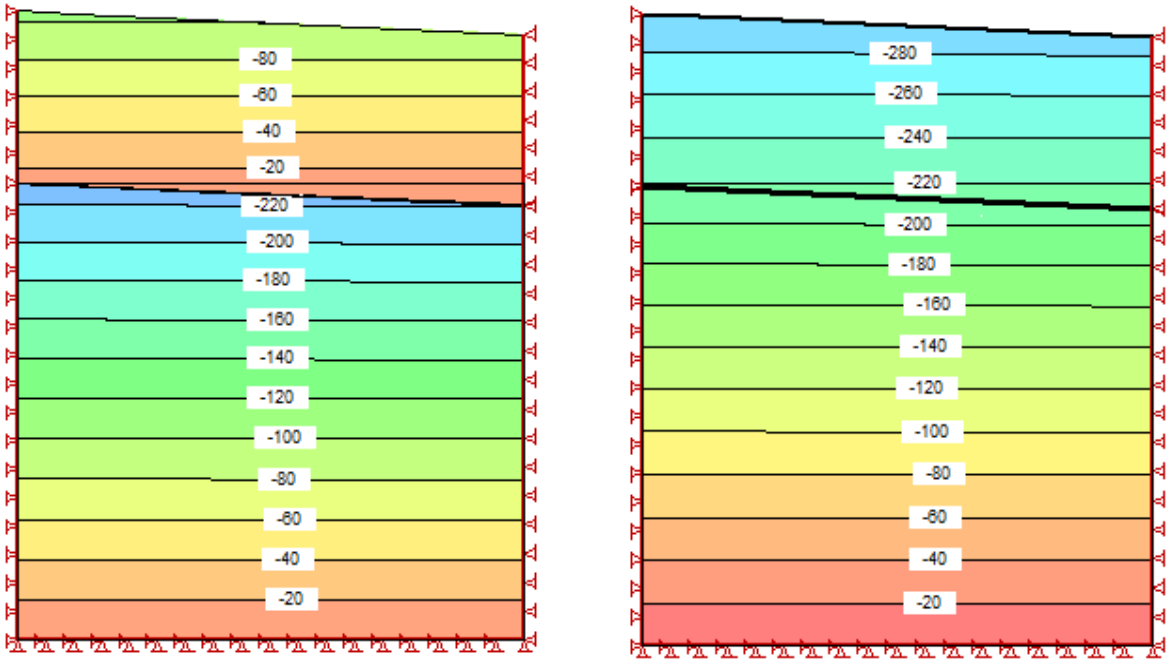

Figure 74. Graph. Pore pressure contours (psf) : (a) with geotextile and (b) without geotextile.

As can be seen in the figure, the inclusion of the geotextile decreases the suction above it. The effect of this built-up pore pressure above the geotextile on the vertical displacement is shown in Figure 75. In this particular initial condition (drainage before loading), the geotextile layer prevents downward water flow and decreases suction in the ABC, thus leading to more displacement. So, although the subgrade layer is protected from changes in moisture content, the ABC is affected by the increased saturation level if drainage does not occur at a sufficient rate to prevent the build-up of pore pressure.

Second Sets of Experimental Profile Modeling

The results of the second set of experimental profile simulations are presented here. The first set of simulations was performed to study the performance of the geotextile as a drainage/moisture barrier under drainage conditions. In the second series, only seepage analysis was conducted to study the performance of one DMBL in practical situations. The analysis was performed in three stages:

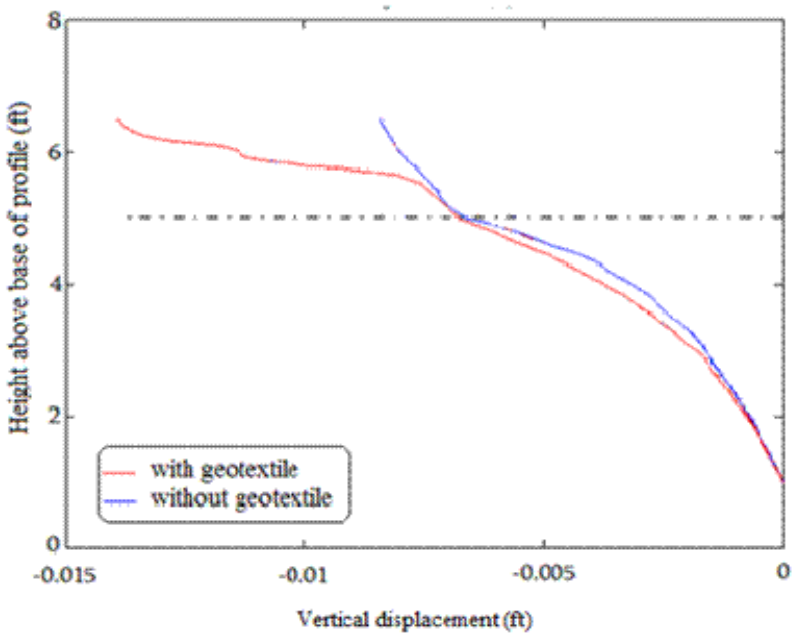

Figure 75. Graph. Deformations under the left edge of loading.

- *In situ* stress analysis due to body forces
- Seepage analysis: rainstorm for 24 hr
- Seepage analysis: drainage conditions for 24 hr

In Stage 1, the soil was loaded under its own weight to model initial *in situ* stress. The water table was placed at the bottom of the profile to model the groundwater table, and hydrostatic pressure distribution was initiated throughout the subgrade. A constant pore pressure (381 psf) corresponding to the optimal water content (~15%) was selected for the ABC. This pore pressure distribution in Stage 1 was selected to estimate the initial hydraulic conditions for Stage 2. Figure 76 shows the pore pressure distribution in Stage 1. In Stage 2, a constant water flux of 0.07 ft/hr was applied at the top of the profile to simulate a rainstorm. The rainstorm was continued for 24 hours. Then, in Stage 3, infiltration due to the rainstorm was stopped, and the pore pressure at the end of Stage 2 was selected as the initial condition for Stage 3. In Stage 3, water was drained from the bottom of the profile by gravity for 24 hours. The hydraulic boundary conditions for Stages 2 and 3 are as follows:

- Zero pressure head at the bottom of the profile (representing the groundwater table)
- No flow boundary conditions at the left and right boundaries (except at the right side of the ABC and geotextile layers)
- Potential seepage boundary for the right side of the ABC and DMBL.

In this set of simulations, both the DMBL and ground surface were placed inclined at a slope of 4.4 percent.

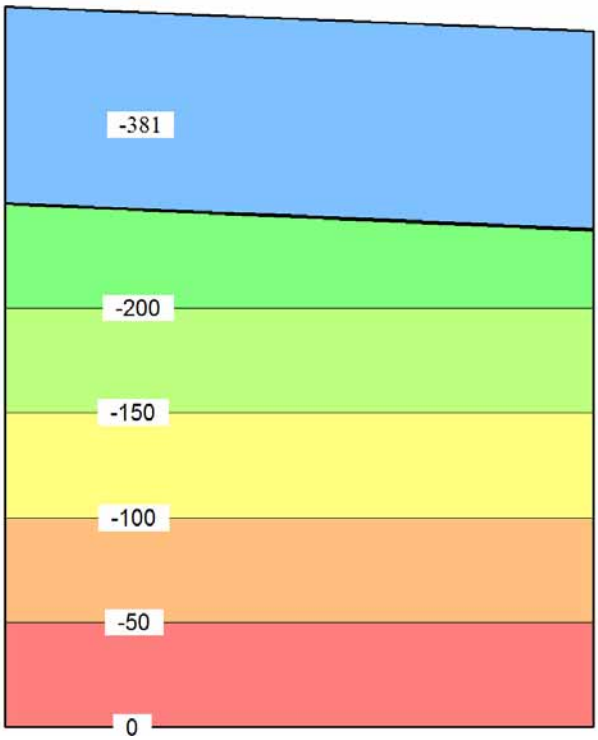

Figure 76. Graph. Pore pressure distribution in Stage 1.

Second Set of Experimental Profile Models: Stage 2

The pore pressure distribution at the end of Stage 1 (initial hydraulic condition for Stage 2) is shown in

Figure 77 after 10 hours of simulated rainfall. In this case, the pore pressure contours are approximately horizontal, which also holds for all the other simulation hours.

Figure **78** shows the pore pressure distribution along the centerline for Stage 2 and for the two cases (with and without DMBL) considered in the analysis. As seen in

Figure **78**, after five hours of rainfall, the inclusion of the DMBL has a small effect on the pore pressure throughout the profile. However, as the moisture front advances in the ABC, the presence of the DMBL changes the pore pressure distribution in both the ABC and the subgrade.

Under unsaturated conditions, the DMBL exhibits very low hydraulic conductivity and prevents water from breaking into the subgrade, leading to a decrease in suction in the ABC. Over time and with the increase in infiltration volume, the suction decreases and the hydraulic conductivity of the DMBL increases and, consequently, water can break into the subgrade and eventually exit the profile from the right edge of the DMBL. As a result, suction increases in the ABC and decreases in the subgrade.

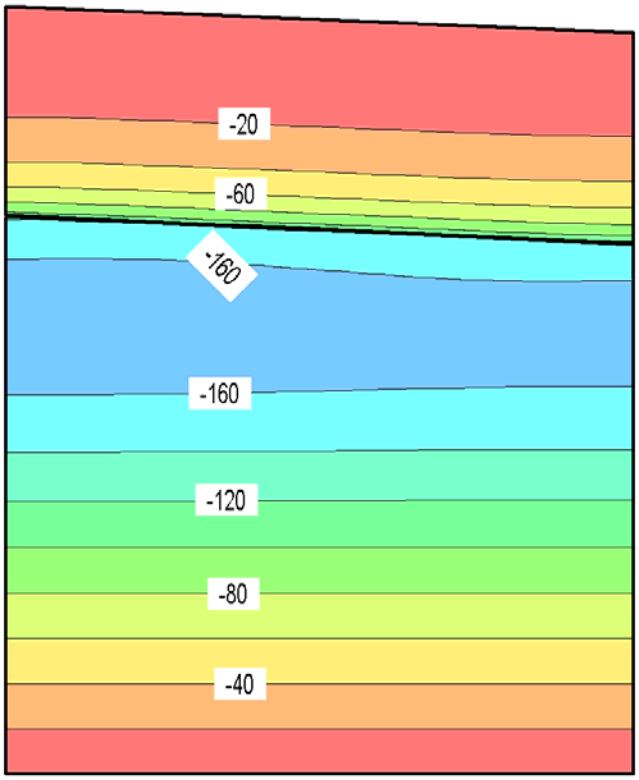

Figure 77. Graph. Pore pressure contours after 10-hr rainstorm.

Thus, given the initial and boundary conditions and the specified rainfall magnitude, the inclusion of one DMBL at the interface of the ABC and subgrade first decreases suction in the ABC. After approximately 16 hr, the suction in the ABC increases compared to the case without a DMBL. On the other hand, the presence of a DMBL increases suction in the subgrade during 24 hours of rainfall. The difference between the pore pressure profiles with and without a DMBL becomes smaller when the DMBL becomes saturated and water breaks into the subgrade. As the DMBL approaches saturation, it can drain more water from the ABC toward the edge drains. This occurrence leads to an increase in suction in the ABC and prevents increasing its degree of saturation. One important parameter that controls this feature of the DMBL is its AEV (i.e., the suction at which an initially saturated medium will first begin to desaturate).

The effect of changing the AEV of the DMBL on pore pressure distribution is considered later in this report. In the next section, results of Stage 3 are presented.

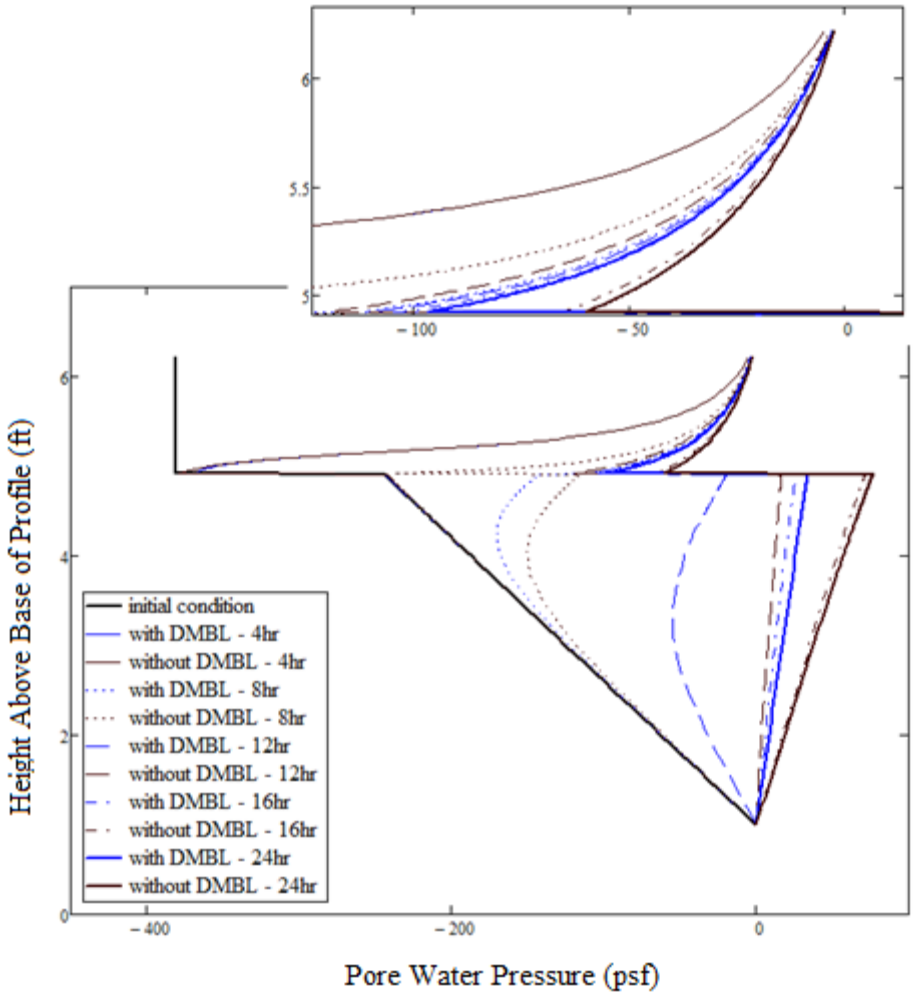

Figure 78. Graph. Pore pressure distribution along the centerline: Stage 2.

Second Set of Experimental Profile Modeling: Stage 3

In Stage 3 of the analysis, the initial hydraulic conditions of Stage 2 were employed, and water was drained from the bottom of the profile under gravity flow for 24 hours.

Figure 79 shows the pore pressure distribution for Stage 3 with and without a DMBL.

Data presented in

Figure 79 show that, after the 24-hr rainfall, inclusion of the DMBL leads to an increase in suction throughout the profile. In Stage 3, when water is drained under gravity, the DMBL becomes unsaturated, and its hydraulic conductivity decreases. Consequently, suction decreases in the ABC, whereas it remains higher in the subgrade as compared to the case without the DMBL. If the DMBL remains conductive under unsaturated conditions, moisture can be drained from the ABC, and its degree of saturation thereby decreases.

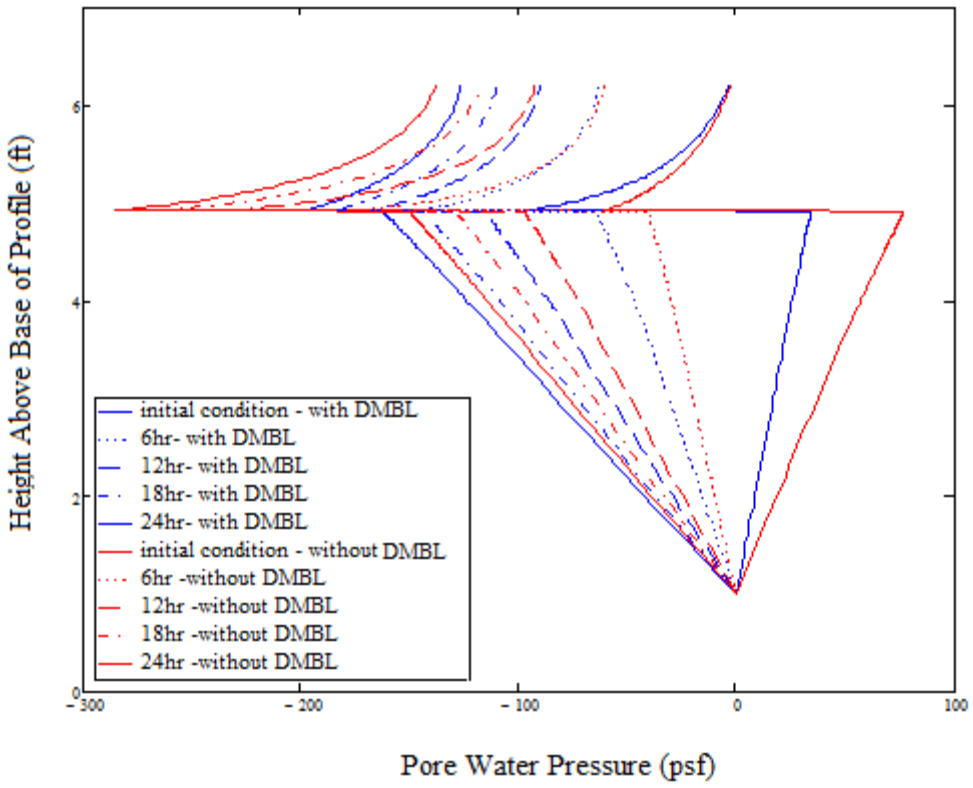

Figure 79. Graph. Pore pressure distribution: Stage 3.

Second Set of Experimental Profile Modeling: DMBL in the Middle of ABC

In the previous simulations, the DMBL is placed at the interface of the ABC and the subgrade. To study the effect of the location of the DMBL on pore pressure, here the DMBL is placed in the middle of the ABC. Figure 80 shows the pore pressure distribution during rainfall (Stage 2) for the case with a DMBL in the middle of the ABC and the case without a DMBL.

As the data in Figure 80 show, at the beginning of the rainfall event and after 2 hours, the suction above the DMBL decreases while it increases below the DMBL. The pore pressure magnitude does not change in the subgrade compared to the case without the DMBL due to the unsaturated hydraulic conductivity of

the DMBL, which is less than the unsaturated hydraulic conductivity of the ABC at the beginning of the rainfall event (see data presented in Figure 72). Over time, the unsaturated hydraulic conductivity of the DMBL increases faster than that for the ABC until it reaches a value that is higher than the hydraulic conductivity value of the ABC. Thus, the DMBL remains unsaturated during the rainfall event, and the hydraulic conductivity of the system is controlled by the unsaturated hydraulic conductivity of the ABC.

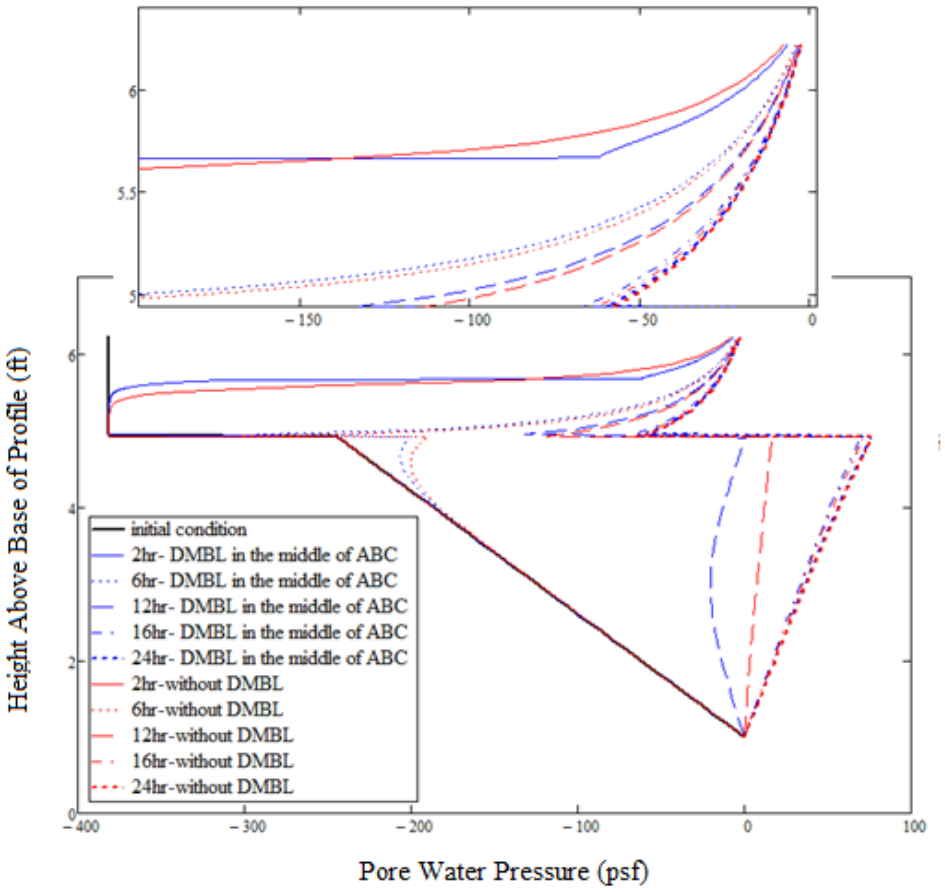

Figure 80. Graph. Pore pressure distribution: DMBL in the middle of ABC.

After reaching this state (after 16 hr), the DMBL does not affect the pore pressure distribution throughout the profile. Thus, given the initial and boundary conditions used in this simulation, placing the DMBL at the interface of the ABC and subgrade layers seems to be more effective than the other configurations, because this configuration leads to an increase in subgrade suction, and after about 16 hr, suction increases throughout the whole profile. In contrast, placing the DMBL in the middle of the ABC does not affect the pore pressure after 16 hr of rainfall. As mentioned previously, if the DMBL has a high conductivity under unsaturated conditions, the suction in the ABC and subgrade should increase during

rainfall and drainage. To investigate this assumption, DMBLs with different AEVs were modeled, and the results are presented next.

Second Set of Experimental Profile Modeling: Different AEVs for DMBLs

The AEV is the suction at which a porous matrix becomes unsaturated. Below that degree of suction, the DMBL is saturated and exhibits high hydraulic conductivity (close to its saturated hydraulic conductivity). Thus, by increasing the AEV, the DMBL remains saturated under high suction, and its hydraulic conductivity is close to its saturated hydraulic conductivity. Keeping all other parameters constant, increasing the AEV implies an increase in the WEV of the DMBL as well. Therefore, water can enter the DMBL – and, thus, the DMBL can function as a drainage layer – at high suction levels. In the Van Genuchten equation, the AEV is approximated by the $1/\alpha$ parameter, and a decreasing α value increases the AEV. In this simulation, three different AEVs were used for the DMBL: 3.76, 4.62, and 6.02 psf. Figure 81 and 82 show the soil water characteristics curves (SWCCs) and hydraulic conductivity curves for the DMBLs with the different AEVs, along with those for silty sand and crushed stone, respectively.

As shown in Figure 82, increasing the AEV increases the hydraulic conductivity of the DMBL under suction. In addition, the DMBL with a high AEV reaches its saturated hydraulic conductivity under higher suction. Thus, the DMBL with a high AEV exhibits higher hydraulic conductivity and conveys more water, both toward the edge drain and into the subgrade layer. Pore pressure distributions along the centerline of the profiles with different AEVs during a 12-hr rainfall event are shown in Figure 83. For up to 4 hours, the AEV does not affect the pore pressure distribution. After 4 hours, the higher AEV leads to less suction in the subgrade because the DMBL with the higher AEV causes more water to flow into the subgrade, and consequently, decreases the suction in the subgrade.

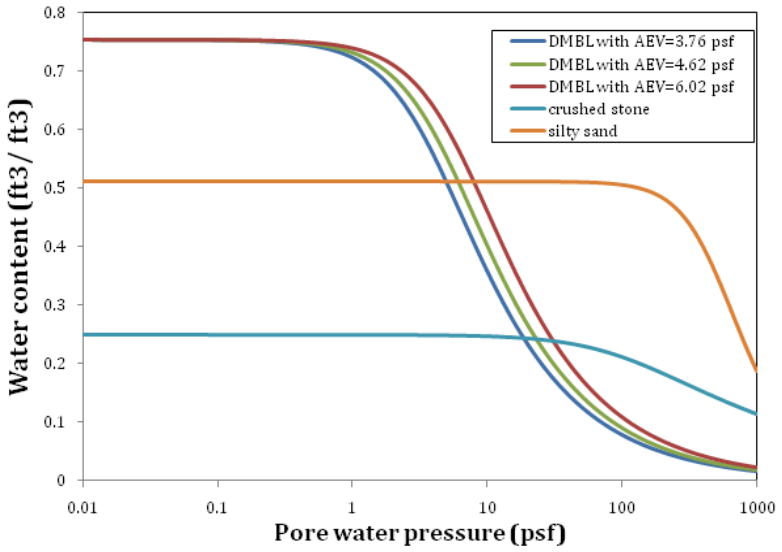

Figure 81. Graph. SWCCs for DMBLs with different AEVS

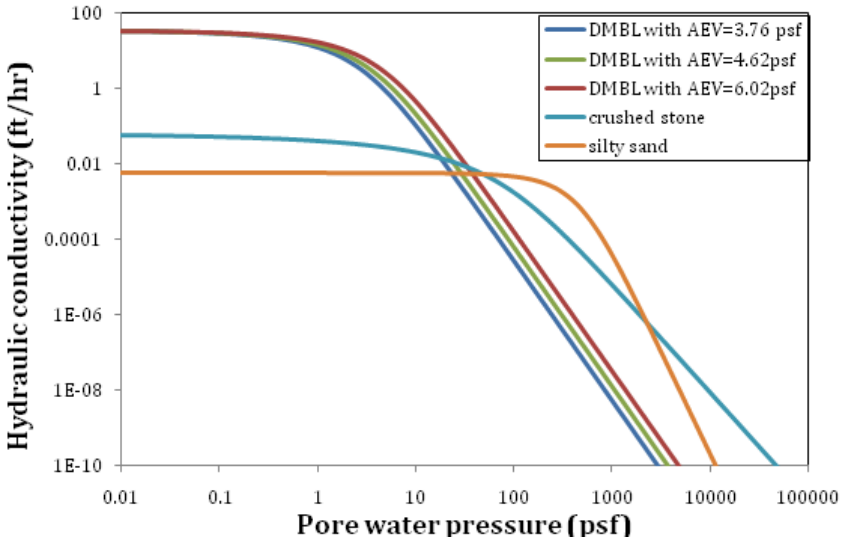

Figure 82. Graph. Hydraulic conductivity curves for DMBLs with different AEVS

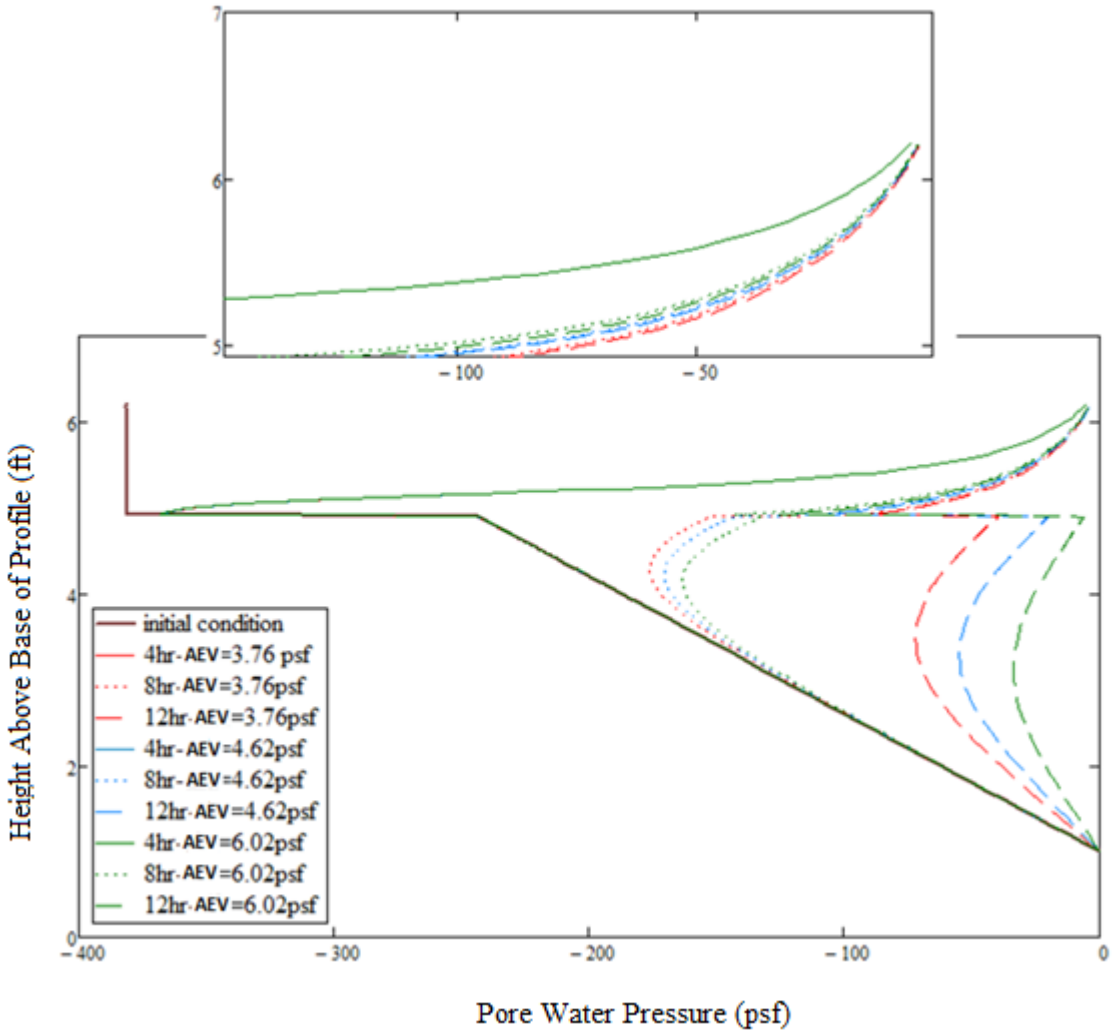

Figure 83. Graph. Pore pressure distributions for DMBLs with different AEVs.

This downward water flow into the subgrade causes a small increase in suction in the ABC. Thus, although a DMBL with a high AEV can drain more water from the ABC, it conveys most of this water into the subgrade because the cross-section area adjacent to the subgrade is much larger than the edge of the DMBL. Over time and with continued rainfall, the DMBL becomes saturated and functions as a drainage layer and conveys most of the rainfall from the ABC into the subgrade, and therefore, decreases the suction in the subgrade.

Figure 84 shows the pore pressure distribution after 24 hours. In terms of the continuation of rainfall, the pore pressure distribution in the profile is almost identical for all three cases. Accordingly, increasing the AEV increases the unsaturated hydraulic conductivity of the DMBL and, if the downward water flow into the subgrade can be eliminated or limited, the ABC can drain while the suction in the subgrade remains relatively unchanged. One possibility to eliminate downward water flow into the subgrade is to use a geomembrane below the DMBL.

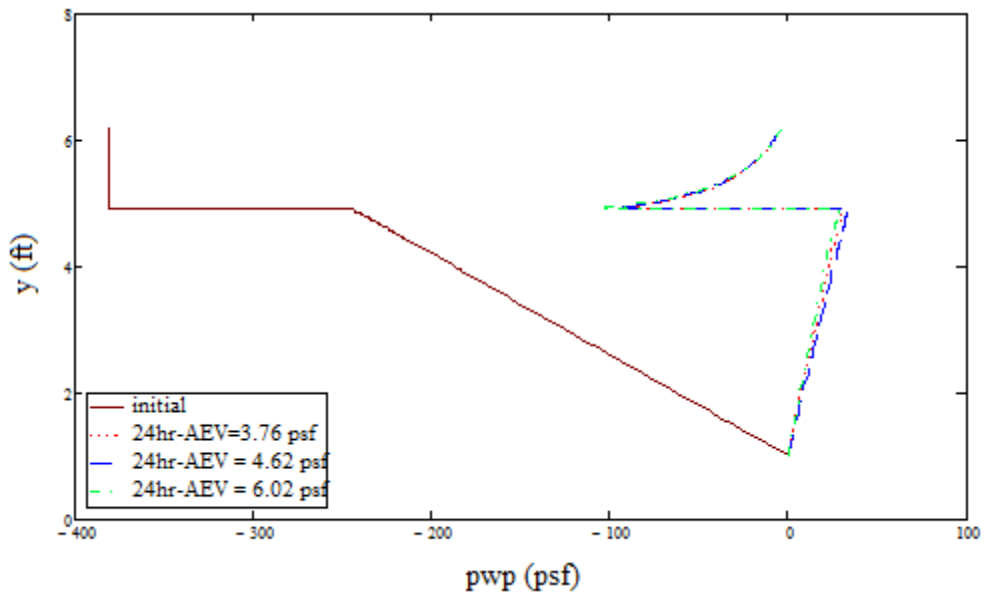

Figure 84. Graph. Pore pressure distribution after 24-hr rainfall event.

Second Set of Experimental Profile Modeling: DMBL Overlying a Geomembrane

To investigate the effects of placing a geomembrane underneath the DMBL, 6-in. thick crushed stone was modeled overlying a DMBL with an AEV of 6.02 psf. The boundary condition at the bottom of the DMBL was selected as a no flow boundary to simulate the geomembrane. The boundary condition at the right side of the ABC and DMBL is the so-called potential seepage boundary condition. Similar to the previous analyses, a flux of 0.07 ft/hr was applied at the top of the ABC to simulate rainfall. Figure 85 shows the pore pressure contours after 3 hours and 6 hours of rainfall.

In this case, using a geomembrane underneath the DMBL causes an accumulation of water and positive pore pressure above the DMBL because the water cannot break into the subgrade due to the presence of the geomembrane, and the DMBL does not have enough storage capacity and hydraulic conductivity to convey all the water coming from the ABC toward the edge for drainage. The hydraulic conductivity of the DMBL was then doubled, and simulations were performed. Figure 86 shows the pore pressure contours after a 6-hr rainfall event (0.07 ft/hr). Although doubling the hydraulic conductivity of the DMBL decreased the pore water pressure in the ABC, placing the geomembrane underneath the DMBL still generated positive pore pressure in the ABC. Thus, given the assumptions made in the analysis, conditions that include a geomembrane underneath the DMBL lead to build-up and positive pore pressure in the ABC.

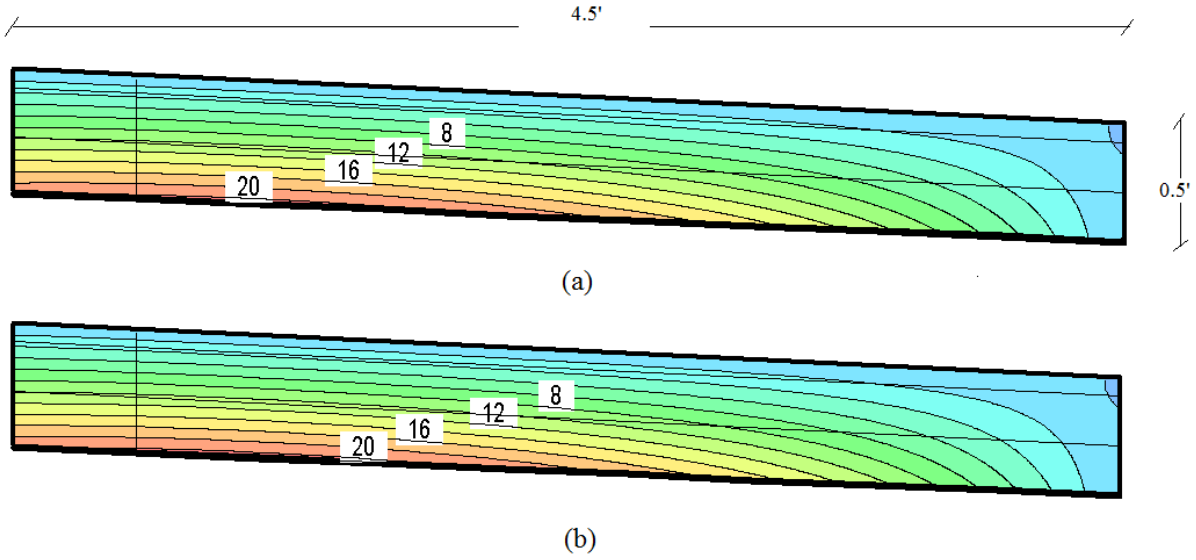

Figure 85. Graph. Pore pressure contours after: a) 3-hr, and b) 6-hr rainfall event.

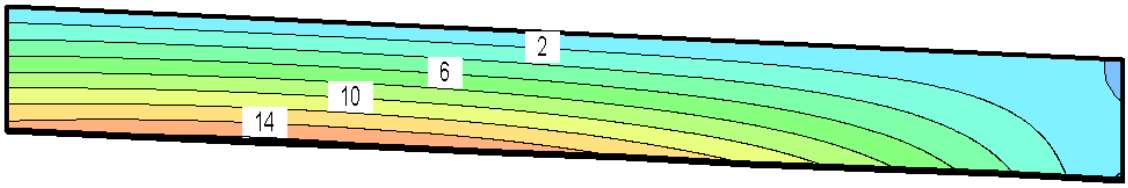

Figure 86. Graph. Pore pressure contours after 6-hr rainfall event: DMBL with doubled hydraulic conductivity.

A possible approach to decrease the positive pore pressure in the ABC is to place a second DMBL with a very low AEV, instead of placing a geomembrane, below the first DMBL. In this case, before the second DMBL becomes saturated, it functions as a barrier and prevents infiltration from decreasing suction in the subgrade. Once the second DMBL becomes saturated, it functions as a drainage layer, doubles the storage capacity and then its drainage capacity, and prevents the accumulation of water in the ABC. Small profiles were modeled to study the use of two DMBLs at the interface of the ABC and subgrade; this modeling is presented next.

Two-Layer DMBL Modeling

As mentioned previously, in order to model a DMBL, the layer is discretized using very fine mesh. In order to model two DMBLs, the mesh needs to be fine enough to overcome the mesh and time step

dependency problem. Adding one more DMBL to the experimental profile increases the number of elements to almost twice that of the original. Because the software cannot handle this number of elements due to memory capacity, a "small" profile was used. The dimensions of the small profile are shown in Figure 87.Similar to the previous analyses, the simulations for the small profile for two DMBLs were performed in three stages:

- *In situ* stress analysis due to body forces
- Seepage analysis: infiltration from rainstorm for 24 hours
- Seepage analysis, then a drainage condition for 24 hours

All the boundary and initial conditions are similar to those in the second set of experimental profile simulations. Four different AEVs (3.76, 6.02, 15.15, and 133.33 psf) were selected for the upper DMBL to study the effects of the changing hydraulic properties of the DMBL on its function as a drainage/moisture barrier. The first two AEVs are lower than the AEV of fiberglass (8.66 psf) and correspond to those of conventional geotextiles used for drainage purposes (i.e., those geotextiles that exhibit high hydraulic conductivity and low AEVs.)

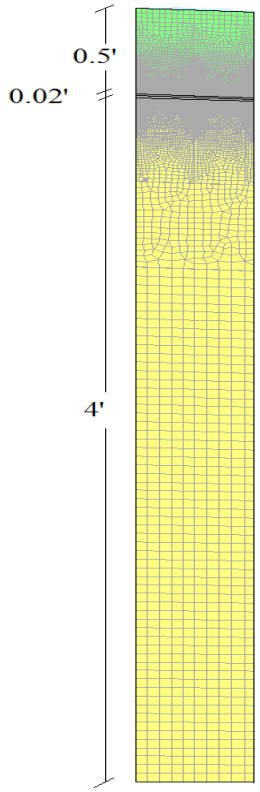

Figure 87. Schematic. Small DMBL profile.

The AEV of 15.15 psf corresponds to that of sandy soil that exhibits high hydraulic conductivity and high AEVs. Two types of sand and their properties were extracted from the UNSODA database and are shown in Table 19. The AEV of 133.33 psf is higher than the AEV of crushed stone (108.26 psf) and is chosen to study ways that a high AEV affects the functionality of the DMBL. For the lower DMBL, a relatively low AEV of 1 psf was selected to simulate a layer such as a geonet. Profiles with one DMBL and without a DMBL were simulated as well for comparative purposes.

Table 19. Properties of two sands (UNSODA 1999).

	θs	θr	AEV (psf)	n	K_s (ft/hr)	bulk density (pcf)	specific gravity
Sand-2562	0.274	0	27.78	1.865	37.8	121.7	2.65
Sand-2253	0.445	0.03	11.45	6.215	14.36	93.6	2.71
Grain Size Distribution (GSD)	**sand-2562**		**sand-2253**				
	Particle size (μmm)	**% finer**	**Particle size (μmm)**	**% finer**			
	2000	100	1000	100			
	50	1.1	50	10			
	2	0	5	4			

Two-Layer DMBL Modeling: Stage 2

In Stage 2, a flux of 0.07 ft/hr was applied at the top of the profile for 24 hours to simulate a rainstorm. Figure 88 shows the pore pressure distribution along the centerline of the profile with an AEV of 3.76 psf for the upper DMBL during the 24-hr rainfall event.

Using two layers increases the suction in the subgrade compared to a one-layer system and a profile without a DMBL. The lower layer functions as a barrier while it is unsaturated, and the upper layer of the composite section functions as a drainage layer because it has a higher AEV. Suction in the lower DMBL decreases over time and the DMBL starts to function as a drainage layer as well, thereby increasing the storage capacity of the DMBL.

These results show that the use of two DMBLs not only mitigates the breakthrough of water into the subgrade layer, but drains water from the ABC as well. Therefore, suction increases in the subgrade and does not change much in the ABC. In comparison, using a geomembrane underneath the DMBL causes positive pore pressure in the ABC.

Figure 89 shows the pore pressure distribution after 24 hours of rainfall in profiles with different AEVs for one and two DMBLs, as well as without a DMBL. In all cases with different AEVs, the suction increases in the subgrade with a slight change in the ABC as compared to the case with one DMBL or without a DMBL. The effects of using different AEVs for the upper DMBL on pore pressure distribution and the results for the profiles of a composite DMBL with different AEVs for the upper layer are shown in Figure 90

Figure 90 shows the effects of the AEV of the upper DMBL on pore pressure distribution. After 6 hours of rainfall, the profile with an AEV of 15.15 psf for the upper DMBL has the highest suction value in the subgrade. Except for the case where AEV = 133.33 psf, increasing the AEV of the upper DMBL increases the suction in the subgrade up to 7 hours of rainfall. Any change in the AEV of the upper DMBL has a small effect on the suction in the ABC compared to that of the subgrade. With continued rainfall and an increasing degree of saturation in the DMBLs, suction in the subgrade remains relatively constant with the changing AEV of the upper DMBL. Thus, given the boundary and initial conditions, increasing the AEV of the upper DMBL increases the suction in the subgrade during the early hours of rainfall (up to 7 hours). On the other hand, increasing the AEV of the upper DMBL more than the AEV of the crushed stone decreases the suction in the subgrade compared to the cases where the AEV = 15.15 psf and AEV = 6.02 psf.

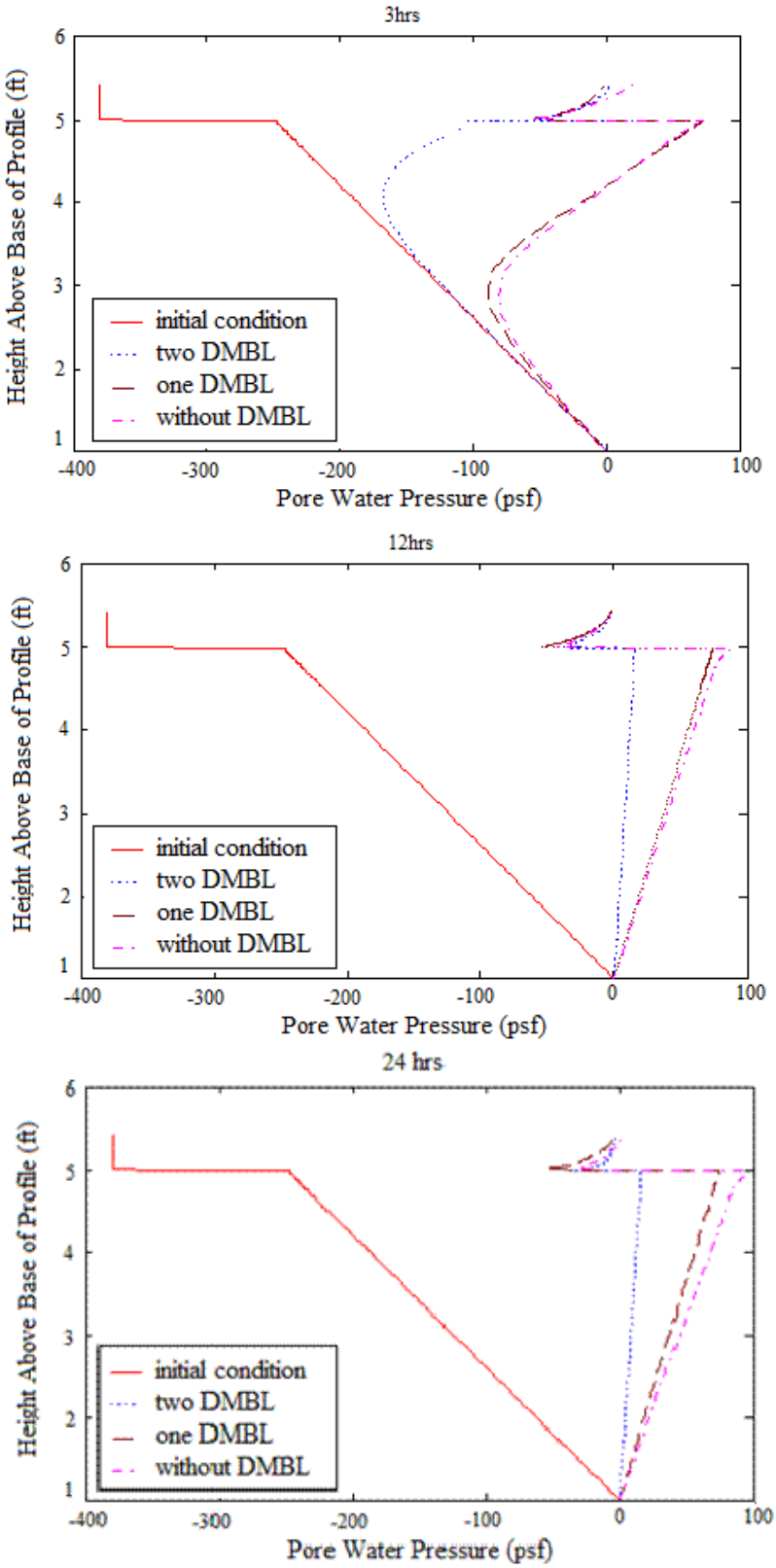

Figure 88. Graph. Pore pressure distribution for DMBL with AEV of 3.76 psf after: a) 6-hr, b) 12-hr, and c) 24-hr rainfall event.

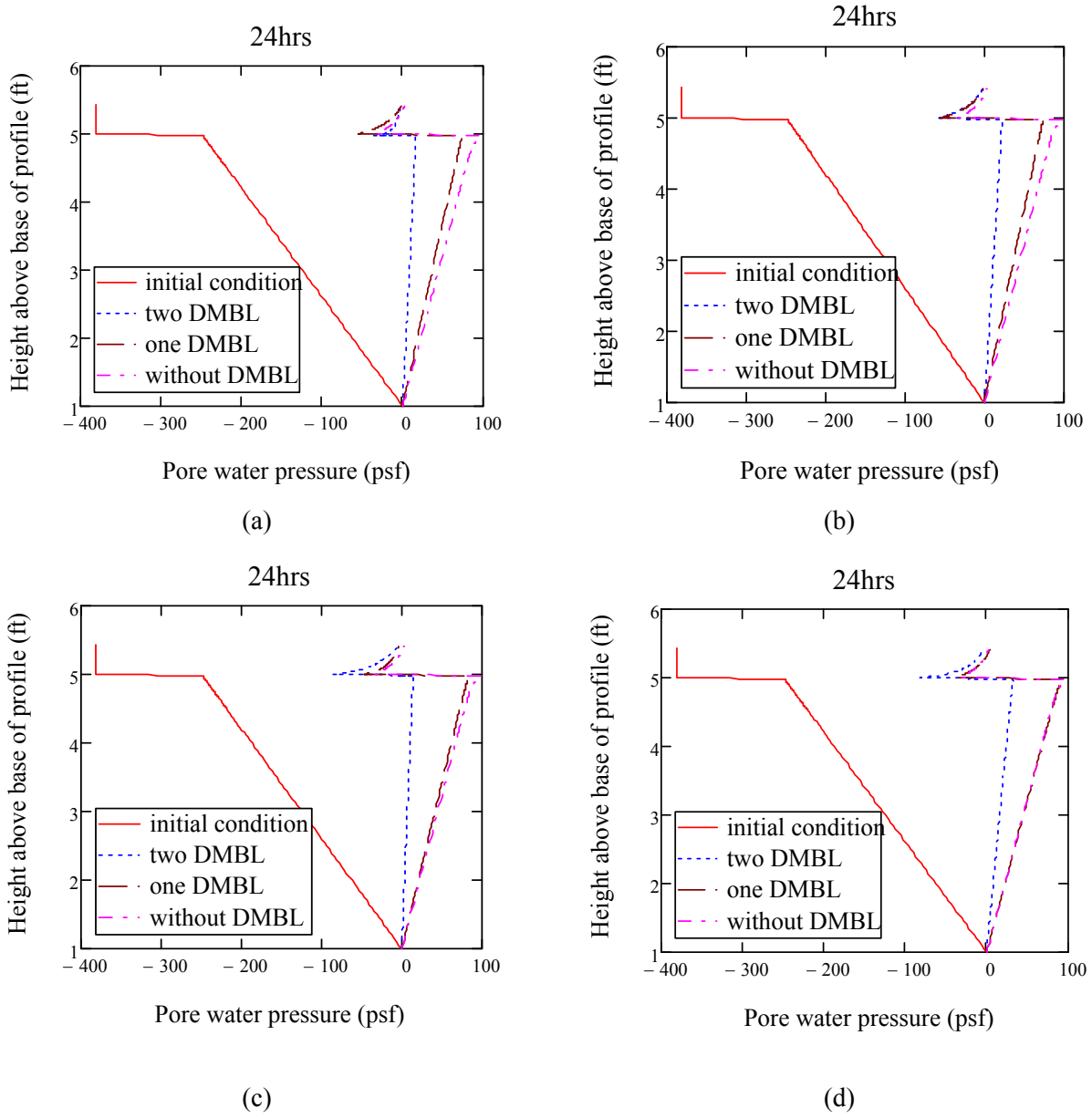

Figure 89. Graph. Pore pressure distributions after 24-hr rainfall event for the profiles with AEVs of: a) 3.76 psf, b) 6.02 psf, c) 15.15 psf, and d) 133.33 psf.

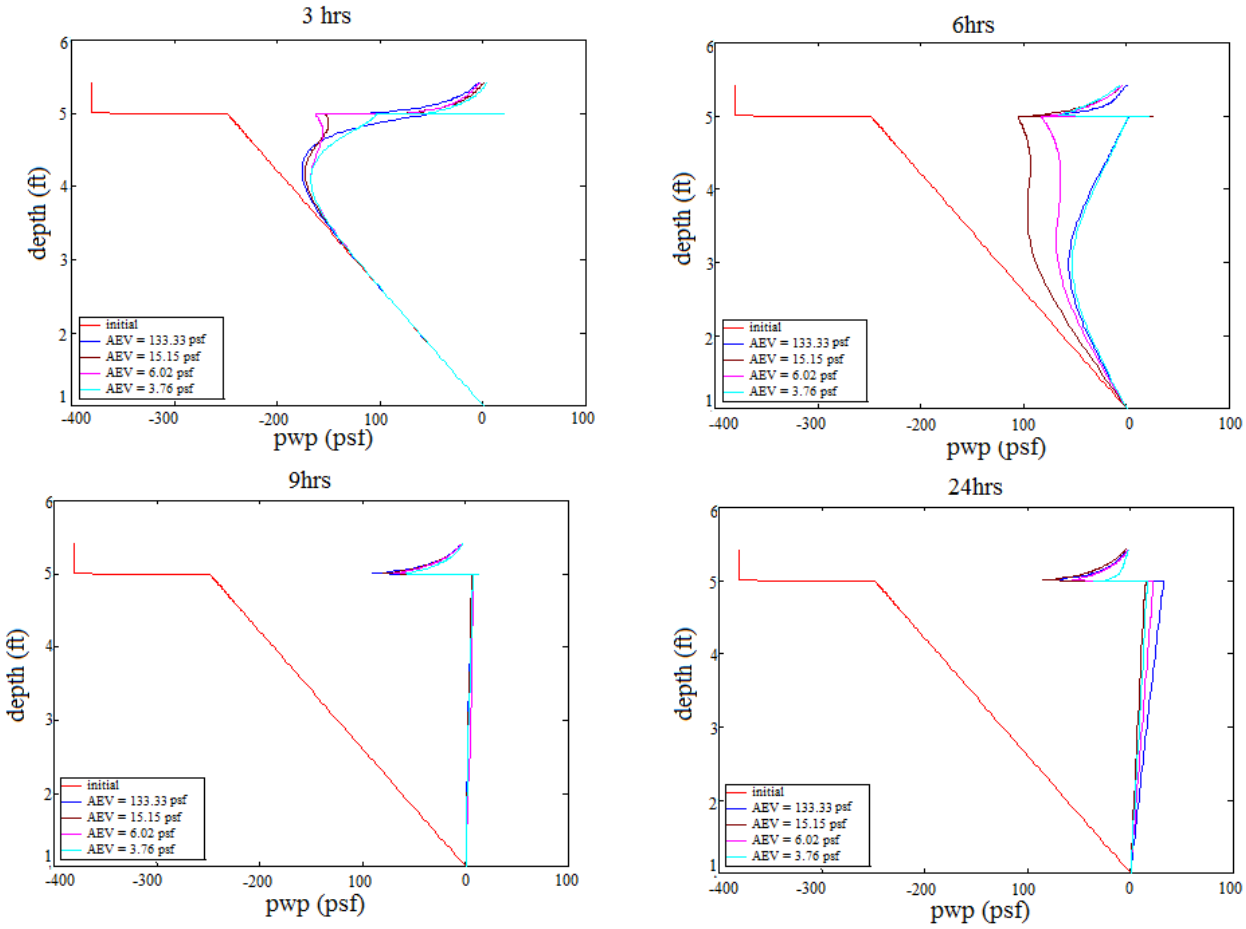

Figure 90. Graph. Pore pressure distribution for different AEVs of the upper DMBL.

The reason can be attributed to the hydraulic properties of the materials. Figure 91 shows the SWCCs and hydraulic conductivity curves for all the DMBLs as well as for the silty sand and crushed stone. When the AEV of the upper DMBL is higher than the AEV of the crushed stone, its WEV will be higher than the AEV of the crushed stone as well. Thus, once the water can leave the crushed stone it can enter the upper DMBL (at a suction of about 100 psf).

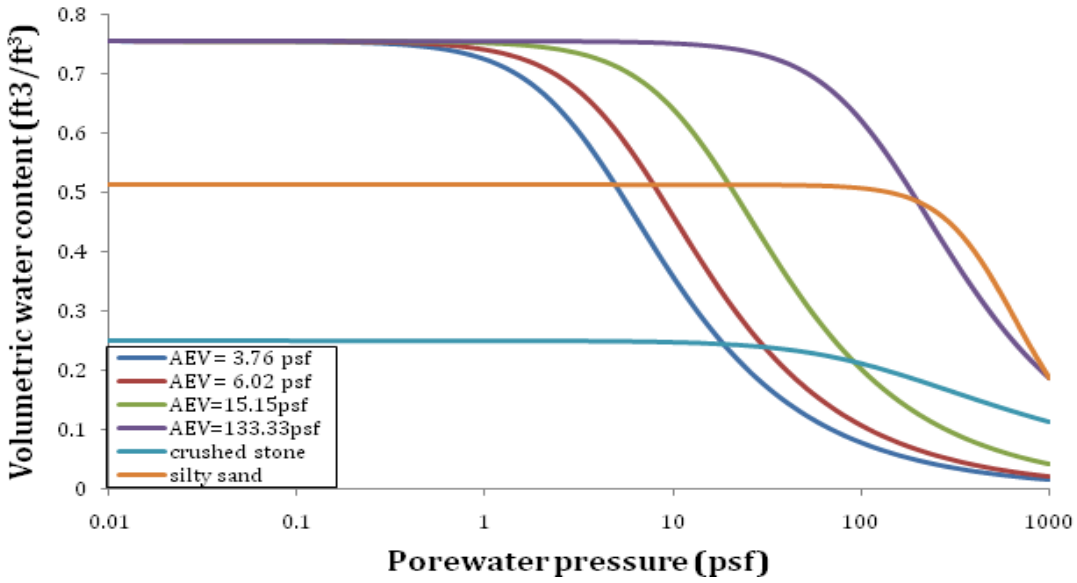

(a)

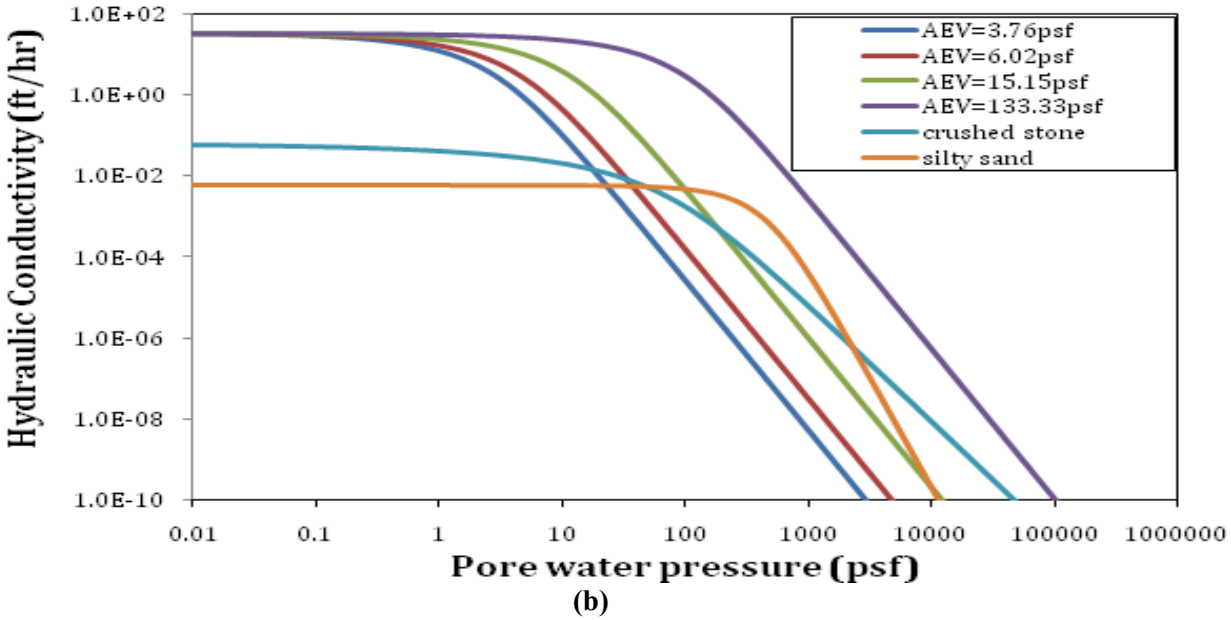

(b)

Figure 91. Graph. a) SWCCs and b) hydraulic conductivity curves.

As can be observed from Figure 91 (b), at a suction of 100 psf, the hydraulic conductivity of the upper DMBL is higher than the hydraulic conductivity of the crushed stone and is close to its saturated hydraulic conductivity. Thus, the upper DMBL conveys water toward the lower DMBL, but because its hydraulic conductivity is less than that for crushed stone, it remains unsaturated. As a result, water cannot drain from the edge of the upper DMBL (due to the imposed boundary condition) and water breaks into the lower DMBL. Once the pore pressure reaches the WEV of the lower DMBL, water flows into the lower DMBL and then toward the edge and into the subgrade. Consequently, the suction in the subgrade decreases. Therefore, increasing the AEV of the upper DMBL increases suction in the subgrade. However, if the AEV of the upper DMBL exceeds the AEV of the crushed stone (and also if the hydraulic conductivity of the upper DMBL is higher than the hydraulic conductivity of the crushed stone at a suction value equal to the AEV of the crushed stone), then the suction in the subgrade decreases. It should be mentioned that this observation depends on the selected boundary conditions in which outflow from the edge of the DMBL occurs only when the DMBL is saturated. If moisture outflow from the model domain is possible under unsaturated conditions, water may drain rather than infiltrate into the subgrade.

Two Layer DMBL Modeling: Stage 3

The pore pressure at the end of Stage 2 was selected as the initial condition for Stage 3, and water was drained under gravitational force. Figure 92 shows the pore pressure distribution for the different AEVs during 24 hours of drainage. Results indicate that changing the AEV of the upper DMBL has a small effect on the pore pressure distribution throughout the profile. In order to compare the results, the pore pressure distribution for two DMBLs, one DMBL (AEV = 3.76 psf), and without a DMBL is presented in Figure 93.

After 24 hours of rainfall, the profile with two DMBLs yields higher suction in the subgrade than the one in the profile that contains one DMBL or the one without a DMBL. Consequently, during the first hours of drainage (up to 9 hours), suction in the subgrade of the profile that contains two DMBLs is greater than the profile with one DMBL or without a DMBL (using only one DMBL does not change the pore pressure distribution in the subgrade compared to the case without a DMBL). The reason is that the lower DMBL has a low AEV, and as it becomes unsaturated under low suction values (~0.1 psf), its hydraulic conductivity decreases rapidly. Consequently, the lower DMBL prevents the downward water flow into the subgrade and increases the degree of saturation in the ABC. As shown in Figure 93, the ABC has the lowest value of suction, and the subgrade has the highest value of suction for the profile with two DMBLs. Although using two DMBLs decreases suction in the ABC, the pore pressure is still negative, and the ABC is under suction (~100 psf).

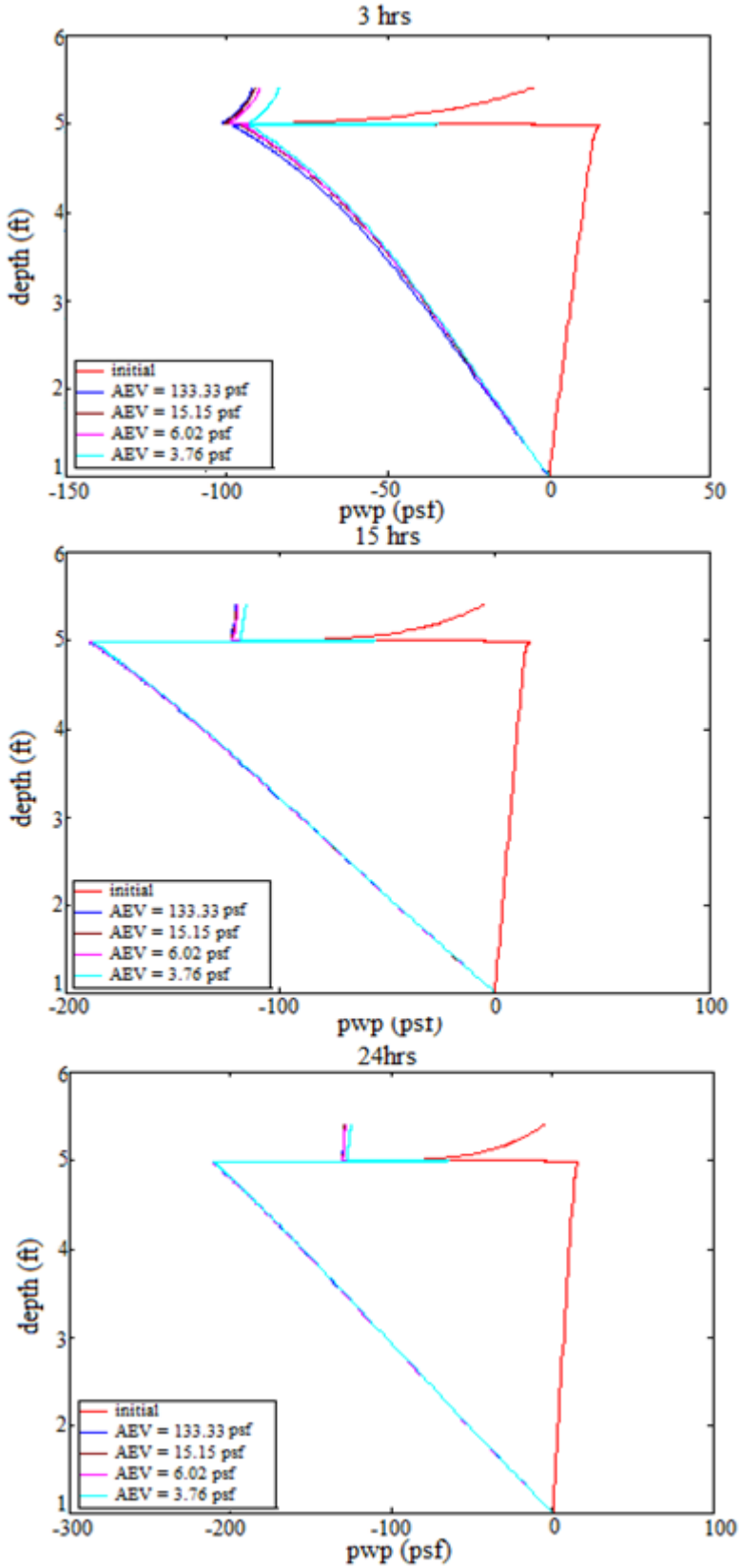

Figure 92. Graph. Pore pressure distribution during 24-hr drainage.

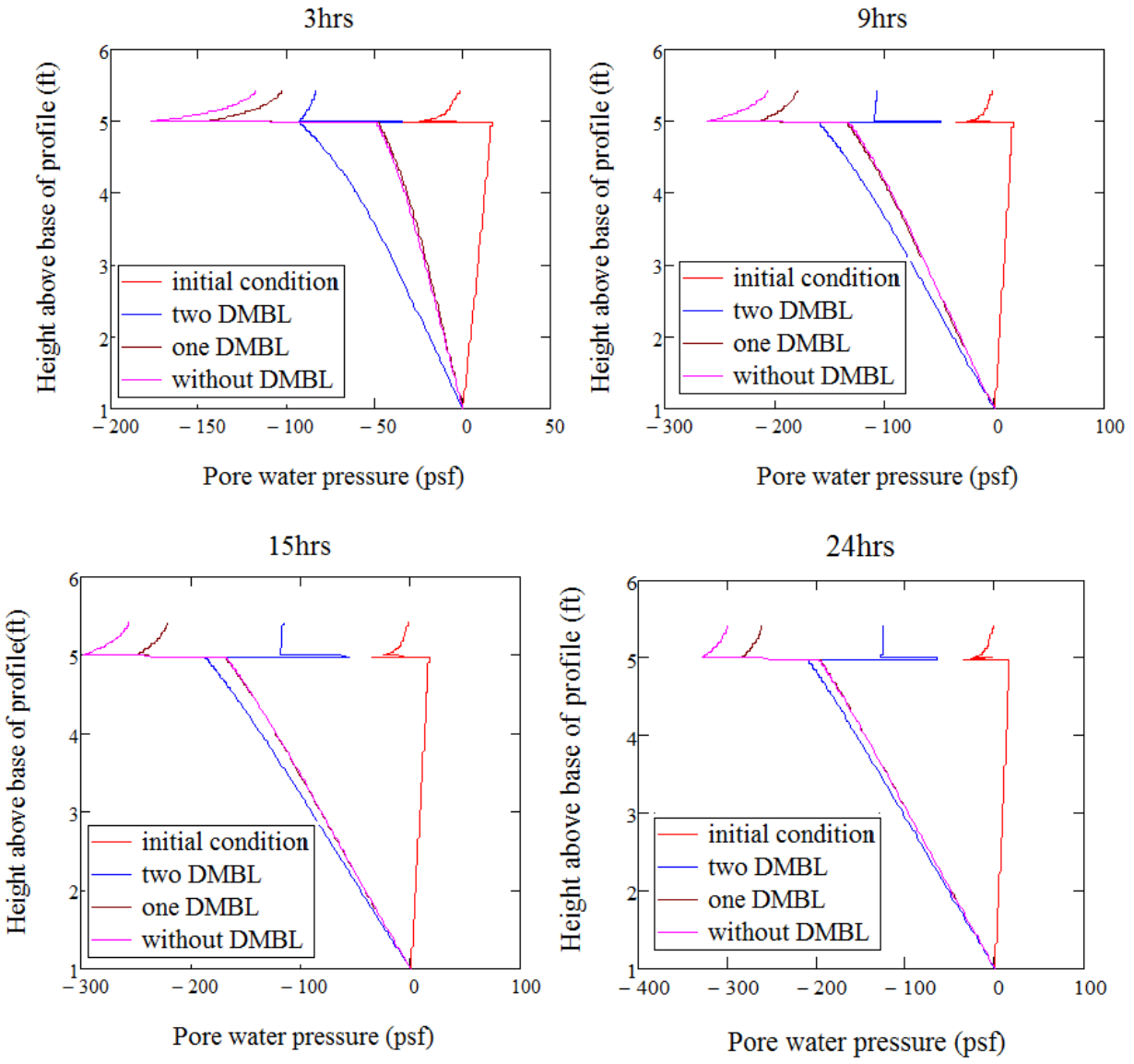

Figure 93. Graph. Pore pressure distribution: Stage 3.

Two-Layer DMBL Modeling: Decreased Rainstorm Intensity

In order to study the effects of rainfall intensity, the applied flux in Stage 2 was halved (0.035 ft/hr). With a decrease in rainfall intensity, the amount of water flowing into the ABC is not sufficient to saturate it. For the same reason, suction in the DMBL and subgrade increases, but both layers do not become saturated. Due to the boundary conditions on the right side of the ABC and DMBL, water cannot leave the profile either from the ABC or from the DMBL. Thus, after about 6 hours, the suction decreases throughout the whole profile, but the specified rainfall amount is not intense enough to cause saturation.

Water moves downward only, and the suction remains almost constant and low throughout the profile. This pore pressure distribution, however, is due to the type of boundary condition selected for the right sides of the ABC and DMBL. For a more realistic scenario, the ABC needs to drain water from its edge under unsaturated conditions. Unfortunately, this scenario is not a readily implementable lateral boundary condition in the current study due to the limitations of the software.

Two-Layer DMBL Modeling: Different Saturated Hydraulic Conductivity

In order to study ways that changing the saturated hydraulic conductivity (K_s) of the upper DMBL affects the moisture distribution throughout the profile, three saturated hydraulic conductivity values of 24.15, 34.15, and 44.15 ft/hr were selected with an AEV of 6.02 psf. Figure 94 shows the pore water pressure distribution along the centerline of the profile for these three saturated hydraulic conductivity values. The middle value is the K_s of fiberglass. Results indicate that changing the saturated hydraulic conductivity of the upper DMBL by 10 ft/hr has a minor effect on the pore pressure distribution. Recall that increasing the AEV of the upper DMBL from 6.02 psf to 15.15 psf increases the suction in the subgrade by about 45% during the first 6 hours of rainfall (Figure 90) due to the shape of the hydraulic conductivity curves for each case.

Figure 95(a) shows the hydraulic conductivity curves of a DMBL with an AEV of 6.02 psf and three different saturated hydraulic conductivity values, and Figure 95 (b) shows the hydraulic conductivity curves of a DMBL where K_s = 34.15 ft/hr and for two AEVs of 6.02 and 15.15 psf. To enhance clarity, the hydraulic conductivity is plotted in both arithmetic and logarithmic scales. Changing the saturated hydraulic conductivity changes the hydraulic conductivity at low suction values (<2 psf), whereas high AEVs cause greater hydraulic conductivity under high suction. Based on the results presented previously, during rainfall events and when water infiltrates the lower DMBL, the upper DMBL becomes unsaturated and remains under suction for most of the analysis (~ 5 to 60 psf). Thus, changing the saturated hydraulic conductivity and, consequently, the hydraulic conductivity of the upper DMBL under low suction, does not have a significant effect on the pore water pressure distribution.

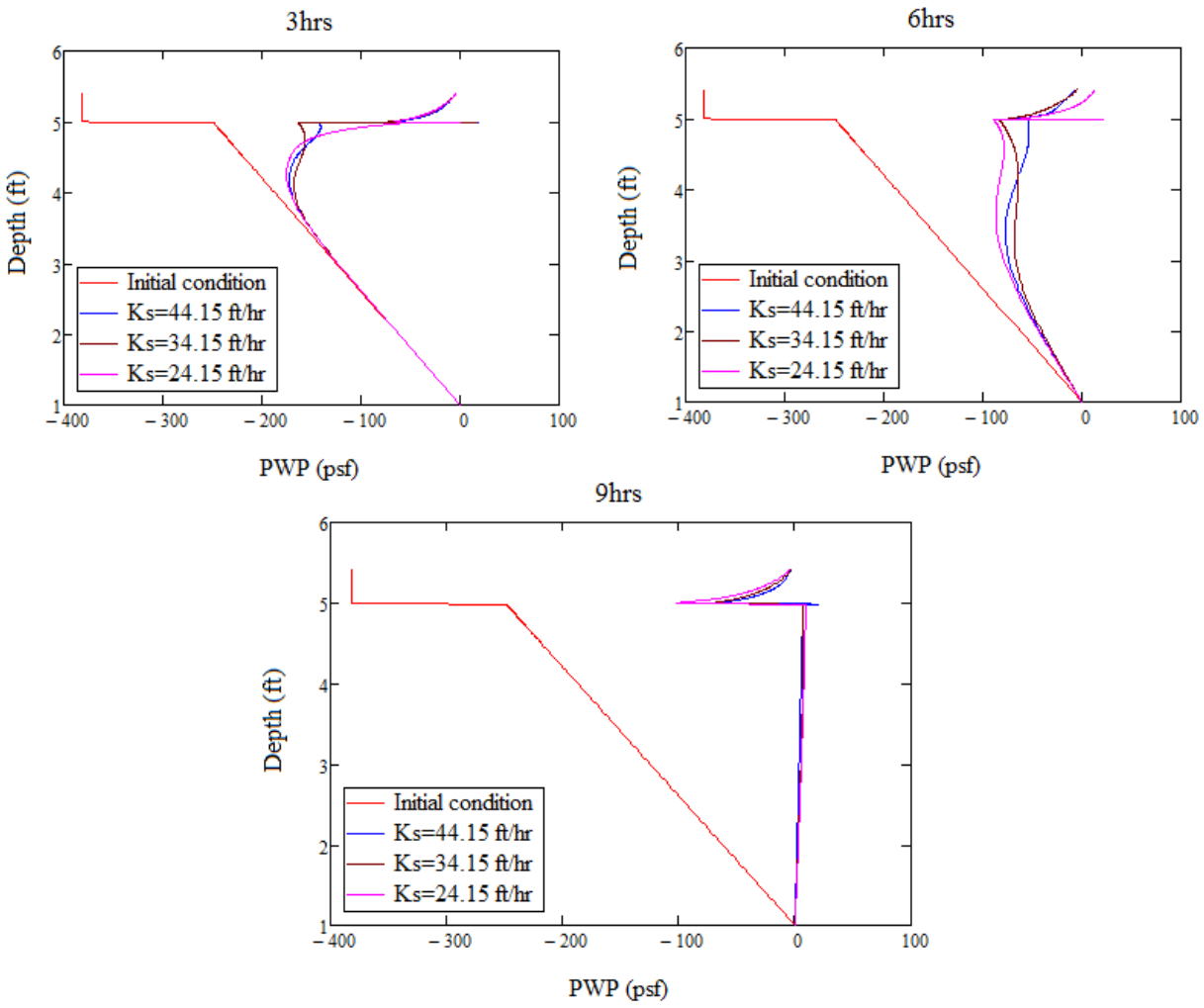

Figure 94. Graph. Pore water pressure distributions for different saturated hydraulic conductivity values.

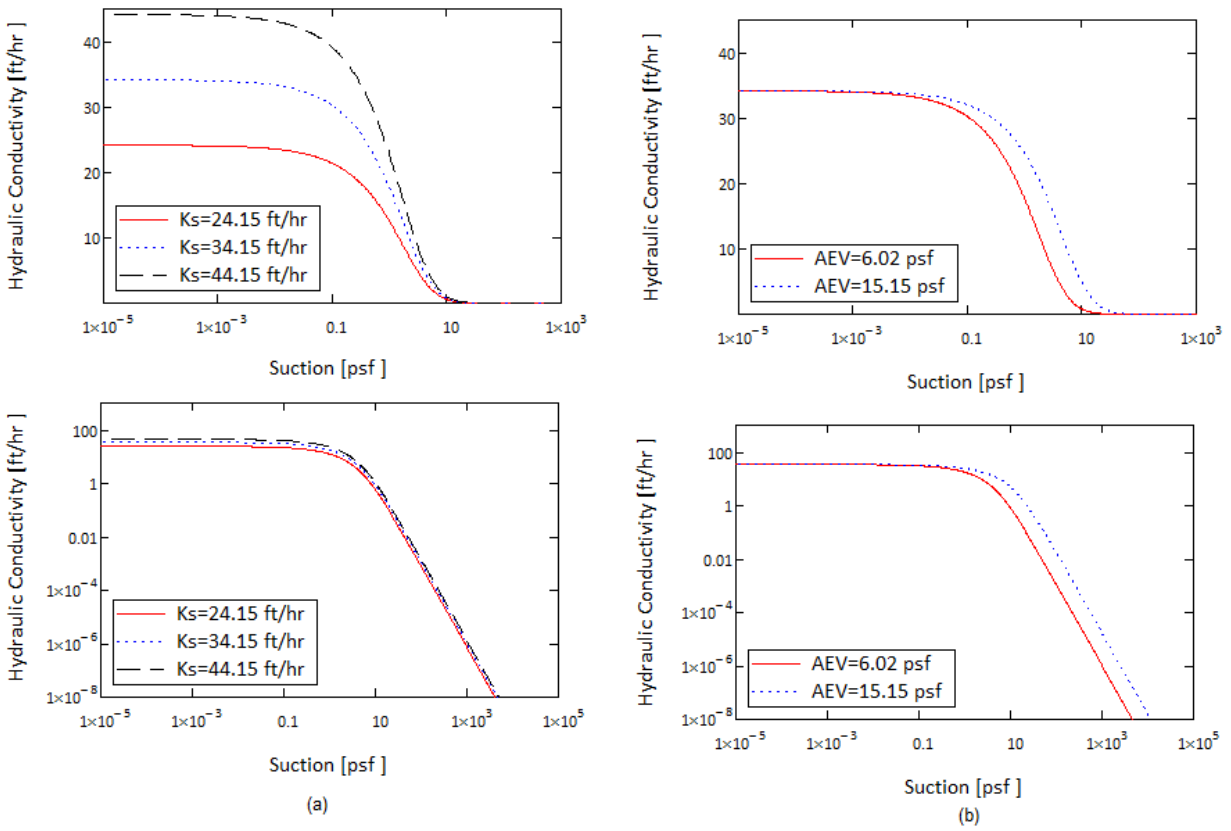

Figure 95. Graph. Hydraulic conductivity curves for: a) different saturated hydraulic conductivity values, and b) different AEVs.

CHAPTER 9 – CONCLUSIONS AND RECOMMENDATIONS

The main objective of this study is to develop recommendations to guide and advance the use of geosynthetic materials as moisture barriers in roadways over soils that are susceptible to volume change due to moisture variations. The study plan encompasses large- and small-scale testing programs and modeling. The scope of the large-scale experimental testing is limited to two tests due to budget constraints. The experimental program is used to obtain data for the analytical model and further study the performance of DMBLs under controlled conditions. The modeling work is aimed at providing systematic data to explain the performance of DMBLs in roadway sections, and then to use these data to propose guidelines to assist in the design of DMBLs.

In this study, the material properties of a fiberglass geosynthetic were measured and compared to data reported in the literature. A composite DMBL was tested in a large-scale test pit for its ability to prevent water from entering the subgrade of a simulated road section. Cyclic loading of the simulated sections, with and without a DMBL, was performed. Based on the findings of this study, the following conclusions are advanced:

1. The small-scale testing performed in this research confirms the results of Stormont and Ramos (2004) with regard to the unsaturated properties of TGLASS material. The Van Genuchten α value for the drying curve is found to be 0.13 psf^{-1} compared to 0.1 psf^{-1} measured by Stormont and Ramos (2004).The value for the wetting curve is determined to be 0.12 psf^{-1} and is approximately the same as the value measured by Stormont and Ramos (2004). The TGLASS material is deemed to be the most appropriate material for a transmission layer due to its ability to convey water under unsaturated conditions. However, it is approximately 5 to 10 times more expensive than traditional polymeric geotextiles used in drainage applications.
2. Data are lacking regarding the unsaturated properties of geotextiles. The interpretation of data reported in the literature suggests a range of AEVs from 7 psf to 33 psf for a variety of products, with these values obtained using a variety of testing approaches. The reliability of such data is not clear, as several parameters, such as thickness and/or Apparent Opening Size (AOS) often were not reported. Yet the performance of the DMBL in a roadway section is highly dependent on the proper selection of the AEVs of the system layers.
3. The limited results from the large-scale testing confirm the performance of the DMBL in a simulated road section. Results show its ability to prevent the infiltration of water into the subgrade during rainfall events.

4. The DMBL system's performance under loading shows that roadway sections that include a DMBL exhibit less deformation than a control section with similar soil properties, although it is not clear whether the improvement in the performance is due to the effect of the moisture control or the reinforcement effect of the DMBL, or a combination of the two. However, the TGLASS geotextile used in the DMBL system is not traditionally used for reinforcement.
5. After seven days of static loading, the simulated roadway control section (without a DMBL) yields measured displacements on the order 0.9 in., and the section with a DMBL yields measured displacements on the order of 0.1 in. Displacements observed during the application of rainfall events also are larger in the control section than in the section that contains a DMBL. From the measured displacements, it appears that the DMBL section installed at the interface of the ABC and subgrade layers improves the performance of the road section. The results, however, should be viewed in conjunction with the assumptions, conditions and properties used in this study.
6. Simulations performed using UNSAT-H to model heat and vapor flow indicate that a change in temperature from 32°F to 100°F affects the hydraulic conductivity of the geotextile, with no significant effect on the hydraulic conductivity of the soil. Although the conductivity of the geotextile is not a direct function of temperature, it is a function of suction. When the geotextile is placed at the bottom of the profile and water moves downward due to gravitational force, the suction level decreases with temperature, and the geotextile exhibits low conductivity under simulated drainage conditions. In this case, the geotextile layer works better as a moisture barrier at high temperatures.
7. Under simulated capillary conditions where water moves upward due to capillary force, a low temperature leads to a decrease in the hydraulic conductivity of the geotextile and induces the geotextile to work more efficiently as a moisture barrier. This finding is important, especially for cold regions where preventing capillary rise and minimizing frost heave is desirable.
8. The 2-D finite element modeling results show that when only one DMBL is used, suction in the ABC decreases under infiltration and drainage conditions, whereas suction increases in the subgrade layer. The decreased suction in the ABC results in a decrease in the shear strength of the ABC and consequently leads to greater deformation under the applied load. One way to minimize the decrease in suction in the ABC is to increase the unsaturated hydraulic conductivity of the DMBL under suction by increasing its AEV.
9. Results from the 2-D finite element modeling of roadway sections show that when only a geotextile layer is used as the DMBL, suction in the ABC decreases under infiltration and drainage conditions, whereas it increases in the subgrade layer. The decreased suction in the ABC

results in a decrease in the shear strength of the ABC and consequently leads to greater deformation under the applied load.

10. One way to minimize the decrease in suction in the ABC is to increase the unsaturated hydraulic conductivity of the DMBL under suction by increasing its AEV. However, when a geotextile alone is used as the DMBL, increasing the AEV of the DMBL decreases the suction in the subgrade during rainfall infiltration due to the downward water flow into the subgrade, because increasing the AEV of the DMBL also increases both the lateral and downward water flow.
11. A composite DMBL decreases the downward flow into the subgrade when the AEV of the lower layer is on the order of 1 psf. In this case, increasing the AEV of the upper layer increases the suction in the subgrade under both rainfall and drainage conditions, whereas the ABC remains unsaturated.
12. Increasing the AEV of the upper layer of the composite DMBL from 3.76 psf to 15.15 psf increases the suction in the subgrade by about 45% during the first 6 hours of rainfall infiltration, whereas the suction in the ABC does not decrease. The results also show that increasing the saturated hydraulic transmissivity of the upper layer does not have a significant effect on the pore pressure distribution in the profile as long as it is under suction greater than 2 psf.
13. The results show that placing the DMBL at the interface of the ABC and subgrade increases suction in the subgrade and ABC layers during infiltration more than when the DMBL is placed in the middle of the ABC

Recommendations

The following recommendations are made based on the experimental results and modeling, taking into consideration the profile, initial and boundary conditions, and infiltration rates (0.07 ft/hr and 0.035 ft/hr) used in the study:

i. A composite DMBL, composed of a transmission layer (geotextile) underneath a capillary break layer (geonet), is found to protect the subgrade from infiltrating water. During the load testing phase, the DMBL section was found to outperform the control section under both static and cyclic loading. A recommended typical cross-section for such a system is shown in Figure 96. The configuration of the DMBL is as recommended by Henry and Stormont (2000).

ii. The DMBL should be placed at the interface of the ABC and subgrade. This configuration is in concert with that reported in the literature.

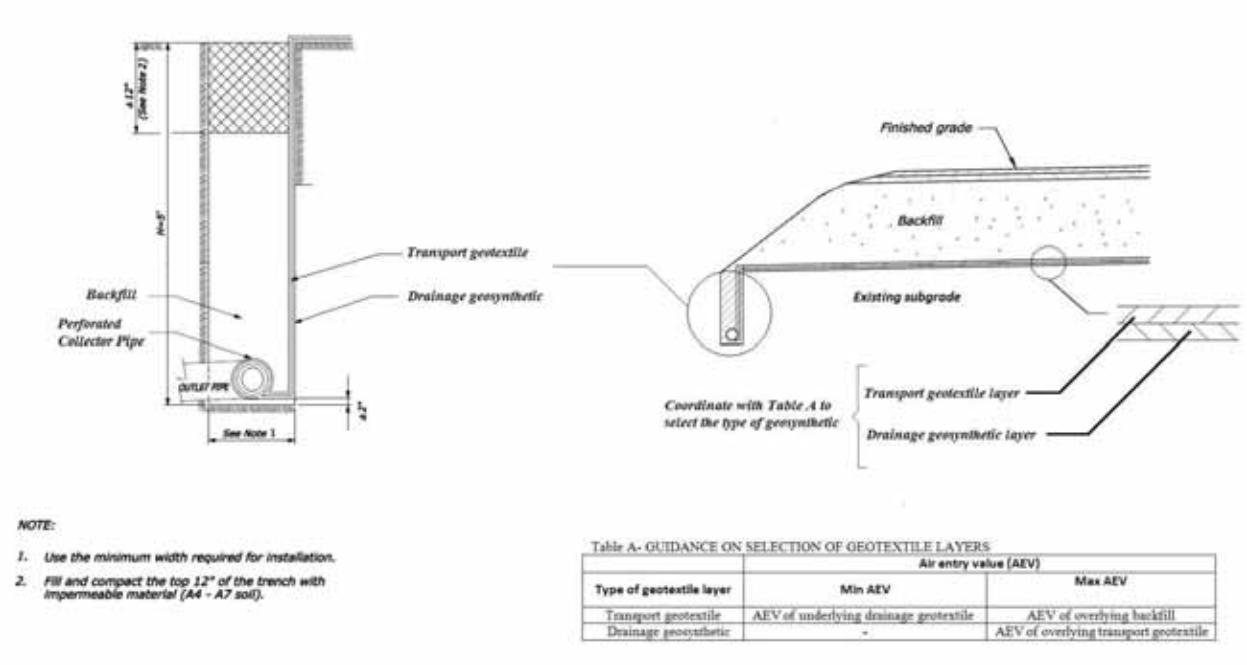

Table A- GUIDANCE ON SELECTION OF GEOTEXTILE LAYERS

	Air entry value (AEV)	
Type of geotextile layer	Min AEV	Max AEV
Transport geotextile	AEV of underlying drainage geotextile	AEV of overlying backfill
Drainage geosynthetic	-	AEV of overlying transport geotextile

Figure 96. Schematic. Typical cross-section of system and connection details.

iii. To diminish water flow into the subgrade and to drain the ABC during rainfall infiltration, the lower DMBL must have a lower AEV than the upper DMBL. The AEV can be estimated based on ASTM D6836, *Standard Test Methods for Determination of the Soil Water Characteristic Curve for Desorption Using a Hanging Column, Pressure Extractor, Chilled Mirror Hygrometer, and/or Centrifuge*, while noting the modifications and procedures followed in this study. It is important to recognize that using a geotextile layer with an AEV that is incompatible with the surrounding layers may lead to the inability of the geotextile layer to transmit water under unsaturated conditions and to act mainly as a barrier. As such, with the continuous introduction of moisture to the system, the ABC may become saturated, leading to a reduction in strength and an increase in rutting.

iv. A high AEV for the upper layer of the DMBL increases suction in the subgrade while maintaining saturation in the ABC. However, the AEV of the upper layer of the DMBL should not exceed the AEV of the overlying ABC.

v. Using a geomembrane underneath the DMBL leads to an increase in the degree of saturation in the ABC. Suction decreases in the ABC because downward water flow is prevented by the geomembrane. With an increase in the degree of saturation to 100%, a positive pore pressure in the ABC is generated, thus leading to a decrease in shear strength and, therefore, more rutting.

vi. During drainage, the use of two DMBLs (a composite two-layer configuration) increases the degree of saturation in the ABC, but does not lead to the generation of positive pore pressure, and the ABC remains unsaturated.

vii. The best configuration for moisture barriers is the use of two layers, as recommended by Stormont et al. (2000), i.e., a layer with a low AEV (1 psf) underneath a layer with a relatively high AEV. The upper layer of the composite section should, however, have an AEV that is lower than that of the ABC. Although it is tempting to suggest ratios of the AEV between the layers, the guiding design principle should be an AEV that is as low as possible for the lower layer and as high as possible for the upper layer, but that does not exceed the AEV of the ABC.

viii. An extensive experimental study should be performed under controlled conditions to investigate the performance of DMBLs, not only for the control of moisture distribution, but also to study the associated system stiffness and deformation responses under applied cyclic loading. Invariably, and in addition to the moisture attenuation, the DMBLs provide some level of reinforcement to a composite section. The aspects of DMBL behavior in response to the combined moisture attenuation and reinforcement effects are noticeably absent from the literature.

(blank page)

REFERENCES

ASTM D6836 – 02. (2008) “Standard Test Methods for Determination of the Soil Water Characteristic Curve for Desorption Using a Hanging Column, Pressure Extractor, Chilled Mirror Hygrometer, and/or Centrifuge.” Book of Standards Vol. 04.09, American Society for Testing and Materials, ASTM International, West Conshohocken, PA.

Bathurst, R., Ho, A. F., and Siemens, G. (2007) “A column apparatus for investigation of 1-D unsaturated –saturated response of sand-geotextile systems.” *Geotechnical Testing Journal*, Vol. 30 (6).

Beskow, G. (1946) Supplement: Some results of Scandinavian soil frost research 1935–1946. In Soil freezing and frost heaving with special applications to roads and railroads. Swedish Geological Society, Series Cv, No. 375, Year Book 3. Translated by J. O. Osterberg. CRREL Special Report 91-23, U.S. Army Corps of Engineers, Cold Regions Research and Engineering Laboratory, Hanover, NH., 161–169.

Bouazza, A., Fruend, M., and Nahlawi, H. (2006). "Water retention of nonwoven polyester geotextiles." *Polymer Testing,* 25 (8), 1038.

Carsel, R. and Parrish, R. S. (1988) “Developing joint probability distribution of soil water retention characteristics.” *Water Resources Research*, 24 (5), 755-769.

Casagrande, L. (1938) “Examination of the sub-soil of roads.” *Proceedings of the 8th International Road Congress*, The Hague, 1–27.

Cass, A. Campbell, G.S. and Jones, T. L. (1981) “Hydraulic and thermal properties of soil samples from the Buried Waste Test Facility.” PNL-4015, Pacific Northwest Laboratory, Richland, WA.

Cass, A. Campbell, G.S. and Jones, T. L. (1984) “Enhancement of thermal water vapor diffusion in soil.” *Soil Science Society of America*, 48, 25-32

Christopher, B. R., Hayden, S. A., and Zhao, A. (2000) “Roadway Base and Subgrade Geocomposite Drainage Layers,” in Testing and Performance of Geosynthetics in Subsurface Drainage, ASTM STP 1390.

Enhanced Integrated Climate Model (EICM) version 3.2 Beta. (2006) Jointly developed by the Texas Transportation Institute, Texas A&M University, and the Department of Civil Engineering, University of Illinois.

Evans, T. M., Meyers, D. K., Gharios, K. M., Hadj-Hamou, T., and Kavazanjian, E. (2000) "The use of a capillary barrier final cover for reclamation of a closed municipal solid waste landfill.” *Proceedings of the Third Annual SWANA Arid Climate Symposium*, Albuquerque, NM, 16.1-16.9.

Fallow, D. J., Brown, D. M., Lauzon, J. D., and Parkin, G. W. (2007) “Risk assessment of unsuitable winter conditions for manure and nutrient application across Ontario.” *Journal of Environmental Quality*, 36, 31-43.

Flerchinger, G. N. and Saxton, K. E. (1989) “Simultaneous heat and water model of a freezing snow-residue-soil system. Theory and development.” *Transactions of the American Society of Agricultural Engineers*, 32, 565-571.

Garcia, E. F. (2007) "Function of permeable geosynthetics in unsaturated embankments subjected to rainfall infiltration." *Geosynthetics International,* 14 (2), 89.

Hansson, K., Simunek, J., Mizoguchi, M., and Lundin, L.-Ch. (2004) “Water flow and heat transport in frozen soil: Numerical solution and freeze/thaw applications.” *Vadose Zone*, 3, 693–704.

Henry, K. S. (1988) “Use of geotextiles to mitigate frost heave in soils.” *Proceedings of the 5th International Conference on Permafrost*, Trondheim, Norway, 2, A.A. Balkema, Brookfield, VT., 1096–1011.

Henry, K. S. and Holtz, R. D. (1997). "Capillary rise of water in geotextiles." *Proceedings of the 1997 International Symposium on Ground Freezing and Frost Action in Soils,* 227-233.

Henry, K. S. and Stormont, J. C. (2000) “Geocomposite capillary barriers drain.” US Patent No. 6,162,653.

Henry, K. S. and Stormont, J. C. (2002) "Geocomposite Capillary Barrier Drain for Limiting Moisture Changes in Pavement Subgrades and Base Courses." NCHRP-IDEA 68 Final Report, Transportation Research Board.

Henry, K. S., Stormont, J. C., Barna, L. A., and Ramos, R. D. (2002) "Geocomposite capillary barrier drain for unsaturated drainage of pavements." *Proceedings of the 7th International Conference on Geosynthetics*, 877-880.

Hillel, D. (1980) Fundamentals of Soil Physics. Academic Press, New York.

Ho, A. F. (2000) “Experimental and Numerical Investigation of Infiltration Ponding in One-dimensional Sand–geotextile Columns”. MSc thesis, Queen’s University, Kingston, Ontario, 212 pp.

Iryo, T. and Rowe, R. K. (2003) “On the hydraulic behavior of unsaturated nonwoven geotextiles.” *Geotextiles and Geomembranes*, 21 (6), 381–404.

Iryo, T. and Rowe, R. K. (2004) “Numerical study of infiltration into a soil-geotextile column.” *Geosynthetics International*, 11 (5), 377-389.

Iryo, T. and Rowe, R. K. (2005) “Hydraulic behavior of soil-geocomposite layers in slopes.” *Geosynthetics International*, 12 (3), 145-154.

Knight, M. A. (2001) "Measurement of geotextile-water characteristic curves using a controlled outflow capillary pressure cell." *Geosynthetics International,* 8 (3), 271.

Krisdani, H., Rahardjo, H., and Leong, E. C. (2008) “Measurement of geotextile-water characteristic curve using capillary rise principle.” *Geosynthetics International*, 15 (2), 86-94.

Kool, J. B. and Parker, J. C. (1987) “Development and evaluation of closed-form expression for hysteretic soil hydraulic properties.” *Water Resources Research*, 23, 105-114.

Kuhn, J. A., McCartney, J. S., and Zornberg, J. G. (2005) "Impinging flow over drainage layers including a geocomposite." *Proceedings of the Sessions of the Geo-Frontiers 2005 Congress*, Austin, Texas, USA, American Society of Civil Engineers, New York, 4013.

Lafleur, J., Lebeau, M., Faure, Y. H., Savard, Y., and Kehila, Y. (2000) "Influence of Matric Suction on the Drainage Performance of Polyester Geotextiles." In Filters and Drainage in Geotechnical and Environmental Engineering, Wolkski, and Mlynarek, eds., Balkema, Rotterdam, 381.

McCartney, J. (2007). "Hydraulic interaction between geosynthetic drainage layers and unsaturated low plasticity clay." *Geotech Spec Publ*, (165), 3.

McCartney, J. S., Kuhn, J. A., and Zornberg, J. G. (2005) Geosynthetic drainage layers in contact with unsaturated soils. *Proceedings of the 16th International Conference of Soil Mechanics and Geotechnical Engineering*, Osaka, Japan, 2301–2305.

Morris, C. M. and Stormont, J. C. (1999) “Parametric study of unsaturated drainage layers in a capillary barrier” *Journal of Geotechnical and Geoenvironmental Engineering*, 125 (12), 1057-1065.

Morris, C. E. (2000) "Unsaturated flow in nonwoven geotextiles." *GeoEng 2000: An International Conference on Geotechnical and Geological Engineering*, Technomic Publishing, Inc., Lancaster, PA .

Nahlawi, H., Bouazza, A., and Kodikara, J. (2007) "Characterisation of geotextiles water retention using a modified capillary pressure cell." *Geotextiles and Geomembranes*, 25 (3), 186.

Park, K. D. and Fleming, I. R. (2006) "Evaluation of geosynthetic capillary barrier." *Geotextiles and Geomembranes*, 24 (1), 64-71.

Preston, G. M. and McBride, R. A. (2004) “Assessing the use of poplar tree systems as a landfill evapotranspiration barrier with the SHAW model.” *Waste Management and Research*, 22, 291-305.

Ramos, R. D. (2001) "Performance of a Fiberglass Based Geocomposite Capillary Barrier Drain." M.Sc. thesis, University of New Mexico, Albuquerque, .

Ross, B. (1990) "The diversion capacity of capillary barriers." *Water Resources Research*, 26, 2625-2629

Rowe, R. K. and Iryo, T. (2003) "On the hydraulic behavior of unsaturated nonwoven geotextiles." *Geotextiles and Geomembranes*, 21 (6), 381.

Scanlon, B., Keese, K., Reedy, R. C., Simunek, J., and Andraski, B. (2003) "Variations in flow and transport in thick desert vadose zones in response to paleoclimatic forcing (0–90 kyr): Monitoring, modeling, and uncertainties." *Water Resource Research*, 39 (7), 1179-1189.

SEEP/W 2002 (Version 5.20) Manual, GEO-SLOPE International, Ltd. Calgary, Alberta, Canada.

SIGMA/W 2007 (Version 7.14, Build 4606) Manual, GEO-SLOPE International, Ltd. Calgary, Alberta, Canada.

Stockton, T. B. (2001) "Performance Experimental Testing of Diversion Lengths for a Geocomposite Unsaturated Drainage System." M.Sc. thesis, University of New Mexico, Albuquerque, NM.

Stormont, J. C., Henry, K. S., and Evans, T. M. (1997) "Water retention functions of four nonwoven polypropylene geotextiles." *Geosynthetics International*, 4 (6), 661-672.

Stormont, J. C., Evans, T. M., Stockton, T., and Ray, C. (1998) "Unsaturated hydraulics properties of a nonwoven polypropylene geotextile." *Proceedings of the '98 Joint Conference on the Environment, Waste-Management Education and Research Consortium*, Albuquerque, NM.

Stormont, J. C. and Morris, C. E. (2000) "Characterization of unsaturated nonwoven geotextiles." *Advances in Unsaturated Geotechnics Proceedings*, Geotechnical Special Publication No. 99, C. D. Shackelford, S. L. Houston, and N. Y. Chang, eds., Geo-Institute of the ASCE, Denver, CO, Aug. 2000, 529–542.

Stormont J. C., and Stockton, T. B. (2000) "Preventing Positive Pore Water Pressures with a Geocomposite Capillary Barrier Drain," in Testing and Performance of Geosynthetics in Subsurface Drainage, ASTM STP 1390, L.D. Suits, J.B Goddard and J.S. Baldwin, Eds. American Society for Testing and Materials, West Conshohocken, PA.

Stormont, J. C., Ramos, R. D., and Henry, K. S. (2001) "Geocomposite capillary barrier drain system with fiberglass transport layer." *Transportation Research Record* (1772), 131.

Stormont, J. C., Ray, C., and Evans, T. M. (2001) "Transmissivity of a nonwoven polypropylene geotextile under suction." ASTM Geotechnical Testing Journal, 24 (2), 164.

Stormont, J. C., and Ramos, R. D. (2004) "Characterization of a fiberglass geotextile for unsaturated in-plane water transport." ASTM Geotechnical Testing Journal , 27 (2), 214.

Stormont, J. C., Henry, K. S., and Roberson, R. (2008). "Geocomposite Capillary Barrier Drain for Limiting Moisture Changes in Pavements: Product Application." Contract No. NCHRP-113 (Draft Final Report), MnDOT.

Stormont, J. C., Henry, K. S., and Roberson, R. (2009) "Geocomposite Capillary Barrier Drain for Limiting Moisture Changes in Pavements: Product Application." Contract No. NCHRP-113 Final Report.

Suits, L. D., Goddard, J. B., and Baldwin, J. S., eds. (2000) American Society for Testing and Materials, West Conshohocken, PA.

Taber, S. (1929) “Frost heaving.” *Journal of Geology*, 38: 303–317. In Historical Perspectives in Frost Heave Research. CRREL Special Report 91-23, U.S. Army Cold Regions Research and Engineering Laboratory, Hanover, NH., 29–35.

Travis, B. J. and Birdsell, K. H. (1991) ‘‘TRACR3D: A model of flow and transport in porous media’. LA-11798-M (UC-814), Los Alamos National Laboratories, Los Alamos, NM.

UNSODA (1999) The Unsaturated Soil Hydraulic Database, User’s Manual, V.1.0. EPA/600/R-96/095.

Zornberg, J. G. and Mitchell, J. K., (1994) “Reinforced soil structures with poorly draining backfills. Part I: Reinforcement interactions and functions.” *Geosynthetics International* 1 (2), 103–147.